Wayne State University Dissertations

1-1-2010

Photodissociation Dynamics In Titan's Atmosphere

Welvidanalage Ruchira Silva
Wayne State University

Follow this and additional works at: http://digitalcommons.wayne.edu/oa_dissertations

Recommended Citation

PHOTODISSOCIATION DYNAMICS IN TITAN'S ATMOSPHERE

by

W. RUCHIRA SILVA

DISSERTATION

Submitted to the Graduate School

of Wayne State University,

Detroit, Michigan

in partial fulfillment of the requirements

for the degree of

DOCTOR OF PHILOSOPHY

2010

MAJOR: CHEMISTRY (Physical)

Approved by:

_____
Advisor   Date

_____

_____

_____

DEDICATION

~ To my Parents, Madu and Netuli...

ACKNOWLEDGMENTS

First and foremost, I owe my deepest gratitude to my advisor, Professor Arthur G. Suits, whose guidance, encouragement and support enabled me to complete my graduate studies through Wayne State University. This dissertation would not have been possible without his forgiveness, kind considerations, great efforts and continuous support. I am very fortunate to have an advisor like Prof. Suits who not only guided me to understand the subject but also helped me to overcome every major difficulty I faced in my life over the last five years. If it was not his support my dreams would not have become a reality. His passion towards research is inspiring and motivating. I'm grateful for him for everything I learnt throughout my graduate career. I admire him as a great scientist and a kind hearted mentor.

I am indebted to my committee members, Dr. Charles Winter, Dr. Vladmire Chernyak, and Dr. David Cinabro for their considerations and support in numerous ways. I am grateful to Dr. Andrew Feig for his efforts in resolving the issues I had with graduate school and helping me in many ways to complete my studies through Wayne State University. Also, I would like to thank Dr. James Rigby and all the faculty members in chemistry department for their considerations in giving me the opportunity to complete my studies. Many thanks to Ms. Melissa Barton for her invaluable help and guidance in numerous ways for completing this dissertation.

TABLE OF CONTENTS

LIST OF TABLES

LIST OF FIGURES

This Dissertation is largely based on the work presented in the following

publications:

1. Silva, R.; Gichuhi, W. K.; Huang, C.; Doyle, M. B.; Kislov, V. V.; Mebel, A. M.; Suits, A. G., H elimination and metastable lifetimes in the UV photoexcitation of diacetylene. *Proc. Natl. Acad. Sci. U. S. A.* 2008, *105* (35), 12713-12718.

2. Silva, R.; Gichuhi, W. K.; Kislov, V. V.; Landera, A.; Mebel, A. M.; Suits, A. G., UV Photodissociation of Cyanoacetylene: A Combined Ion Imaging and Theoretical Investigation. *J. Phys. Chem. A* 2009, *113* (42), 11182-11186.

3. Silva, R.; Gichuhi, W. K.; Doyle, M. B.; Winney, A. H.; Suits, A. G., Photodissociation of heptane isomers and relative ionization efficiencies of butyl and propyl radicals at 157 nm. *Phys. Chem. Chem. Phys.* 2009, *11* (23), 4777-4781.

Chapter 1

Titan

1.1 Introduction

Titan, Saturn's largest satellite, is the only solar system body besides Earth and Venus that has a dense atmosphere[1,2]. Titan is known to have the second largest volume of any of our solar system's satellites, with the radius of 2575 km, roughly 50% greater than that of Earth's moon[3]. It was first discovered in 1655 by a Dutch astronomer Christiaan Huygens[4]. It was well known as a planet-like satellite because of its size and it was also considered as the largest moon in the solar system until Voyager 1 arrived in 1980. However, now it is clear that the dense atmosphere of Titan, which extends many kilometers above its surface, increases the visible radius of Titan, giving it a larger apparent size.

Titan's atmosphere, mostly N_2, has a value of column density ten times greater than that of Earth[5,6,7]. Unlike the Earth's atmosphere, there is no chemical equilibrium in Titan's atmosphere. It has an irreversible formation of complex negative and positive ions at the thermosphere, which involves solar EUV, UV radiation and impact from high energy electron and ions as a result of magnetospheric-ionospheric-atmospheric interactions[8]. On the other hand CH_4, the second most abundant molecule in Titan's atmosphere, dissociates

irreversibly ultimately leading to formation of ethane, acetylene and simple nitriles[5],[7]. These molecules eventually undergo photochemical reactions to produce larger organic molecules, such as benzene and naphthalene[5, 9]. These molecules start condensing at about 950 km altitude, and trigger the process of haze formation[8],[10]. The haze particles strongly absorb UV and visible radiation and initiate the heating process in Titan's stratosphere and drive the wind system in the middle atmosphere[11]. These haze particles act as ozone in Earth's stratosphere[5], shielding the surface from UV radiation. Finally, these complex molecules precipitate on the surface of Titan, thereby connecting the upper thermosphere with the surface[8].

Most of the detailed information on Titan's atmosphere and the surface to-date was revealed from Cassini-Huygens mission, which arrived in the Saturnian system in 2004[12],[13]. However, the origin, the atmosphere and the surface of Titan are still a mystery in most aspects and scientists face extraordinary challenges in understanding the processes involved. On the other hand it is an interesting body to study, as Titan is known to have diverse geophysical and chemical processes comparable to the Earth's atmosphere[8]. Therefore, Titan is an ideal world for geophysicists and astrochemists to explore the mysteries of this satellite as well as making the connection to the Earth.

1.2 Origin of Titan

The origin of Titan has been extensively studied over the last decade through data obtained from space and ground based measurements, models, and laboratory studies. Although we are still not close to a complete understanding of Titan, these data and models have helped enormously to understand the formation and evolution of Titan as well as to get an idea of how it captured an atmosphere[8].

However, it is a quite difficult task to find the best connection between a model for the solar nebula and a model for the formation of planets that includes its own satellite system. Any thriving model for satellite formation should be able to predict the probable composition of the atmosphere and surface as well as the density and variety of satellites[8]. Those are the crucial properties that can be employed as useful parameters to elucidate the limitations of satellite formation models by comparison with current observations. By considering the 3-D hydro-dynamical model[14] it is clear that satellite formation took place in the protosatellitary disk. At the last stage of planetary formation, the contracting atmosphere in protosatellitary disk helped to capture the materials, which became the building blocks of the satellites.

Scenarios have been developed for satellite formation based on two end-member type hypotheses[8].

Hypothesis 1

It is hypothesized that planetesimals, which consists only of silicates and moderately refractory volatile compounds, were formed in the cold- and gas-dominated solar nebula which is at the end of its lifetime. This could have happened due to rapid degeneration of primary subnebula[15]. In this case, CH_4, H_2S and Xe can be trapped as clathrate hydrates while NH_3 and CO_2 condensed in migrating planetesimals which ultimately formed Titan[15-16]. This will explain the low abundance of CO and ^{36}Ar in Titan's atmosphere as the lack of water ice at later age restricted the trapping of less stable molecules such as CO and Ar which prefer to clathrated at low temperatures[8].

Hypothesis 2

In this hypothesis, it is assumed that planetesimals were formed within the warm sub nebula with the formation of Saturn. These planetesminal were the origin of Titan and other satellites in Saturn[8]. Silicates and other moderately volatile materials must have incorporated into Titan by this formation. However, considering the temperature of planetesminals, it would be rather difficult to entrap the volatile noble gases like Xe, Ar and CH_4 in ice grains; however it would facilitate accommodation of H_2O, NH_3, CO_2 and nonvolatile compounds[17,10,18,19]. Detection of Ar on a small scale from the Huygens GCMS[20] has provided an indication of ambient temperatures for the formation in the sub nebula ~ 100 K[18,19] assuming Ar was trapped in amorphous ice. Even though

CH_4 is the second most abundant constituent in Titan's current atmosphere; it was not initially included in Titan. CH_4 was produced from the reaction of C compounds such as CO_2 with H, which was produced from H_2O by water-rock reactions[10]

Both of these hypotheses proposed that NH_3 escaped from the planetesimals throughout the accumulation and formed the early atmosphere. Then these hypotheses suggest that NH_3 would have converted to N_2 due to photolysis reactions of the hot proto-atmosphere of Titan[21] or impact-induced chemical reactions[22]. However, it is also suggested that CH_4 outgassed from the inner part of the Titan[20,23]. Even though these two processes lead to different isotopic ratio of H:D in vaporized water and methane, these provide a comparable guideline for formation[8] of Titan's atmosphere.

1.3   Titan as a model for the early Earth

Life on Earth originated about 4 billion years ago. Investigation of the processes that led to the origin of life is extremely difficult and challenging due to the fact that most of the processes and environmental conditions at that time have been erased by the evolutionary mechanisms. Therefore, it is very important for scientists to have an extraterrestrial place, which is parallel to our primitive Earth, to understand the emergence of life on our planet.

Titan has many similarities with early Earth even though it has a lower temperature[24]. Titan is the only outer solar system body with an atmospheric pressure (1.5 bar) close to the Earth's atmosphere. Moreover, both Titan and Earth consist of an N_2 dominated atmosphere[5,1]. In addition, there are many structural similarities ranging from ionosphere to troposphere in both atmospheric systems. When CH_4 is considered, it exists in all three phases on Titan: gaseous, solid and liquid. This resembles the presence of H_2O in the Earth[8],[10]. Further, Titan is the only extraterrestrial body that is known to have liquid on its the surface, in the form of hydrocarbon lakes.

1.3.1 Complex Prebiotic chemistry in Titan's atmosphere

It is well known that several of the organic molecules that are formed in Titan today are important molecules in prebiotic chemistry. HCN, HC_3N and C_2N_2 are some of the key molecules found in Titan's atmosphere and also crucial for prebiotic chemistry[25,26]. N_2 and CH_4 in Titan's atmosphere initiate the formation of gas phase complex organic molecules and solid state products such as tholins[27] which also can be produced in the laboratory. Data collection at the region of troposphere and stratosphere using gas chromatography mass spectrometer (GCMS) shows that there is a low abundance of volatile organic species other than CH_4[7]. This is due to the condensation of volatile organic substances on aerosol particles. After analyzing their composition using Huygens

analytic predictor-corrector (APC) instrument, it is clear that these aerosol particles are made of refractory organic compounds, which are covered by condensation of volatile compounds[20]

Several organic compounds have been detected by the ion and neutral mass spectrometer (INMS) instrument in Cassini at very high altitudes (1100 km-1300 km)[28]. The extrapolation of data obtained by INMS indicated the possibility of the formation of higher molecular weight species in the ionosphere[8]. Therefore, if confirmed, these data would definitely revolutionize our understanding of Titan's atmosphere, implying it has the ability of forming high molecular weight complex organic molecules[29] in its ionosphere, a surprising change in perspective.[28, 30]

After formation, these complex higher molecular weight organic molecules will tend to accumulate simultaneously with other volatile organic compounds, ultimately depositing on Titan's surface[8]. This is the beginning of aerosol particle formation and these aerosol particles will undergo chemical evolution, perhaps forming biologically interesting molecules[31]. It has been shown by laboratory experiments that tholins can form amino acids when there are interactions with liquid water[32]. These processes could happen on Titan's surface where cryovolcanism occurs[33]. Unfortunately, it is impractical to study long time chemical evolution processes in the laboratory; therefore Titan is an ideal candidate for observation of the chemical evolution of prebiotic Earth.

1.4   Titan as a complex system to study

Compared to other objects in our solar system, Titan is the best satellite to show parallel coupling between the magnetosphere, stratosphere, ionosphere, troposphere, surface and interior as seen in the Earth[34]. Therefore, Titan is also studied as a complex system analogous to the Earth.

On Earth, H_2O is the working fluid that has a well understood complex life cycle. In Titan, CH_4 acts as water in Earth[10]. It is known to present in the interior, trapped as clatharate hydate[15-16] or dissolved in a liquid layer under the crust of Titan. The presence of CH_4 in the interior of Titan affects the ice crust chemically, mechanically and thermally[10]. Outgassing of interior CH_4 can be happen via cryovolcanoes[11]. These volcanisms, which supply CH_4, could be facilitated by the presence of a liquid water mantle[35]. All these predictions were supported by data collected by the Cassini Visible and Infrared mapping Spectrometers (VIMS) as well as from the information obtained by its RADAR imaging systems[12].   Also, the escaped methane facilitates the formation of clouds, helping to maintain the basic radiative balance of the dense atmosphere in Titan[35]. In the upper atmosphere of Titan, CH_4 is dissociated and reacts with N_2 to form complex organic molecules that will eventually form a dense aerosol layer[5]. All of these complex molecules and aerosol particles precipitate on the surface nourishing the lakes, seas and dunes[10,8].

1.4.1 Surface of Titan

The Cassini/Huygens mission has shown and provided a vast array of information of Titan. This information is available for geophysists to predict or obtain a better understanding of Titan's surface. Geomorphologicanl information has been gathered by using high resolution (0.5km/pixel) RADAR mapper with coverage of approximately 1% of Titan's surface[12]. In addition to that, the Cassini Visible and Infrared Mapping Spectrometer (VIMS) with a moderate resolution (few km/pixel) has covered $100km^2$ geographical areas on Titan's surface[36,37]. According to the observations, the surface of Titan appears to be young, and low frequency impact craters have been found[38]. In addition, Cassini RADAR images provided information on complex geological features on the surface of Titan. Dome shaped volcanic constructs, cryovolcanic flows and twisting channels are some of the interesting geological features that have been observed on Titan's surface[12]. The Synthetic Aperture Radar (SAR) mode of the Cassini RADAR maps assisted in identifying frozen hydrocarbons on the surface[12]. Moreover, scattering and dielectric data obtained from these instruments clearly indicated the presence of porous ice structure[12]. Also, it is clear that there are erosion features such as deltas, river channels, hydrocarbon lakes, mountains, widespread aeolian, glacial-flow assembles as well as dunes on the surface[11, 36, 39].

1.4.2 Interaction between upper atmosphere and magnetosphere

Titan's upper atmosphere, extending from 400 km, is the most essential part of Titan's entire atmosphere when its chemistry and physics are considered[40]. In this region, EUV and VUV radiation play a key role in dissociating N_2 and CH_4 to form primary organic constituents[5]. These dissociation products will ultimately undergo more complex photochemical reactions that affect all other layers in Titan's atmosphere[1, 21]. On the other hand, Titan's upper atmosphere actively interacts with Saturn's magnetosphere resulting in the formation of an induced magnetosphere in Titan[41]. In the induced magnetosphere, N_2 and CH_4 can be easily ionized and dissociated[1, 5] producing primary nitriles and hydrocarbons that can create photochemical effects on all other layers.

Previous Voyager and recent Cassini/Huygens observations have provided valuable information on an extraordinary relationship between Titan's upper atmosphere and magnetosphere. Moreover, these observations have assisted in understanding the complex upper atmospheric chemistry to great extent. Huygens has given the information on vertical profile of total composition of the atmosphere from 1400km[13]. It was able to obtain detailed information from ~ 140km altitude to the surface[8]. On the other hand Cassini provided data up to 950km altitude[13]. These accumulated measurements not only directly help to identify ~100 new complex organic molecules at the upper atmosphere of Titan[7,

[20] but also observed haze particles at high altitude, longitude dependent composition and a strong relationship between magnetic field and the ionosphere. Detection of heavy negative ions using mass/charge and energy/charge spectrometer in Cassini was an important finding[28]. This observation of very large negative ion (~8kDa) at high altitude (~1000km) ionosphere proposed that there is an ionospheric contribution for the formation of aerosol in the lower layers of Titan's atmosphere[42]. Additional information was obtained from ground based observations and the Cassini Magnetospheric Imaging Instrument (MIMI)[43]. Observation of very high gas escape rates, detection of neutral hydrogen clouds, which spread out for several Titan's radii, and identification of energetic neutral atoms[44] (ENA) that can be used to study magnetospheric dynamics facilitate to obtain a better understanding of the relationship between Titan's upper atmosphere and Saturn's magnetosphere. Taken together, the study of Titan's upper atmosphere and magnetosphere is very important in understanding the entire atmosphere. However, future studies are needed to better understand this broad transition region that would give us relevant information on the entire atmosphere.

1.4.3 Neutral atmosphere of Titan

Titan's atmosphere, very much like Earth's atmosphere, is connected to its ionosphere through chemical reactions, the surface through precipitation and

evaporation, and the interior through outgassing. Observing the variation of chemical composition and temperature profile in Titan's atmosphere would allow scientists to get a thorough understanding of Titan's neutral atmosphere. Titan's temperature profile is similar to the temperature profile of Earth[45]. At the Earth's surface H_2O, CO_2, which are greenhouse gases, warm up the atmosphere by ~35K. In Titan, the surface is warmed due to pressure induced heat absorption by N_2, H_2 and CH_4 by ~20K[46]. The temperature starts to decrease gradually with altitude in both atmospheres up to the tropopause (around ~10-15km from surface on Earth and ~40km on Titan)[45]. However, when altitude increases above the tropopause, again temperature starts to increase due to the presence of ozone in Earth and CH_4 and haze layers on Titan[45]. The balance between heating and cooling a region in Titan is achieved by the presence of molecules. CH_4 is important in heating while haze, C_2H_2, C_2H_6 and HCN are crucial for cooling this region[46]. Therefore, the molecules in the haze layer act as anti-greenhouse gases which absorb ~ 30% of solar radiation and blocking illumination of lower atmosphere[46]. This anti-greenhouse effect and warming effect change considerably with seasons and latitude[47] because of the variation of number density of C_2H_2, C_2H_6 and HCN gases with latitude and with season. This variation of abundance is caused by seasonal winds[48,11]. Moreover, the distribution of haze and its photolysis byproducts such as C_2H_2, C_2H_6 and HCN gases, condensation and deposition on the surface can be influenced by the

atmospheric circulation of Titan[49].   This atmospheric circulation is directly affected by the variation of number density of anti-greenhouse gases.

Though CH_4 is a major constituent of Titan's atmosphere, the understanding of Titan's methane cycle is still not clear. Regardless of irreversible destruction of methane by reactions, a greater saturation of methane in the troposphere has been observed by Huygens[50]. However, H_2O covers 75% of Earth's surface while liquid CH_4 in seas and lakes only covers about 1% of Titan's surface[39]. In addition, Earth's atmosphere only contains ~2.5 cm of precipitable H_2O where as Titan's atmosphere contains up to ~5m of precipitable CH_4[8]. Therefore, it is surprising to observe the lower atmosphere of Titan contains more methane than predictions. A great amount of methane release must have come from volcanoes, contributing to the methane cycle in Titan's atmosphere while leaving the surface dry[8,10].

Only 10% of the incident sunlight can contribute to weather by reaching Titan's surface, whereas 60% of sunlight   on Earth reaches the surface[8]. The formation of clouds on Titan is still not understood although various theories have been proposed. There is a development of large number of storms, which changing with season[51], in Titan's atmosphere. The Cassini probe has observed several instances of clouds throughout the thick haze layer near the South Pole and near 40° S region using near infrared spectroscopy and imaging[31]. Formation of clouds as well as their location, frequency and composition can be explained by theoretical models that consider and describe the large scale

circulation[52], cryovolcanism and surface heating. Figure 1.2 summarizes and shows the major coupling between Titan's neutral atmospheric processes[8].

1.5   Haze formation in Titan's atmosphere

Understanding elementary chemical reactions in detail is the key goal of chemical dynamics. Most of the chemical processes that occur in earth and other planetary atmospheres are usually initiated by light, and, thus, photochemistry has a great significance in such study, including a broad range of issues of fundamental importance in astrochemical physics. Titan's haze layers are assumed to be composed of hydrocarbons and nitriles formed from its dense atmosphere[1,5,53]. Photochemistry and impact from high energetic electrons initiate reactions involving 4% of methane in Titan's dense nitrogen atmosphere to form complex hydrocarbons and carbon-nitrogen compounds[5]. This complex hydrocarbon production undergoes a series of reactions involving hydrocarbon radicals and ions that remain poorly understood. It is believed that haze is known to play an important role in Titan's energy balance and atmospheric dynamics. After the Cassini/Huygens mission, lots of new information is now becoming available and this information will help to get a good understanding of Titan's atmosphere and the mechanism of its haze formation[54,6,55]. When constructing a photochemical model to describe the atmospheric composition in Titan's atmosphere, it is very important to have a solid database of the relevant physical
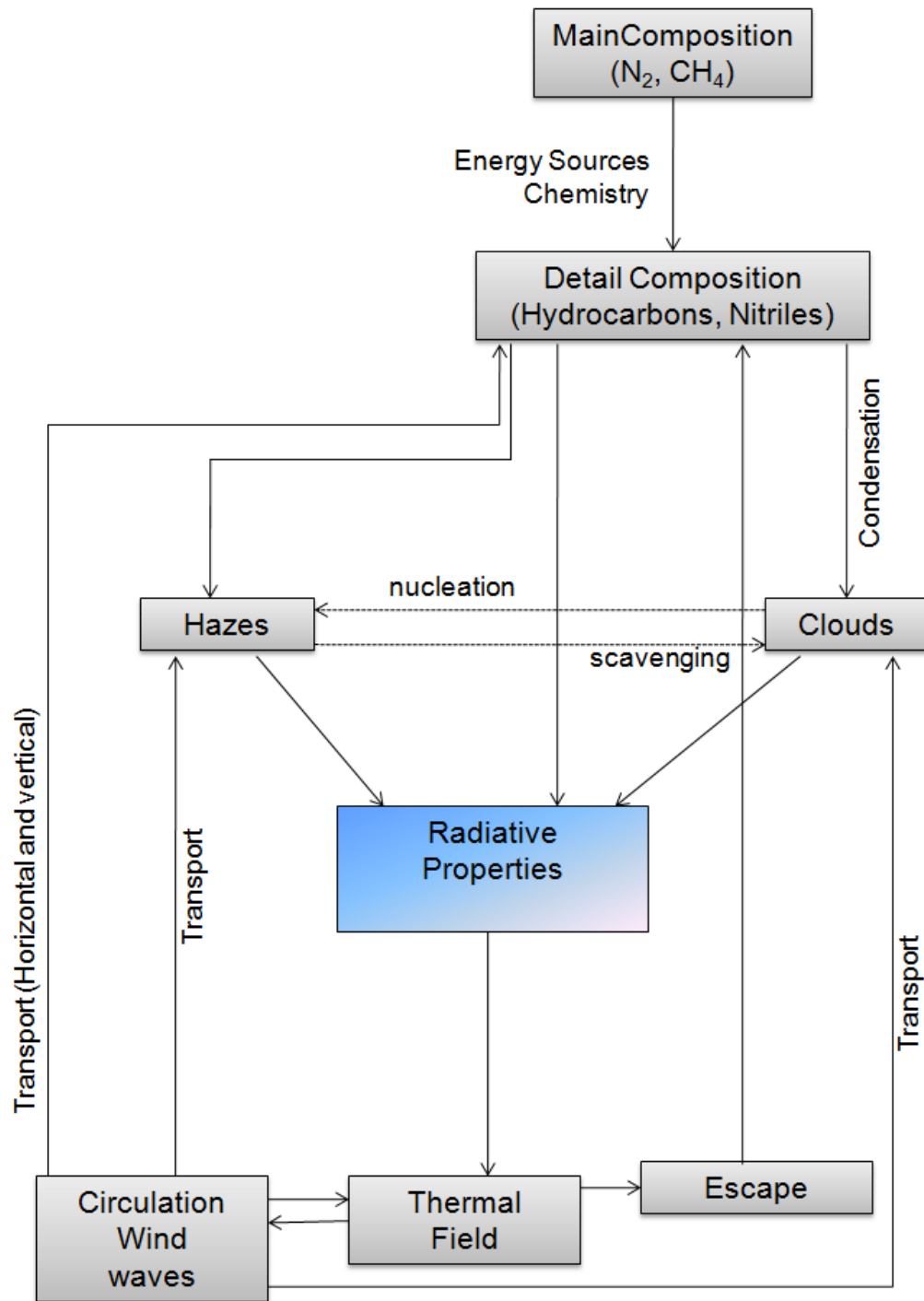
Figure 1.1 (Adapted from reference 5) coupling between Titan atmospheric processes[8]

and chemical parameters. Table 1.1 summarizes the main physical and chemical

data in Titan's atmosphere[5].

1.5.1 Primary chemical reactions in Titan's atmosphere

Dissociation of thermospheric N_2 with the interaction of energetic electrons

coming from induced magnetosphere initiate chemical reaction process in Titan's

atmosphere[5, 56]. This dissociation generates ground and excited state N atoms,

which can readily abstract an H atom from CH_4[57].

$$2\,[\,N_2 \;+\; e \;\longrightarrow\; N \;+\; N\,(^2D) \;+\; e\,]$$

$$2\,[\,N\,(^2D) \;+\; CH_4 \;\longrightarrow\; NH \;+\; CH_3\,]$$
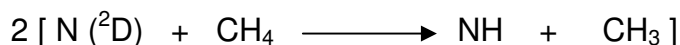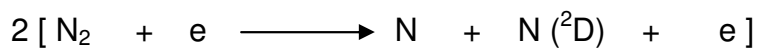
NH radical can interact with ground state N to form N_2 and H. This H

radical reacts with another NH radical and produces H_2 and N

$$NH \;+\; N \;\longrightarrow\; N_2 \;+\; H$$

$$NH \;+\; H \;\longrightarrow\; N \;+\; H_2$$
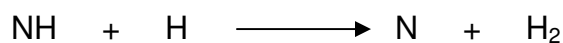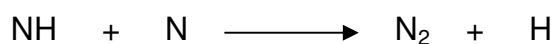
Formation of CH_3 from H abstraction reaction can initiate HCN formation[58].

$$2\,[\,CH_3 \;+\; N \;\longrightarrow\; HCN \;+\; H_2\,]$$

_____

net $N_2 \;+\; 2CH_4 \;\longrightarrow\; 2HCN \;+\; 3H_2$
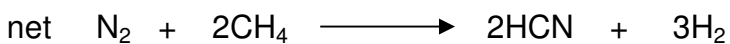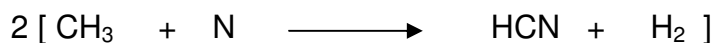
HCN then is transported to the stratosphere and condenses in the

troposphere.

Table1.1
At the Surface (altitude z=0) r_0 = distance to center = 2575km g_0 = gravity = 135cm s^{-2} P_0 = total pressure = 1.5 bar T_0 = temperature = 94K n_0 = number density = 1.2×10^{20} cm^{-3}
Composition of the Troposphere (volume mixing ratio) N_2 > 0.97 CH_4 < 0.03 H_2 = 0.002 **At Troposphere (z = 45km)** P = 130 mbar T = 71.4 K n = 1.1×10^{19} cm^{-3}
Composition of Stratosphere (volume mixing ratio) CH_4 = 1-3x10^{-2} C_4H_2 = 10^{-8}-10^{-7} H_2 = 2.0x10^{-3} HCN = 2x10^{-7} C_2H_6 = 2x10^{-5} HC_3N = 10^{-8}-10^{-7} C_2H_2 = 2x10^{-6} C_2N_2 = 10^{-8}-10^{-7} C_2H_4 = 4x10^{-7} CO = 6x10^{-5} C_3H_8 = 2-4x10^{-6} CO_2 = 1.5x10^{-9} CH_3C_2H = 3x10^{-8} H_2O < 1x10^{-9}
Composition of Mesosphere and thermosphere N_2 = 2.7x10^8 cm^{-3} at z = 1280km CH_4 = 1.2x10^8 cm^{-3} at z = 1140km (mixing ratio = 0.08) C_2H_2 mixing ratio 1% - 2% at z = 840km

Table 1.1 Chemical and physical composition of Titan's atmosphere[5](adapted from reference 5)

Photodissociation of CH_4 is very crucial in Titan's mesosphere. It is found that the H elimination pathway plays very minor role at VUV radiation[59]. There are three major pathways of CH_4 dissociation with the quantum yield of 0.41, 0.51 and 0.08 respectively[59-60,61].

$$CH_4 + h\nu \longrightarrow {}^*CH_2 + H_2$$
$$\longrightarrow CH_2 + 2H$$
$$\longrightarrow CH + H + H_2$$
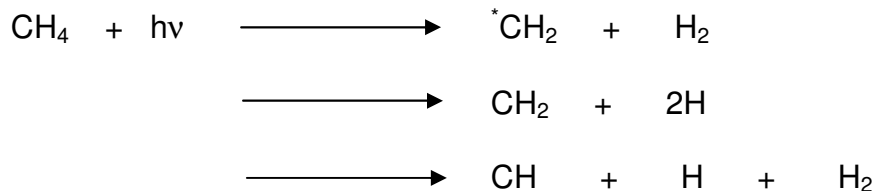
Where ${}^*CH_2$ and CH_2 are singlet excited and ground triplet state of CH_2 respectively. Triplet CH_2 can react with its own radical to produce C_2H_2. On the other hand CH_2 can collide with CH_3, which forms in the previous reaction with N (^2D), to form C_2H_4 in mesosphere[62,63]. Moreover, CH can be reacted with CH_4 to form C_2H_4.

$$2CH_2 \longrightarrow C_2H_2 + H_2$$
$$CH_2 + CH_3 \longrightarrow C_2H_4 + H$$
$$CH + CH_4 \longrightarrow C_2H_4 + H$$
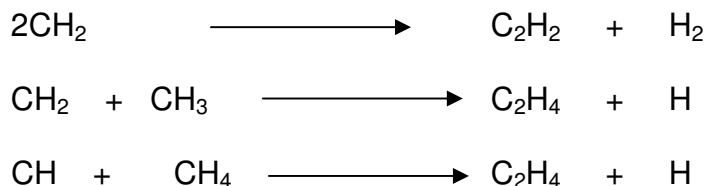
Further reaction between CH_2 and C_2H_2 can initiate the formation of CH_3C_2H by distributing the excess energy to a third body[63].

$$CH_2 + C_2H_2 + M \longrightarrow CH_3C_2H + M$$
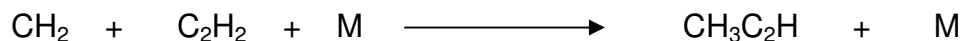
Formation of C_2H_6 can be driven by two major reaction pathways. The ultimate reaction step of both pathways is recombination of two CH_3 radicals. However formation of CH_3 radical can occur two different ways. Both reaction parts start

from singlet CH_2 radical. CH_2 can react either with H_2, which forms for CH_4 dissociation, or with another CH_4 to form CH_3[5].

$$^*CH_2 \ + \ H_2 \longrightarrow CH_3 \ + \ H$$

$$2CH_3 \ + \ M \longrightarrow C_2H_6 \ + \ M$$

Or

$$^*CH_2 \ + \ CH_4 \longrightarrow 2CH_3$$

$$2CH_3 \ + \ M \longrightarrow C_2H_6 \ + \ M$$
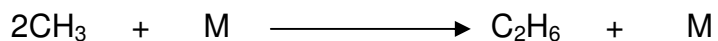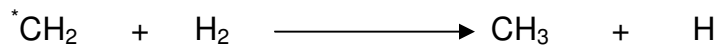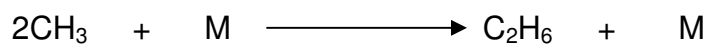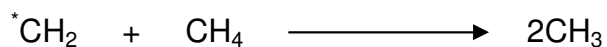
After formation of C_2H_6, it can be condensed in the troposphere to form surface lakes and seas on Titan or it can further react with C_2H, which is formed by photodissociation of C_2H_2, to form C_2H_5. This C_2H_5 can readily interact with CH_3 radical to produce C_3H_8[5].

$$C_2H_2 \ + \ h\nu \longrightarrow C_2H \ + \ H$$

$$C_2H \ + \ CH_4 \longrightarrow C_2H_2 \ + \ CH_3$$

$$C_2H \ + \ C_2H_6 \longrightarrow C_2H_2 \ + \ C_2H_5$$

$$CH_3 \ + \ C_2H_5 \ + \ M \longrightarrow C_3H_8 \ + \ M$$
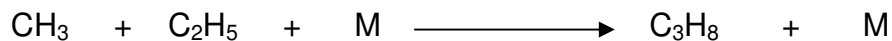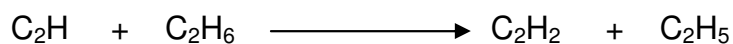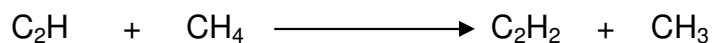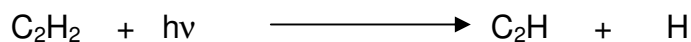
Formation of C_4H_2, which is very important in polyacetylene formation, is initiated by photodissociation of C_2H_2 in the stratosphere[64,63,65].

$$C_2H_2 \ + \ h\nu \longrightarrow C_2H \ + \ H$$

$$C_2H \ + \ C_2H_2 \longrightarrow C_4H_2 \ + \ H$$
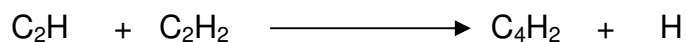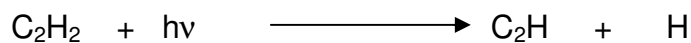
Furthermore, cyanoacetylene can be generated in the stratosphere by the reaction of C_2H with HCN molecule[64,63,65].

$$C_2H_2 \ + \ h\nu \longrightarrow C_2H \ + \ H$$

$$C_2H \quad + \quad HCN \quad \longrightarrow \quad HC_3N \quad + \quad H$$
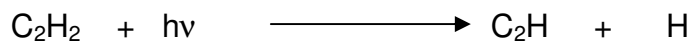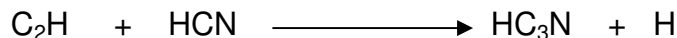
Photodissociation of HCN leads to the formation of CN radical that rapidly reacts with another HCN molecule to form C_2N_2[63-65].

$$HCN \quad + \quad h\nu \quad \longrightarrow \quad CN \quad + \quad H$$

$$CN \quad + \quad HCN \quad \longrightarrow \quad C_2N_2 \quad + \quad H$$
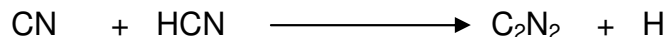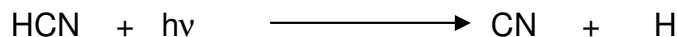
Thermospheric H_2O, which originates from meteorites, can be sublimated and photodissociated to form OH radical. OH radical can further react with CH_3 to form CO and this CO can again collide with an OH radical to produce CO_2[66,67].

$$H_2O \quad + \quad h\nu \quad \longrightarrow \quad OH \quad + \quad H$$

$$OH \quad + \quad CH_3 \quad \longrightarrow \quad CO \quad + \quad 2H_2$$

$$OH \quad + \quad CO \quad \longrightarrow \quad CO_2 \quad + \quad H$$
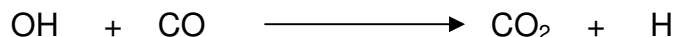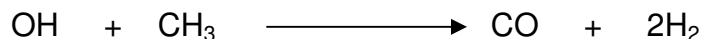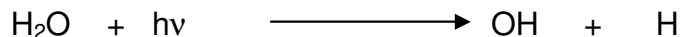
1.5.2 Polymerization process

A important aspect of Titan's atmosphere is the haze layer which may be considered as the destination of hydrocarbon and nitrile chemistry[9]. This thick haze layer mainly divided in to two regions which are known as main haze layer (below ~ 220km) and detached layer[68] (from 300 to 350km). Even though the exact mechanism for haze formation is still uncertain, there are very useful mechanisms of haze particle formation via polyyne formation[2, 5, 69], nitrile polymerization and polyaromatic hydrocarbon formation[70].

Considering the first mechanism, polymerization of C_2H_2 is the key for polyyne formation. After formation of C_2H via the photodissociation of C_2H_2, C_2H can react with another C_2H_2 molecule to form C_4H_2. This polymerization process will proceed till the formation of polyynes[71]

$$C_{2n}H_2 \ + \ C_2H \quad \longrightarrow \quad C_{2n+2}H_2 \ + \ H \qquad (n= 1,2,3..)$$

This chain lengthening process does not undergo one-dimensional polymerization. It automatically cyclizes and assists the nucleation of the soot particle[72] (figure 1.3-a).

At low temperature, the reactivity of polyacetylene radical decreases with the size. The relative size dependent rate constant of polyethynyl reaction can be described as follows[5].

$$k\,(C_{2n}H \ + \ X) \ = \ 3^{1-n}\,k\,(C_2H \ + \ X) \quad \text{where } X = \ H_2, CH_4, C_2H_2 \ldots$$

Considering Titan's atmospheric temperature and mixing ratios, there can be several key reactions for polyacetylene polymer formation in Titan's atmosphere[9].

$$C_6H_2 \ + \ C_4H \quad \longrightarrow \quad \text{PA-polymer}$$

$$C_6H_2 \ + \ C_6H \quad \longrightarrow \quad \text{PA-polymer}$$

$$C_8H_2 \ + \ C_2H \quad \longrightarrow \quad \text{PA-polymer}$$

$$C_8H_2 \ + \ C_4H \quad \longrightarrow \quad \text{PA-polymer}$$

$$C_8H_2 \ + \ C_6H \quad \longrightarrow \quad \text{PA-polymer}$$
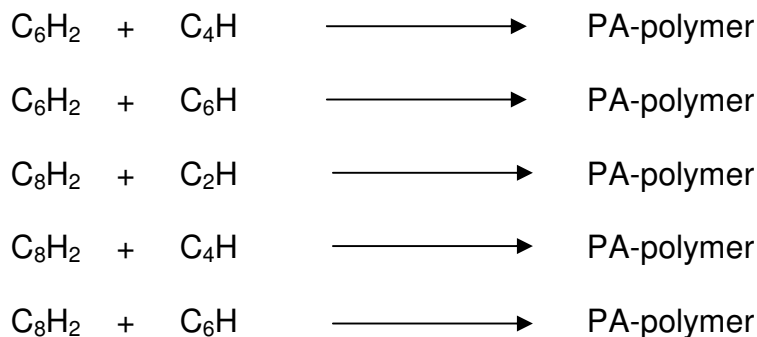
Polymerization of acetylene can lead to formation of polyaromatic Hydrocarbons PAH[9]. Benzene is the first member of this process. Benzene can undergo the
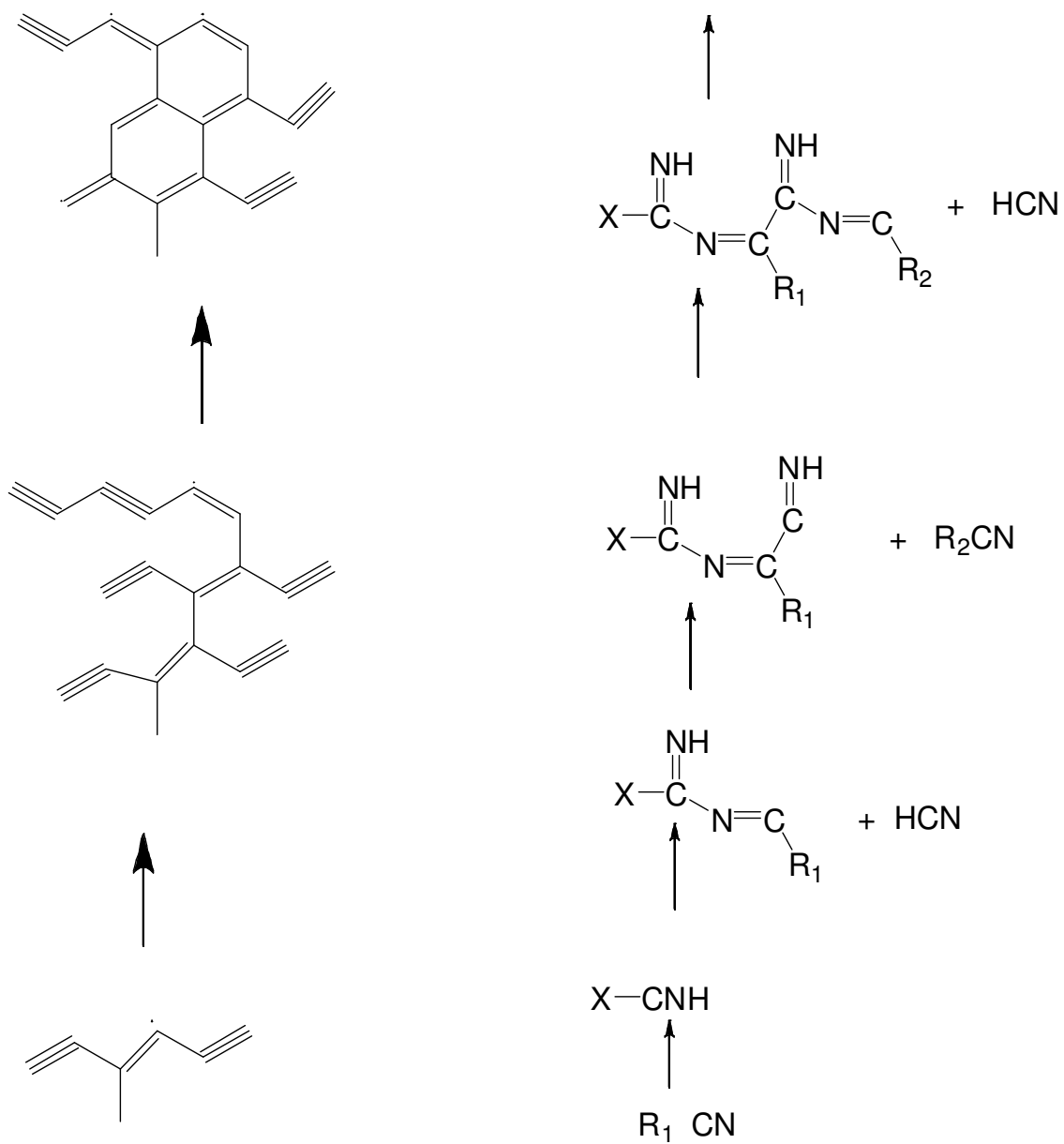
Figure 1.2 (a) cyclization of polyacetylene. (b) Attachment of RCN on to nitrile backbone[9].

reaction with enthynyl radical or phenyl radical can react with acetylene or another benzene molecule to form PAHs

$$C_6H_5 \quad + \quad C_2H_2 \quad \longrightarrow \quad \text{PAH-polymer}$$

$$C_6H_6 \quad + \quad C_2H \quad \longrightarrow \quad \text{PAH-polymer}$$

$$C_6H_5 \quad + \quad C_6H_6 \quad \longrightarrow \quad \text{PAH-polymer}$$
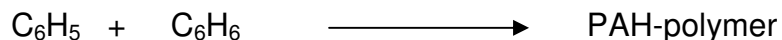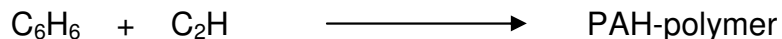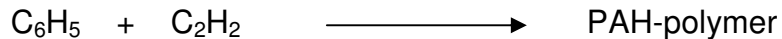
Nitrile polymerization can be initiated by the reaction of excited HCN molecule with another ground state HCN molecule to form HCN dimer[73]. This chain reaction can proceed until pure poly-HCN is formed.

$$^*HCN \quad + \quad HCN \quad \longrightarrow \quad (HCN)_2 \quad \longrightarrow \longrightarrow \longrightarrow \quad (HCN)_n$$
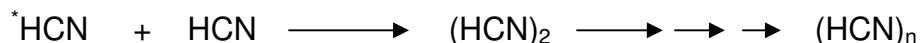
However, most possible nitrile polymerization in Titan's atmosphere requires a heterogeneity which can occur by the attachment of CN and RCN on to nitrile compounds[9] (Figure 1.3-b).

Laboratory studies have indicated that cyanoacetylene (HC_3N) can polymerize much faster than HCN does[74] and 2-5 times faster than C_2H_2[75]. Due to high reactivity of metastable states of HC_3N, it is very important to include copolymerization of $^*HC_3N$. The main reaction product can be written as follows.

$$HC_3N \quad + \quad h\nu \quad \longrightarrow \quad ^*HC_3N$$

$$^*HC_3N \quad + \quad C_2H_2 \quad \longrightarrow \quad \text{Co-polymer}$$

$$HC_3N \quad + \quad C_6H_5 \quad \longrightarrow \quad \text{Co-polymer}$$
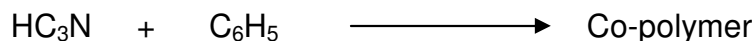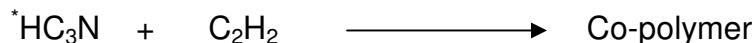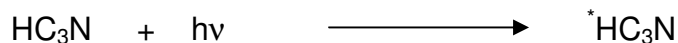
1.6 References

1. Wilson, E. H.; Atreya, S. K., Current state of modeling the photochemistry of Titan's mutually dependent atmosphere and ionosphere. *J. Geophys. Res.-Planets* **2004,** *109* (E6).

2. Toublanc, D.; Parisot, J. P.; Brillet, J.; Gautier, D.; Raulin, F.; McKay, C. P., Photochemical modeling of titans atmosphere. *Icarus* **1995,** *113* (1), 2-26.

3. Dandouras, I.; Garnier, P.; Mitchell, D. G.; Roelof, E. C.; Brandt, P. C.; Krupp, N.; Krimigis, S. M., Titan's exosphere and its interaction with Saturn's magnetosphere. *Philos. Trans. R. Soc. A-Math. Phys. Eng. Sci.* **2009,** *367* (1889), 743-752.

4. Coustenis, A.; Taylor, F. W., Titan: Exploring an Earthlike World (Series on Atmospheric, Oceanic and Planetary Physics) **2008**.

5. Yung, Y. L.; Allen, M.; Pinto, J. P., Photochemistry of the atmosphere of titan - comparison between model and observations. *Astrophysical Journal Supplement Series* **1984,** *55* (3), 465-506.

6. Raulin, F.; Owen, T., Organic chemistry and exobiology on Titan. *Space Science Reviews* **2002,** *104* (1-2), 377-394.

7. Niemann, H. B.; Atreya, S. K.; Bauer, S. J.; Carignan, G. R.; Demick, J. E.; Frost, R. L.; Gautier, D.; Haberman, J. A.; Harpold, D. N.; Hunten, D. M.; Israel, G.; Lunine, J. I.; Kasprzak, W. T.; Owen, T. C.; Paulkovich, M.; Raulin, F.; Raaen, E.; Way, S. H., The abundances of constituents of Titan's atmosphere

from the GCMS instrument on the Huygens probe. *Nature* **2005,** *438* (7069), 779-784.

8.   Coustenis, A.; Atreya, S. K.; Balint, T.; Brown, R. H.; Dougherty, M. K.; Ferri, F.; Fulchignoni, M.; Gautier, D.; Gowen, R. A.; Griffith, C. A.; Gurvits, L. I.; Jaumann, R.; Langevin, Y.; Leese, M. R.; Lunine, J. I.; McKay, C. P.; Moussas, X.; Muller-Wodarg, I.; Neubauer, F.; Owen, T. C.; Raulin, F.; Sittler, E. C.; Sohl, F.; Sotin, C.; Tobie, G.; Tokano, T.; Turtle, E. P.; Wahlund, J. E.; Waite, J. H.; Baines, K. H.; Blamont, J.; Coates, A. J.; Dandouras, I.; Krimigis, T.; Lellouch, E.; Lorenz, R. D.; Morse, A.; Porco, C. C.; Hirtzig, M.; Saur, J.; Spilker, T.; Zarnecki, J. C.; Choi, E.; Achilleos, N.; Amils, R.; Annan, P.; Atkinson, D. H.; Benilan, Y.; Bertucci, C.; Bezard, B.; Bjoraker, G. L.; Blanc, M.; Boireau, L.; Bouman, J.; Cabane, M.; Capria, M. T.; Chassefiere, E.; Coll, P.; Combes, M.; Cooper, J. F.; Coradini, A.; Crary, F.; Cravens, T.; Daglis, I. A.; de Angelis, E.; de Bergh, C.; de Pater, I.; Dunford, C.; Durry, G.; Dutuit, O.; Fairbrother, D.; Flasar, F. M.; Fortes, A. D.; Frampton, R.; Fujimoto, M.; Galand, M.; Grasset, O.; Grott, M.; Haltigin, T.; Herique, A.; Hersant, F.; Hussmann, H.; Ip, W.; Johnson, R.; Kallio, E.; Kempf, S.; Knapmeyer, M.; Kofman, W.; Koop, R.; Kostiuk, T.; Krupp, N.; Kuppers, M.; Lammer, H.; Lara, L. M.; Lavvas, P.; Le Mouelic, S.; Lebonnois, S.; Ledvina, S.; Li, J.; Livengood, T. A.; Lopes, R. M.; Lopez-Moreno, J. J.; Luz, D.; Mahaffy, P. R.; Mall, U.; Martinez-Frias, J.; Marty, B.; McCord, T.; Salvan, C.; Milillo, A.; Mitchell, D. G.; Modolo, R.; Mousis, O.; Nakamura, M.; Neish, C. D.; Nixon, C. A.; Mvondo, D.; Orton, G.; Paetzold, M.; Pitman, J.; Pogrebenko, S.; Pollard, W.;

Prieto-Ballesteros, O.; Rannou, P.; Reh, K.; Richter, L.; Robb, F. T.; Rodrigo, R.; Rodriguez, S.; Romani, P.; Bermejo, M.; Sarris, E. T.; Schenk, P.; Schmitt, B.; Schmitz, N.; Schulze-Makuch, D.; Schwingenschuh, K.; Selig, A.; Sicardy, B.; Soderblom, L.; Spilker, L. J.; Stam, D.; Steele, A.; Stephan, K.; Strobel, D. F.; Szego, K.; Szopa, C.; Thissen, R.; Tomasko, M. G.; Toublanc, D.; Vali, H.; Vardavas, I.; Vuitton, V.; West, R. A.; Yelle, R.; Young, E. F., TandEM: Titan and Enceladus mission. *Experimental Astronomy* **2009,** *23* (3), 893-946.

9.   Wilson, E. H.; Atreya, S. K., Chemical sources of haze formation in Titan's atmosphere. *Planetary and Space Science* **2003,** *51* (14-15), 1017-1033.

10.   Atreya, S. K.; Adams, E. Y.; Niemann, H. B.; Demick-Montelara, J. E.; Owen, T. C.; Fulchignoni, M.; Ferri, F.; Wilson, E. H., Titan's methane cycle. *Planetary and Space Science* **2006,** *54* (12), 1177-1187.

11.   Tomasko, M. G.; Archinal, B.; Becker, T.; Bezard, B.; Bushroe, M.; Combes, M.; Cook, D.; Coustenis, A.; de Bergh, C.; Dafoe, L. E.; Doose, L.; Doute, S.; Eibl, A.; Engel, S.; Gliem, F.; Grieger, B.; Holso, K.; Howington-Kraus, E.; Karkoschka, E.; Keller, H. U.; Kirk, R.; Kramm, R.; Kuppers, M.; Lanagan, P.; Lellouch, E.; Lemmon, M.; Lunine, J.; McFarlane, E.; Moores, J.; Prout, G. M.; Rizk, B.; Rosiek, M.; Rueffer, P.; Schroder, S. E.; Schmitt, B.; See, C.; Smith, P.; Soderblom, L.; Thomas, N.; West, R., Rain, winds and haze during the Huygens probe's descent to Titan's surface. *Nature* **2005,** *438* (7069), 765-778.

12.   Elachi, C.; Wall, S.; Allison, M.; Anderson, Y.; Boehmer, R.; Callahan, P.; Encrenaz, P.; Flamini, E.; Franceschetti, G.; Gim, Y.; Hamilton, G.; Hensley, S.;

Janssen, M.; Johnson, W.; Kelleher, K.; Kirk, R.; Lopes, R.; Lorenz, R.; Lunine, J.; Muhleman, D.; Ostro, S.; Paganelli, F.; Picardi, G.; Posa, F.; Roth, L.; Seu, R.; Shaffer, S.; Soderblom, L.; Stiles, B.; Stofan, E.; Vetrella, S.; West, R.; Wood, C.; Wye, L.; Zebker, H., Cassini radar views the surface of Titan. *Science* **2005,** *308* (5724), 970-974.

13.	Waite, J. H.; Niemann, H.; Yelle, R. V.; Kasprzak, W. T.; Cravens, T. E.; Luhmann, J. G.; McNutt, R. L.; Ip, W. H.; Gell, D.; De La Haye, V.; Muller-Wordag, I.; Magee, B.; Borggren, N.; Ledvina, S.; Fletcher, G.; Walter, E.; Miller, R.; Scherer, S.; Thorpe, R.; Xu, J.; Block, B.; Arnett, K., Ion Neutral Mass Spectrometer results from the first flyby of Titan. *Science* **2005,** *308* (5724), 982-986.

14.	Magni, G.; Coradini, A., Formation of Jupiter by nucleated instability. *Planetary and Space Science* **2004,** *52* (5-6), 343-360.

15.	Hersant, F.; Gautier, D.; Lunine, J. I., Enrichment in volatiles in the giant planets of the Solar System. *Planetary and Space Science* **2004,** *52* (7), 623-641.

16.	Hersant, F.; Gautier, D.; Tobie, G.; Lunine, J. I., Interpretation of the carbon abundance in Saturn measured by Cassini. *Planetary and Space Science* **2008,** *56* (8), 1103-1111.

17.	Alibert, Y.; Mousis, O., Formation of Titan in Saturn's subnebula: constraints from Huygens probe measurements. *Astronomy & Astrophysics* **2007,** *465* (3), 1051-1060.

18. Owen, T., *Phys-Usp* **2005,** *48*, 635-639.

19. Owen, T. C.; Niemann, H.; Atreya, S.; Zolotov, M. Y., Between heaven and Earth: the exploration of Titan. *Faraday Discuss.* **2006,** *133*, 387-391.

20. Israel, G.; Szopa, C.; Raulin, F.; Cabane, M.; Niemann, H. B.; Atreya, S. K.; Bauer, S. J.; Brun, J. F.; Chassefiere, E.; Coll, P.; Conde, E.; Coscia, D.; Hauchecorne, A.; Millian, P.; Nguyen, M. J.; Owen, T.; Riedler, W.; Samuelson, R. E.; Siguier, J. M.; Steller, M.; Sternberg, R.; Vidal-Madjar, C., Complex organic matter in Titan's atmospheric aerosols from in situ pyrolysis and analysis. *Nature* **2005,** *438* (7069), 796-799.

21. Atreya, S. K., Evolution of a nitrogen atmosphere on titan. *Science* **1978,** *201*, 611.

22. McKay, C. P.; Pollack, J. B.; Courtin, R., The thermal structure of titans atmosphere. *Icarus* **1989,** *80* (1), 23-53.

23. Tobie, G.; Lunine, J. I.; Sotin, C., Episodic outgassing as the origin of atmospheric methane on Titan. *Nature* **2006,** *440* (7080), 61-64.

24. Lorenz, R. D.; Lunine, J. I.; Withers, P. G.; McKay, C. P., Titan, Mars and Earth: Entropy production by latitudinal heat transport. *Geophys. Res. Lett.* **2001,** *28* (3), 415-418.

25. Clarke, D. W.; Ferris, J. P., Chemical evolution on Titan: Comparisons to the prebiotic earth. *Orig. Life Evol. Biosph.* **1997,** *27* (1-3), 225-248.

26. Matthews, C. N.; Minard, R. D., Hydrogen cyanide polymers, comets and the origin of life. *Faraday Discuss.* **2006,** *133*, 393-401.

27.   Nguyen, M. J.; Raulin, F.; Coll, P.; Derenne, S.; Szopa, C.; Cernogora, G.; Israel, G.; Bernard, J. M., Carbon isotopic enrichment in Titan's tholins? Implications for Titan's aerosols. *Planetary and Space Science* **2007,** *55* (13), 2010-2014.

28.   Waite, J. H.; Young, D. T.; Cravens, T. E.; Coates, A. J.; Crary, F. J.; Magee, B.; Westlake, J., The process of tholin formation in Titan's upper atmosphere. *Science* **2007,** *316* (5826), 870-875.

29.   Atreya, S. K., Atmospheres and ionospheres of the outer planets and their satellites. **1986**, 183-186.

30.   Atreya, S., Titan's organic factory. *Science* **2007,** *316* (5826), 843-845.

31.   Raulin, F., Astrobiology and habitability of Titan. *Space Science Reviews* **2008,** *135* (1-4), 37-48.

32.   Khare, B. N.; Sagan, C.; Ogino, H.; Nagy, B.; Er, C.; Schram, K. H.; Arakawa, E. T., Amino-acids derived from titan tholins. *Icarus* **1986,** *68* (1), 176-184.

33.   Raulin, F.; Nguyen, M. J.; Coll, P., Titan: an astrobiological laboratory in the solar system - art. no. 66940L. In *Instruments, Methods, and Missions for Astrobiology X*, Hoover, R. B.; Levin, G. V.; Rozanov, A. Y.; Davies, P. C. W., Eds. Spie-Int Soc Optical Engineering: Bellingham, 2007; Vol. 6694, pp L6940-L6940.

34.   Lebonnois, S.; Rannou, P.; Hourdin, F., The coupling of winds, aerosols and chemistry in Titan's atmosphere. *Philos. Trans. R. Soc. A-Math. Phys. Eng. Sci.* **2009,** *367* (1889), 665-682.

35.   Sotin, C.; Jaumann, R.; Buratti, B. J.; Brown, R. H.; Clark, R. N.; Soderblom, L. A.; Baines, K. H.; Bellucci, G.; Bibring, J. P.; Capaccioni, F.; Cerroni, P.; Combes, M.; Coradini, A.; Cruikshank, D. P.; Drossart, P.; Formisano, V.; Langevin, Y.; Matson, D. L.; McCord, T. B.; Nelson, R. M.; Nicholson, P. D.; Sicardy, B.; LeMouelic, S.; Rodriguez, S.; Stephan, K.; Scholz, C. K., Release of volatiles from a possible cryovolcano from near-infrared imaging of Titan. *Nature* **2005,** *435* (7043), 786-789.

36.   Barnes, J. W.; Brown, R. H.; Soderblom, L.; Buratti, B. J.; Sotin, C.; Rodriguez, S.; Le Mouelic, S.; Baines, K. H.; Clark, R.; Nicholson, P., Global-scale surface spectral variations on Titan seen from Cassini/VIMS. *Icarus* **2007,** *186* (1), 242-258.

37.   McCord, T. B.; Hansen, G. B.; Buratti, B. J.; Clark, R. N.; Cruikshank, D. P.; D'Aversa, E.; Griffith, C. A.; Baines, E. H.; Brown, R. H.; Ore, C. M. D.; Filacchione, G.; Formisano, V.; Hibbitts, C. A.; Jaumann, R.; Lunine, J. I.; Nelson, R. M.; Sotin, C.; Team, V., Composition of Titan's surface from Cassini VIMS. *Planetary and Space Science* **2006,** *54* (15), 1524-1539.

38.   Lorenz, R. D.; Wood, C. A.; Lunine, J. I.; Wall, S. D.; Lopes, R. M.; Mitchell, K. L.; Paganelli, F.; Anderson, Y. Z.; Wye, L.; Tsai, C.; Zebker, H.;

Stofan, E. R., Titan's young surface: Initial impact crater survey by Cassini RADAR and model comparison. *Geophys. Res. Lett.* **2007,** *34* (7).

39.   Stofan, E. R.; Elachi, C.; Lunine, J. I.; Lorenz, R. D.; Stiles, B.; Mitchell, K. L.; Ostro, S.; Soderblom, L.; Wood, C.; Zebker, H.; Wall, S.; Janssen, M.; Kirk, R.; Lopes, R.; Paganelli, F.; Radebaugh, J.; Wye, L.; Anderson, Y.; Allison, M.; Boehmer, R.; Callahan, P.; Encrenaz, P.; Flamini, E.; Francescetti, G.; Gim, Y.; Hamilton, G.; Hensley, S.; Johnson, W. T. K.; Kelleher, K.; Muhleman, D.; Paillou, P.; Picardi, G.; Posa, F.; Roth, L.; Seu, R.; Shaffer, S.; Vetrella, S.; West, R., The lakes of Titan. *Nature* **2007,** *445* (7123), 61-64.

40.   Vinatier, S.; Bezard, B.; Fouchet, T.; Teanby, N. A.; de Kok, R.; Irwin, P. G. J.; Conrath, B. J.; Nixon, C. A.; Romani, P. N.; Flasar, E. M.; Coustenis, A., Vertical abundance profiles of hydrocarbons in Titan's atmosphere at 15 degrees S and 80 degrees N retrieved from Cassini/CIRS spectra. *Icarus* **2007,** *188* (1), 120-138.

41.   Sittler, E. C.; Hartle, R. E.; Johnson, R. E.; Cooper, J. F.; Lipatov, A. S.; Bertucci, C.; Coates, A. J.; Szego, K.; Shappirio, M.; Simpson, D. G.; Wahlund, J. E., Saturn's magnetospheric interaction with Titan as defined by Cassini encounters T9 and T18: New results. *Planetary and Space Science* **2010,** *58* (3), 327-350.

42.   Coates, A. J.; Crary, F. J.; Lewis, G. R.; Young, D. T.; Waite, J. H.; Sittler, E. C., Discovery of heavy negative ions in Titan's ionosphere. *Geophys. Res. Lett.* **2007,** *34* (22).

43. Krimigis, S. M.; Mitchell, D. G.; Hamilton, D. C.; Livi, S.; Dandouras, J.; Jaskulek, S.; Armstrong, T. P.; Boldt, J. D.; Cheng, A. F.; Gloeckler, G.; Hayes, J. R.; Hsieh, K. C.; Ip, W. H.; Keath, E. P.; Kirsch, E.; Krupp, N.; Lanzerotti, L. J.; Lundgren, R.; Mauk, B. H.; McEntire, R. W.; Roelof, E. C.; Schlemm, C. E.; Tossman, B. E.; Wilken, B.; Williams, D. J., Magnetosphere imaging instrument (MIMI) on the Cassini mission to Saturn/Titan. *Space Science Reviews* **2004,** *114* (1-4), 233-329.

44. Mitchell, D. G.; Brandt, P. C.; Roelof, E. C.; Dandouras, J.; Krimigis, S. M.; Mauk, B. H., Energetic neutral atom emissions from Titan interaction with Saturn's magnetosphere. *Science* **2005,** *308* (5724), 989-992.

45. Flasar, F. M.; Achterberg, R. K.; Conrath, B. J.; Gierasch, P. J.; Kunde, V. G.; Nixon, C. A.; Bjoraker, G. L.; Jennings, D. E.; Romani, P. N.; Simon-Miller, A. A.; Bezard, B.; Coustenis, A.; Irwin, P. G. J.; Teanby, N. A.; Brasunas, J.; Pearl, J. C.; Segura, M. E.; Carlson, R. C.; Mamoutkine, A.; Schinder, P. J.; Barucci, A.; Courtin, R.; Fouchet, T.; Gautier, D.; Lellouch, E.; Marten, A.; Prange, R.; Vinatier, S.; Strobel, D. F.; Calcutt, S. B.; Read, P. L.; Taylor, F. W.; Bowles, N.; Samuelson, R. E.; Orton, G. S.; Spilker, L. J.; Owen, T. C.; Spencer, J. R.; Showalter, M. R.; Ferrari, C.; Abbas, M. M.; Raulin, F.; Edgington, S.; Ade, P.; Wishnow, E. H., Titan's atmospheric temperatures, winds, and composition. *Science* **2005,** *308* (5724), 975-978.

46. McKay, C. P.; Pollack, J. B.; Courtin, R., The greenhouse and antigreenhouse effects on titan. *Science* **1991,** *253* (5024), 1118-1121.

47.   Coustenis, A.; Achterberg, R. K.; Conrath, B. J.; Jennings, D. E.; Marten, A.; Gautier, D.; Nixon, C. A.; Flasar, F. M.; Teanby, N. A.; Bezard, B.; Samuelson, R. E.; Carlson, R. C.; Lellouch, E.; Bjoraker, G. L.; Romani, P. N.; Taylor, F. W.; Irwin, P. G. J.; Fouchet, T.; Hubert, A.; Orton, G. S.; Kunde, V. G.; Vinatier, S.; Mondellini, J.; Abbas, M. M.; Courtin, R., The composition of Titan's stratosphere from Cassini/CIRS mid-infrared spectra. *Icarus* **2007,** *189* (1), 35-62.

48.   Lebonnois, S.; Toublanc, D.; Hourdin, F.; Rannou, P., Seasonal variations of Titan's atmospheric composition. *Icarus* **2001,** *152* (2), 384-406.

49.   Cui, J.; Yelle, R. V.; Vuitton, V.; Waite, J. H.; Kasprzak, W. T.; Gell, D. A.; Niemann, H. B.; Muller-Wodarg, I. C. F.; Borggren, N.; Fletcher, G. G.; Patrick, E. L.; Raaen, E.; Magee, B. A., Analysis of Titan's neutral upper atmosphere from Cassini Ion Neutral Mass Spectrometer measurements. *Icarus* **2008,** *200* (2), 581-615.

50.   Tokano, T.; McKay, C. P.; Neubauer, F. M.; Atreya, S. K.; Ferri, F.; Fulchignoni, M.; Niemann, H. B., Methane drizzle on Titan. *Nature* **2006,** *442* (7101), 432-435.

51.   Griffith, C. A.; Penteado, P.; Baines, K.; Drossart, P.; Barnes, J.; Bellucci, G.; Bibring, J.; Brown, R.; Buratti, B.; Capaccioni, F.; Cerroni, P.; Clark, R.; Combes, M.; Coradini, A.; Cruikshank, D.; Formisano, V.; Jaumann, R.; Langevin, Y.; Matson, D.; McCord, T.; Mennella, V.; Nelson, R.; Nicholson, P.;

Sicardy, B.; Sotin, C.; Soderblom, L. A.; Kursinski, R., The evolution of Titan's mid-latitude clouds. *Science* **2005,** *310* (5747), 474-477.

52.   Rannou, P.; Montmessin, F.; Hourdin, F.; Lebonnois, S., The latitudinal distribution of clouds on Titan. *Science* **2006,** *311* (5758), 201-205.

53.   Coustenis, A.; Bezard, B.; Gautier, D.; Marten, A.; Samuelson, R., Titans atmosphere from voyager infrared observations .3. Vertical distributions of hydrocarbons and nitriles near titans north-pole. *Icarus* **1991,** *89* (1), 152-167.

54.   Lebreton, J. P.; Witasse, O.; Sollazzo, C.; Blancquaert, T.; Couzin, P.; Schipper, A. M.; Jones, J. B.; Matson, D. L.; Gurvits, L. I.; Atkinson, D. H.; Kazeminejad, B.; Perez-Ayucar, M., An overview of the descent and landing of the Huygens probe on Titan. *Nature* **2005,** *438* (7069), 758-764.

55.   Schulze-Makuch, D.; Grinspoon, D. H., Biologically enhanced energy and carbon cycling on Titan? *Astrobiology* **2005,** *5* (4), 560-567.

56.   Strobel, D. F.; Shemansky, D. E., EUV emission from titans upper-atmosphere - voyager-1 encounter. *J. Geophys. Res-Space Phys.* **1982,** *87* (NA3), 1361-1368.

57.   Yung, y. L., fixation of nitrogen in the prebiotic atmosphere. *Science* **1979,** *203*, 1002.

58.   Messing, I.; Filseth, S. V.; Sadowski, C. M.; Carrington, T., Absolute rate constants for the reactions of CH with O and N atoms. *J. Chem. Phys.* **1981,** *74* (7), 3874-3881.

59. Slanger, T. G.; Black, G., Photodissociative channels at 1216 a for H_2O, NH_3, and CH_4. *J. Chem. Phys.* **1982,** *77* (5), 2432-2437.

60. Laufer, A. H., Photolysis of methane at 1236-a - quantum yield of hydrogen formation. *J. Chem. Phys.* **1968,** *49*, 2272.

61. Gorden, R., Gas-phase photolysis and radiolysis of methane . Formation of hydrogen and ethylene. *J. Chem. Phys.* **1967,** *46*, 4823.

62. Ashfold, M. N. R.; Hancock, G.; Ketley, G. W.; Minshullbeech, J. P., DIrect measurements of a A-1(1) CH_2 removal rates. *Journal of Photochemistry* **1980,** *12* (1), 75-83.

63. Laufer, A. H., Reactions of ethynyl radicals - rate constants with CH_4, C_2H_6, and C_2D_6. *J. Phys. Chem.* **1981,** *85* (25), 3828-3831.

64. Becker, R. S.; Hong, J. H., Photochemistry of acetylene, hydrogen-cyanide, and mixtures. *J. Phys. Chem.* **1983,** *87* (1), 163-166.

65. Okabe, H., Photochemistry of acetylene at 1470 A. *J. Chem. Phys.* **1981,** *75* (6), 2772-2778.

66. DeMore, W. B., *JPL PUB* **1982**, 8257.

67. Fenimore, C. P., *12TH S Int comb pitt* **1969**, 463.

68. Rages, K.; Pollack, J. B., Vertical-distribution of scattering hazes in titan upper-atmosphere. *Icarus* **1983,** *55* (1), 50-62.

69. Lara, L. M.; Lellouch, E.; LopezMoreno, J. J.; Rodrigo, R., Vertical distribution of Titan's atmospheric neutral constituents. *J. Geophys. Res.-Planets* **1996,** *101* (E10), 23261-23283.

70.   Coustenis, A.; Salama, A.; Schulz, B.; Ott, S.; Lellouch, E.; Encrenaz, T.; Gautier, D.; Feuchtgruber, H., Titan's atmosphere from ISO mid-infrared spectroscopy. *Icarus* **2003,** *161* (2), 383-403.

71.   Allen, M.; Pinto, J. P.; Yung, Y. L., Titan - aerosol photochemistry and variations related to the sunspot cycle. *Astrophys. J.* **1980,** *242* (2), L125-L128.

72.   Krestinin, A. V., Detailed modeling of soot formation in hydrocarbon pyrolysis. *Combust. Flame* **2000,** *121* (3), 513-524.

73.   Rettig, T. W.; Tegler, S. C.; Pasto, D. J.; Mumma, M. J., Comet outbursts and polymers of HCN. *Astrophys. J.* **1992,** *398* (1), 293-298.

74.   Scattergood, T. W.; Lau, E. Y.; Stone, B. M., Titans aerosols .1. Laboratory investigations of shapes, size distributions, and aggregation of particles produced by uv photolysis of model titan atmospheres. *Icarus* **1992,** *99* (1), 98-105.

75.   Clarke, D. W.; Ferris, J. P., Mechanism of cyanoacetylene photochemistry at 185 and 254 nm. *J. Geophys. Res.-Planets* **1996,** *101* (E3), 7575-7584.

Chapter 2

Experimental Overview

2.1   Introduction

Information and measurements from the Cassini/Huygens mission have provided a profound understanding of Titan's atmosphere and its chemistry[1,2,3]. In addition, many laboratory based experiments aimed at understanding the astrochemical problems or observations have been emerged in parallel to the Cassini/Huygens measurements. However, most of these laboratory studies, which are largely dominated by spectroscopic based methods, were done only to support astronomical observation. In the recent years, direct laboratory simulation and modeling techniques of Titan's atmosphere and haze formation have rapidly developed due to the availability of new, detailed information[4,5]. However, for modeling of Titan's atmosphere, it is very crucial to have a large network of elementary reactions with known rate constants at relevant temperatures. Experimental methods that are employed in obtaining kinetics data at appropriate temperatures[6,7,8] and exploring photochemical products in single collision environments[9,10,11] are now being used in modeling studies.

A major objective of recent studies of Titan is to understand the chemical dynamics of Titan's atmosphere[12] since the gross chemical composition is already well understood. Photodissociation is the key step of all chemical dynamics of Titan's atmosphere. Therefore, studying of the photodissociation dynamics of the elementary chemical constituents of Titan under extreme environments is important in obtaining precise measurements that in turn can be used in modeling of Titan's atmosphere.

The DC slice imaging technique, which is described in detail next, is a very powerful method to study chemical dynamics under collisionless environments and low temperatures as in Titan. The other advantage of employing the DC slice imaging technique is to study photodissociation dynamics relevant to Titan to obtain translational energy distributions and angular distribution of the desired product. These studies will be important in obtaining a better understanding of the Titan's atmosphere and for current modeling studies. The main focus of this chapter is to give an overview of the instrumentation of the imaging techniques that are either employed or provided a basis for the current studies of the constituents of Titan's atmosphere under collisionless conditions.

2.2   Ion Imaging

Ion imaging is a prevailing and powerful method of studying photodissociation dynamics or reactive scattering[13]. This fascinating method was

first developed by Chandler and Houston in 1987 and used to measure photodissociation dynamics of methyl iodide[1]. The major components of the ion imaging instrumentation consist of Wiley-McLaren time-of-flight (TOF) mass spectrometer with a repeller electrode and a grounded grid, a two-dimensional (2D) position-sensitive detector, a microchannel plate (MCP) coupled to a fast phosphor screen and a charge coupled device (CCD) camera. In this technique, one of the fragments of photodissociation event can be ionized by a probe laser, and the produced ion cloud is accelerated by the repeller electrode. This accelerated ion cloud moves in the Wiley-McLaren TOF tube towards the MCP detector. MCP detector is coupled to a phosphor screen to produce visible ion spots, which can be viewed by CCD camera. At the detector, the three-dimensional ion cloud is flattened, resulting in a two dimensional ion image. To reconstruct the 3D photofragment ion distribution from the 2D photofragment projection, mathematical methods such as inverse Abel transformation are employed. After obtaining the 3D ion distribution, the central section of interest can be isolated for further studies. The velocity and internal energy distribution of photodissociated fragments can be obtained from the images. The velocity of the photo fragment is calculated by dividing the distance of the ion spot from the center of the image by the time of flight of the ion. Then, the internal energy of the ion can be determined by using conservation of energy and momentum. This technique is also very powerful in obtaining total translational energy and angular

distributions for a photodissociation event, and has been subjected to continuing improvements.

2.3   Velocity map imaging

In 1997, Eppink and Parker[14] significantly improved the ion imaging technique and achieved a great success by introducing a high resolution velocity map imaging technique (VMI). In VMI, the velocity resolution was improved almost one order of magnitude. The major difference of the velocity map imaging technique over ion imaging is the removal of the grid of the Wiley-McLaren setup and its replacement by focusing elements. The replacement of grids with an additional extractor electrode focuses the ions with same velocity at nearly the same point on the detector regardless of their origin position. Figure 2.1 is a schematic representation of typical ion imaging apparatus with velocity mapping ion optics. This setup includes a pulsed molecular beam source, ion optics, imaging detector, and data acquisition unit.

Although the VMI technique achieved a greater success in obtaining high resolution velocity images over other techniques, it is not without limitations. The major drawback of VMI method is the presence of artificial noise on the symmetry axis due the image reconstruction methods. The imaging method inevitably uses numerical inversion techniques such as the inverse Abel transform to reconstruct the velocity distribution from the images. This is indeed

important as imaging techniques always project the three dimensional ion sphere onto the two dimensional detector. The artificial noise arising from image reconstruction leads to poor resolution of translational energy distribution and angular distribution. Moreover, these reconstruction methods are only valid if the experiment has an axis of cylindrical symmetry parallel to the detector plane. Images that do not possess a cylindrical symmetry axis parallel to the imaging plane cannot be transformed to 3D distribution using these mathematical methods[15]. This drawback definitely affects the experiments that use two different lasers with different polarizations. One such an example is studying the orientation and alignment effects of photofragments using a pump-probe strategy. Therefore, an alternative to the VMI was long needed and the one approach to look was the way to find a method to detect only the fragment that has no velocity component along the time of flight axis.

2.4   Direct Current (DC) Sliced Imaging

A slicing technique has been introduced to detect the quantity of interest - the velocity distribution in the plane parallel to the detector – directly. The characteristic feature of this technique is the direct detection of central slice of the 3D photofragment distribution. A related approach was first proposed by Tonokura and Suzuki[16] who used "laser sheet" ionization with a cylindrical lens to probe a slice of a neutral fragment sphere. Kisopoulos and co-workers[17]
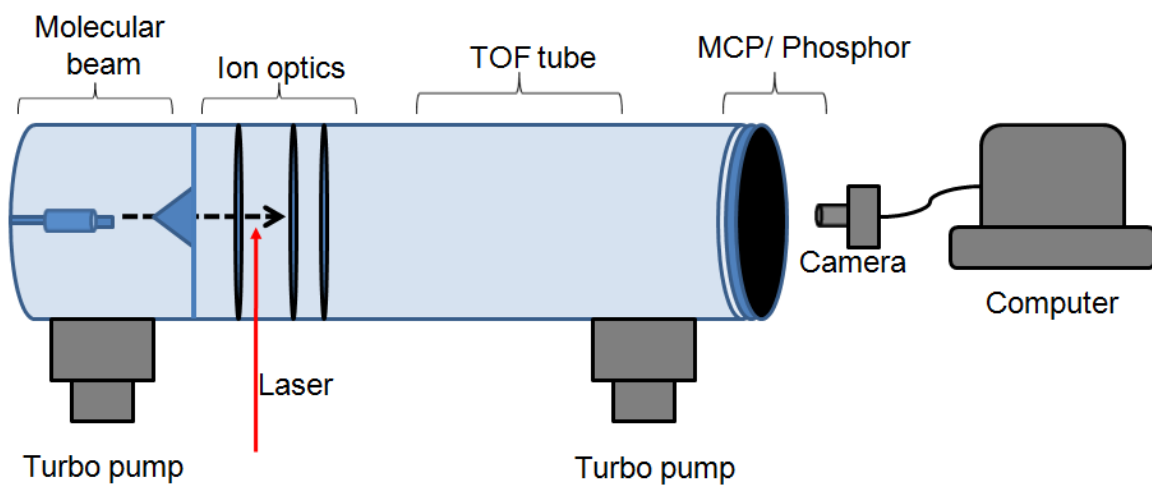
Figure 2.1 Schematic instrumentation setup of Ion imaging with conventional velocity mapping ion optics

recently developed the technique by applying a pulsed electric field to the expanded ion fragments. Introduction of short period of field free expansion to the ion cloud facilitates the spatial expansion of the ion cloud at the detector region. Then, the central section of this ion cloud could be detected exclusively with a narrow time gate at the imaging detector due to the expansion of the ion cloud. A major benefit of slice imaging technique is that the total translational and angular distribution can be obtained directly without applying any mathematical construction methods such as the inverse Abel transformation or complex forward convolution methods. Furthermore, it can be used in any type of systems of interest that have a wide range of photofragment kinetic energy.

This pulsed slice technique, however, has to compromise velocity focusing of the VMI technique, so that offers limited resolution. This drawback can be overcome by introducing multilens velocity mapping ion optics at low voltages without using a mesh grid[15] (no pulsed field).

The Direct current (DC) slice imaging technique was developed by the Suits group as an alternative approach to overcome the limitations associated with previous methods. In this method, a spread of ion cloud is obtained by using a very low repeller voltage. The momentum focusing is then achieved by maintaining the precise voltage ratio which is applied to the repeller and extractor lenses, and adding an additional lens element. This technique does not employ grids or pulsed electric fields, which distort the ion cloud. The important features in DC slice imaging technique are represented in Figure 2.2. In this figure, it
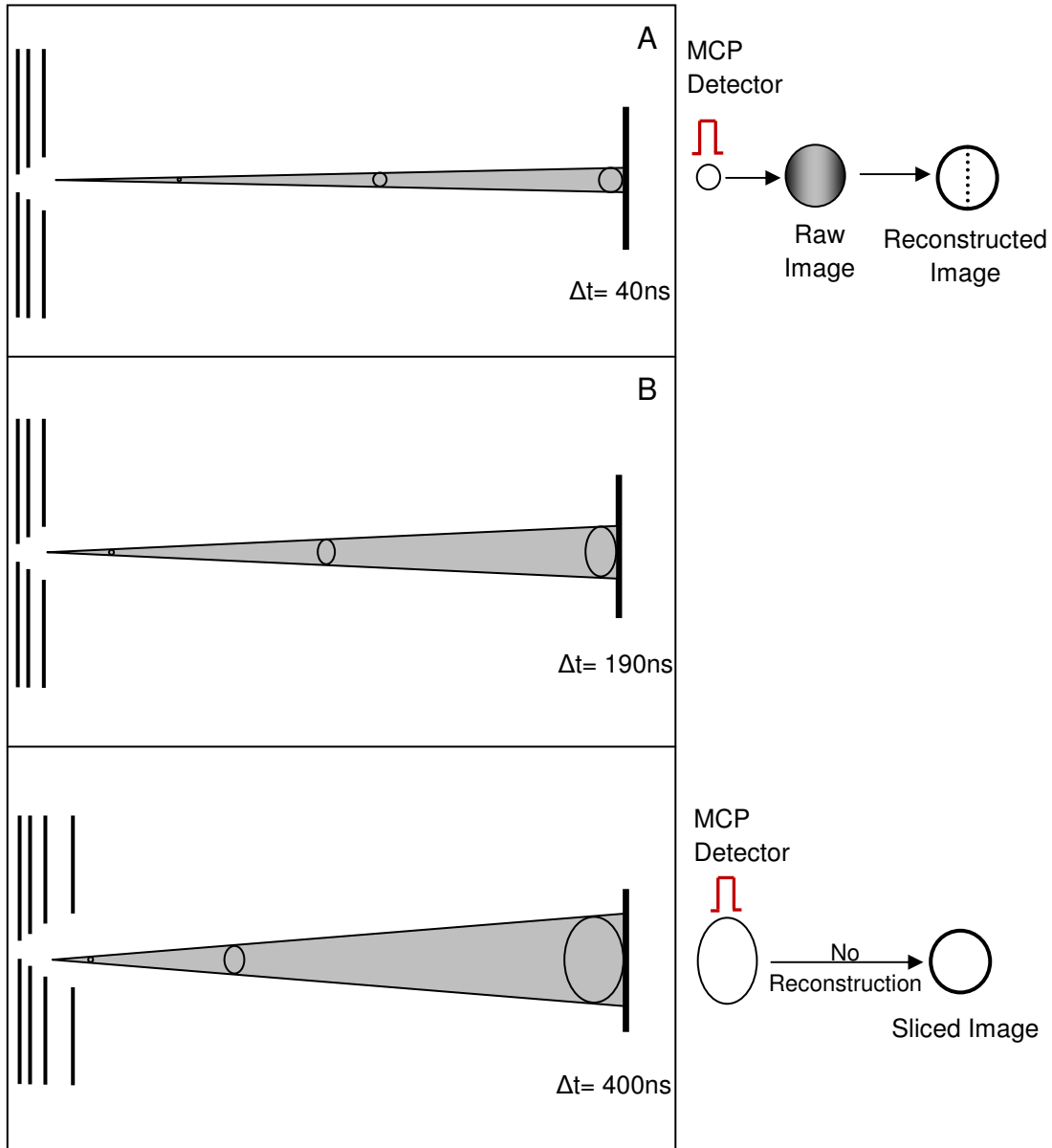
Figure 2.2 Schematic illustration of the simulated expansion of the photofragment ion cloud at 1.5 µs Intervals (Adapted from reference 15).

clearly illustrates the expansion of an isotropic ion cloud through the time-of-flight axis. A conventional velocity mapping condition is shown in Figure 2.2 A. In this instance, the ion cloud is detected within a short temporal spread (40 ns) by the MCP. As stated previously, the expansion of the ion cloud can be achieved by decreasing the repeller voltage, which is shown in Figure 2.2 B. The extent of reducing voltage of repeller is restricted due to the loss of the focus. However, this can be overcome by introducing an additional ion optic. Figure 2.2 C shows the use of two focusing lenses to adequately stretch the ion sphere, which in turn increases the arrival time width. This is very important for detecting the central slice of ion cloud through a narrow gate at the detector. Notably, this technique was used in many experiments performed in Suits research group and is the central to the work in this thesis. Also, this technique has many similarities to the "3D" imaging method, which was separately developed by K. Liu et al[18].

Figure 2.3 is a schematic representation of the components of the experimental setup of DC slice imaging, which was used in our studies of molecules relevant to Titan's atmosphere. A molecular beam seeded in either argon or helium is expanded supersonically into the source chamber. This was achieved through a pulsed nozzle operating at 10/30 Hz and a backing pressure of 3 atm. After it travels through a skimmer (1.0 mm diameter), the collimated beam arrives the velocity mapping electrode assembly, which has been optimized for DC slice imaging. Then it is intersected at 90^0 by two counter-propagating lasers. After ionization of photodissociated fragments by the probe laser, the ion sphere

CCD Camera/ PMT

MCP/ Phosphor
Detector

Flight Tube

L_3

L_2

Probe Laser

L_1

V_R

Photolysis and
Probe Laser

Skimmer

Pulsed Valve

.
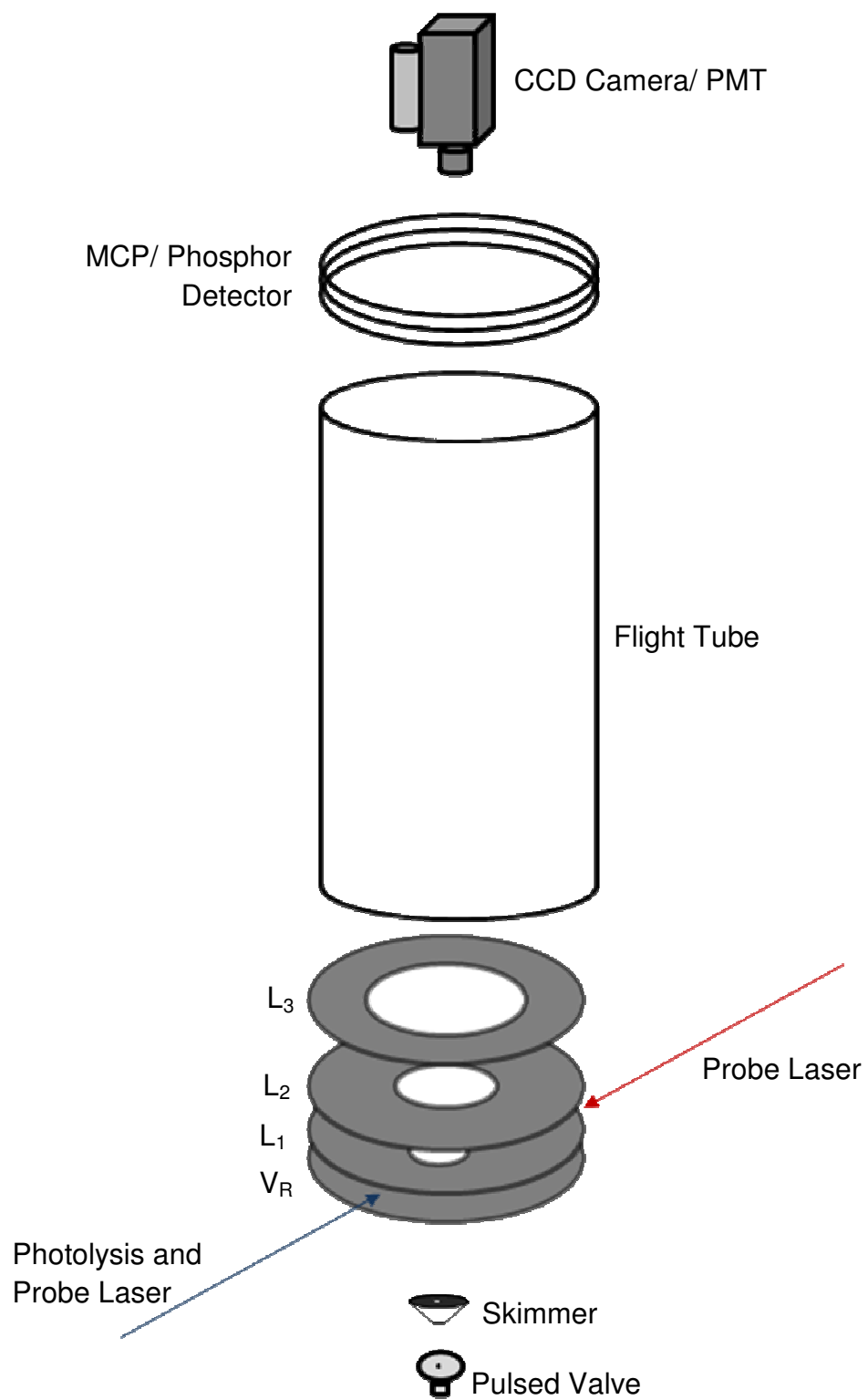
Figure 2.3 Schematic of experimental apparatus for DC slice imaging

moves along the time of flight tube. Next this ion cloud impacts onto a MCP array of 75 or 120 mm diameter. The MCP array is then coupled to a P-47 phosphor screen to give the ion spot signal. Then a narrow (40 ns) time gate at the detector was used to obtain the central slice of the distribution. Finally, a CCD camera and a photomultiplier tube (PMT) were used to record the resulting signal with the help of IMACQ Megapixel acquisition program[19] .

As mentioned previously, this was the experimental setup that was used extensively for our studies and the experimental set up for chapters 3, 4 and 5. In addition, for the use of our study of photodissociation of Titan's atmospheric constituents, Two Color Reduced Doppler method was employed as a reliable and convenient probing strategy, especially in H atom detection

2.5   Two Color Reduced Doppler (TCRD) technique

Doppler free multi photon spectroscopic methods were first introduced in the 1970s[20,21,22,23] for gas phase spectroscopy. Since then, this technique has been extensively used as a versatile method for ionization and detection in various high resolution gas phase spectroscopic studies[24,25,26,27,28]. In this method, the Doppler width of a photofragment is eliminated by absorbing one photon from each of two counter propagating, equal frequency laser beams. Previously, Doppler free methods have extensively been used in absorption spectroscopic studies. Interestingly, It has been recently shown that the Doppler

free method can also be used in resonance enhance multiphoton ionization (REMPI) spectroscopy to obtain a high signal to noise ratio and a ultrasensitive detection efficiency[29]. This higher sensitivity is mainly due to the simultaneous resonance of all of the species in the probe volume. In this technique, two counterpropagating laser lights with a very narrow line width are precisely fixed at the center of the absorption line. This counterpropagating two laser beams can be produced by splitting a parent laser beam and then directing them around the apparatus to obtain the Doppler free effect. Following to those Doppler free REMPI studies, a pioneering work on ion imaging using Doppler free REMPI was done for H atom[30]. In this work, two circular polarized laser beams have been employed to eliminate the one color signal from each laser. This approach offers improved sensitivity and higher signal to noise ratio in imaging studies. However, the major drawback of this method is the presence of background one laser signal.

Two Color Reduced Doppler (TCRD) technique was developed by Suits group as an alternative approach for obtaining same benefits as in Doppler free technique. The major advantage of this method over the Doppler free REMPI is the elimination of one color background signal. Here, two different laser lights are counterpropagated to achieve the resonance transition to excited state of the probing system. The sum of the two wave vectors of each counter propagating laser beams determines the Doppler reduction of the transition, which is not zero as in Doppler free strategy. However, the Doppler width is significantly reduced

compared to normal Doppler-limited 2+1 REMPI, where a single beam is used to absorb two photons to achieve the resonance transition. Our research group has extensively employed TCRD technique to probe Hydrogen atom, which is shown in figure 2.4. In this technique, parent molecule can absorb the shorter wavelength light and undergoes photodissociation. In most instances, longer wavelength light is chosen such that it is transparent to the parent molecule. Then the fragment, which we need to probe, is resonantly excited to a higher excited state by the absorption of a photon from each counter propagating laser beam. Then it can be ionized by absorbing another photon from either of two laser beam. To give a better understanding of this technique, a theoretical explanation behind TCRD is summarized below.

An atom or a molecule with the velocity of **v** in a laser field of a frequency ω_{laser} can detect the relative frequency of ω which can be written in the equation given below[31].

$$\omega = \omega_{laser} - \mathbf{k}.\mathbf{v} \qquad \text{where } \mathbf{k} \text{ is the wave vector}$$

In two color experiment, if the transition involves one photon from each laser beam, then the resonance transition can be obtained from the equation given below.

$$\omega_1 + \omega_2 = \omega_{laser1} + \omega_{laser2} - (\mathbf{k_1} + \mathbf{k_2}).\mathbf{v}$$
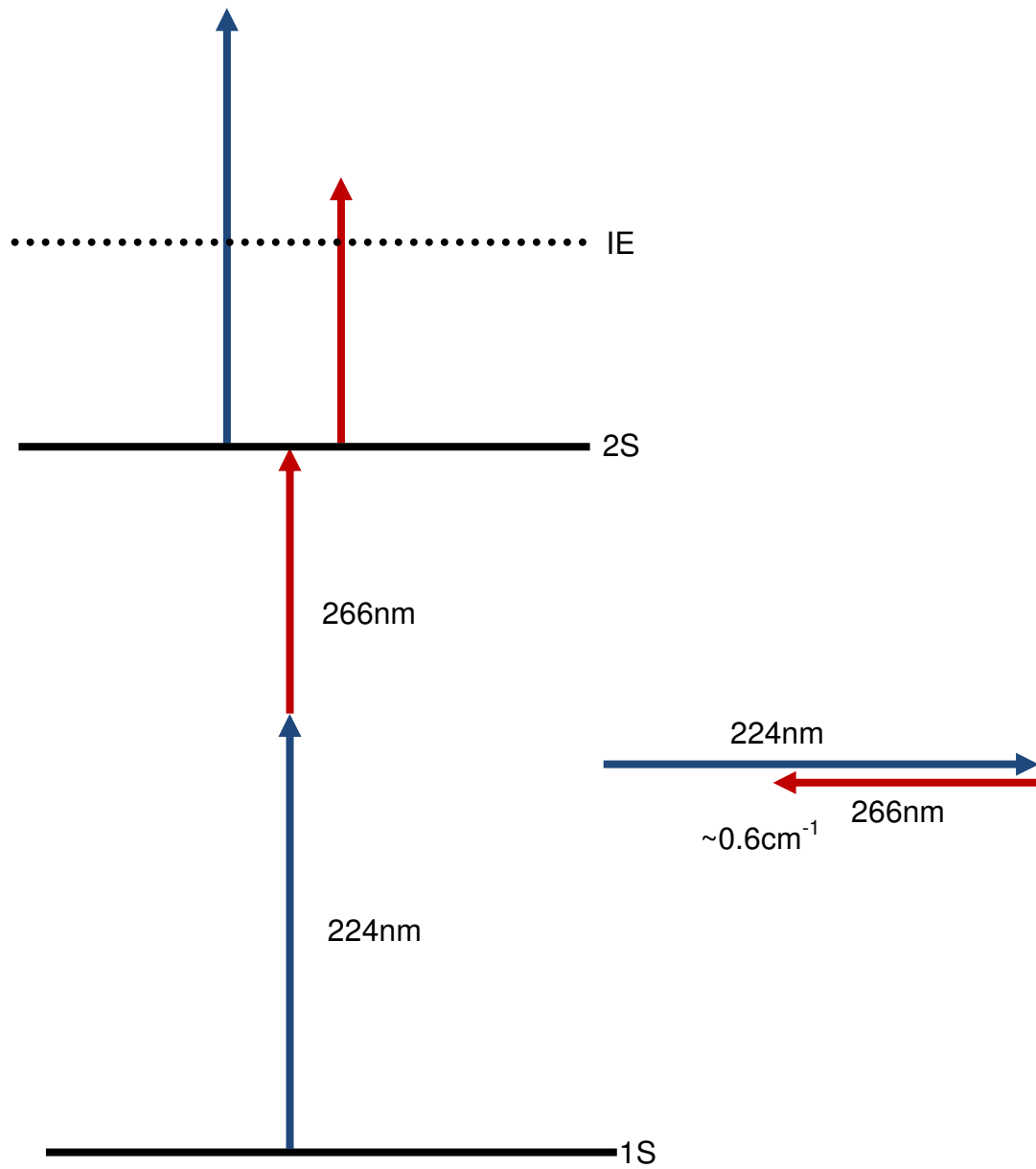
Figure 2.4 Scheme of the Two Color Reduced Doppler REMPI probe (Adapter from reference 31)

In Doppler free condition, k_1 and k_2 have the same magnitude but different sign, which cancel each other and resulting the zero Doppler width. However in TCRD condition, the sum of the two wave vectors[31] is not zero but substantially low. For an example, when two laser wavelengths of 224nm and 266nm (produced from forth harmonic generation of Nd:YAG) are used to probe the D atom from the photodissociation of DBr molecule, the reduced Doppler profile of D atom is 0.6 cm^{-1} (Kinetic energy release of DBr at 224nm = 1.74 eV, therefore v=1.24x10^{4}ms^{-1}). In this case, the Doppler profile of D can be easily masked by 2cm^{-1} bandwidth of 266nm beam. In contrast, the Doppler broadening in conventional REMPI technique is found to be 3.5cm^{-1}, and cannot be covered without scanning of the laser. Therefore, TCRD-REMPI technique has a great benefit over the conventional REMPI method for the detection of products with a higher kinetic energy release. Because of the above mention uses and advantages, TCRD-REMPI method has been widely employed in our experimental set up and is the basis for the results obtained for H probe in diacetylene and cynoacetylene experiments which are discussed in Chapter 3 and 4.

2.6   References

1.   Cravens, T. E.; Robertson, I. P.; Waite, J. H.; Yelle, R. V.; Kasprzak, W. T.; Keller, C. N.; Ledvina, S. A.; Niemann, H. B.; Luhmann, J. G.; McNutt, R. L.;

Ip, W. H.; De La Haye, V.; Mueller-Wodarg, I.; Wahlund, J. E.; Anicich, V. G.; Vuitton, V., Composition of titan's ionosphere. *Geophys. Res. Lett.* **2006,** *33* (7).

2.   Bellucci, A.; Sicardy, B.; Drossart, P.; Rannou, P.; Nicholson, P. D.; Hedman, M.; Baines, K. H.; Burrati, B., Titan solar occultation observed by Cassini/VIMS: Gas absorption and constraints on aerosol composition. *Icarus* **2009,** *201* (1), 198-216.

3.   Waite, J. H.; Niemann, H.; Yelle, R. V.; Kasprzak, W. T.; Cravens, T. E.; Luhmann, J. G.; McNutt, R. L.; Ip, W. H.; Gell, D.; De La Haye, V.; Muller-Wordag, I.; Magee, B.; Borggren, N.; Ledvina, S.; Fletcher, G.; Walter, E.; Miller, R.; Scherer, S.; Thorpe, R.; Xu, J.; Block, B.; Arnett, K., Ion Neutral Mass Spectrometer results from the first flyby of Titan. *Science* **2005,** *308* (5724), 982-986.

4.   Yung, Y. L.; Allen, M.; Pinto, J. P., Photochemistry of the atmosphere of titan - comparison between model and observations. *Astrophysical Journal Supplement Series* **1984,** *55* (3), 465-506.

5.   Lavvas, P. P.; Coustenis, A.; Vardavas, I. M., Coupling photochemistry with haze formation in Titan's atmosphere, Part II: Results and validation with Cassini/Huygens data. *Planet Space Sci.* **2008,** *56* (1), 67-99.

6.   Rowe, B. R.; Canosa, A.; Sims, I. R., Rate coefficients for interstellar gas-phase chemistry. *J. Chem. Soc.-Faraday Trans.* **1993,** *89* (13), 2193-2198.

7.   Sims, I. R.; Queffelec, J. L.; Defrance, A.; Rebrionrowe, C.; Travers, D.; Rowe, B. R.; Smith, I. W. M., Ultra-low temperature kinetics of neutral-neutral

reactions - the reaction CN+O^{-2} down to 26-K. *J. Chem. Phys.* **1992,** *97* (11), 8798-8800.

8.   Sims, I. R.; Smith, I. W. M., rate constants for the radical-radical reaction between CN and O^{-2} at temperatures down to 99-K. *Chem. Phys. Lett.* **1988,** *151* (6), 481-484.

9.   Casavecchia, P.; Balucani, N.; Volpi, G. G., Crossed-beam studies of reaction dynamics. *Annu. Rev. Phys. Chem.* **1999,** *50*, 347-376.

10.   Lee, Y. T., Molecular-beam studies of elementary chemical processes. *Science* **1987,** *236* (4803), 793-798.

11.   Schmoltner, A. M.; Chu, P. M.; Brudzynski, R. J.; Lee, Y. T., Crossed molecular-beam study of the reaction O(3P)+C$_2$H$_4$. *J. Chem. Phys.* **1989,** *91* (11), 6926-6936.

12.   Suits, A. G., Titan: A Strangely Familiar World. *J. Phys. Chem. A* **2009,** *113* (42), 11097-11098.

13.   Chandler, D. W.; Houston, P. L., Two-dimensional imaging of state-selected photodissociation products detected by multiphoton ionization. *J. Chem. Phys.* **1987,** *87* (2), 1445-1447.

14.   Eppink, A.; Parker, D. H., Velocity map imaging of ions and electrons using electrostatic lenses: Application in photoelectron and photofragment ion imaging of molecular oxygen. *Rev. Sci. Instrum.* **1997,** *68* (9), 3477-3484.

15.   Townsend, D.; Minitti, M. P.; Suits, A. G., Direct current slice imaging. *Rev. Sci. Instrum.* **2003,** *74* (4), 2530-2539.

16.   Tonokura, K.; Suzuki, T., Slicing photofragment spatial-distribution by laser sheet ionization. *Chem. Phys. Lett.* **1994,** *224* (1-2), 1-6.

17.   Gebhardt, C. R.; Rakitzis, T. P.; Samartzis, P. C.; Ladopoulos, V.; Kitsopoulos, T. N., Slice imaging: A new approach to ion imaging and velocity mapping. *Rev. Sci. Instrum.* **2001,** *72* (10), 3848-3853.

18.   Lin, J. J.; Zhou, J. G.; Shiu, W. C.; Liu, K. P., Application of time-sliced ion velocity imaging to crossed molecular beam experiments. *Rev. Sci. Instrum.* **2003,** *74* (4), 2495-2500.

19.   Li, W.; Chambreau, S. D.; Lahankar, S. A.; Suits, A. G., Megapixel ion imaging with standard video. *Rev. Sci. Instrum.* **2005,** *76* (6).

20.   Biraben, F., Experimental evidence of 2-photon transition without doppler broadening. *Physical review letters* **1974,** *32*, 643.

21.   Grynberg, G., Doppler-free multiphotonic spectroscopy. *Reports on progress in physics* **1977,** *40*, 791.

22.   Riedle, E.; Neusser, H. J.; Schlag, E. W., Electronic-spectra of polyatomic-molecules with resolved individual rotational transitions - benzene. *J. Chem. Phys.* **1981,** *75* (9), 4231-4240.

23.   (a) Vasilenko, L. S., LIne shape of 2-photon absorption in a standing-wave field in a gas. *Jetp letters-ussr* **1970,** *12*, 113; (b) Guccionegush, R.; Gush, H. P.; Schieder, R.; Yamada, K.; Winnewisser, G., Doppler-free 2-photon absorption of NH_3 using a CO_2 and diode-laser. *Phys. Rev. A* **1981,** *23* (5), 2740-2743.

24.   Riedle, E.; Moder, R.; Neusser, H. J., Pulsed doppler-free 2-photon spectroscopy of polyatomic-molecules. *Opt. Commun.* **1982,** *43* (6), 388-394.

25.   Riedle, E.; Stepp, H.; Neusser, H. J., Heterogeneous perturbations in the doppler-free S1 -SO 2-photon spectrum of benzene - evidence for intrastate coupling. *Chem. Phys. Lett.* **1984,** *110* (5), 452-458.

26.   Kato, H.; Oonishi, T.; Nishizawa, K.; Kasahara, S.; Baba, M., Doppler-free two-photon absorption spectroscopy of the A(1)A(u)<-X(1)A(g) transition of trans-glyoxal. *J. Chem. Phys.* **1997,** *106* (20), 8392-8400.

27.   Misono, M.; Wang, J.; Ushino, M.; Okubo, M.; Kato, H.; Baba, M.; Nagakura, S., Doppler-free two-photon absorption spectroscopy and the Zeeman effect of the A B-1(2u)<- X (1)A(1g)14(0)(1)1(0)(1) band of benzene. *J. Chem. Phys.* **2002,** *116* (1), 162-171.

28.   Okubo, M.; Misono, M.; Wang, J. G.; Baba, M.; Kato, H., The Doppler-free two-photon absorption spectroscopy of naphthalene with Zeeman effects. *J. Chem. Phys.* **2002,** *116* (21), 9293-9299.

29.   Vrakking, M. J. J.; Bracker, A. S.; Suzuki, T.; Lee, Y. T., Ultrasensitive detection of hydrogen molecules by (2+1) resonance-enhanced multiphoton ionization. *Rev. Sci. Instrum.* **1993,** *64* (3), 645-652.

30.   Riedel, J.; Dziarzhytski, S.; Kuczmann, A.; Renth, F.; Temps, F., Velocity map ion imaging of H atoms from the dissociation of HCO (A(2) A ") using Doppler-free multi-photon ionization. *Chem. Phys. Lett.* **2005,** *414* (4-6), 473-478.

31.   Huang, C. S.; Li, W.; Kim, M. H.; Suits, A. G., Two-color reduced-Doppler

ion imaging. *J. Chem. Phys.* **2006,** *125* (12).

Chapter 3

Photodissociation Dynamics and Metastable Lifetimes of Diacetylene

in Titan's Atmosphere

3.1   Introduction

Titan's haze layer is an important factor controlling the energy balance and atmospheric dynamics in Titan's atmosphere. As discussed in Chapter 1 in detail, the haze layer of Titan is believed to be created of polyhydrocarbons and polynitriles. However, the understanding of the chemical processes that govern the formation of the haze layer is not well understood.   It has been shown previously that diacetylene (C_4H_2), cyanoacetylene (HC_3N), and other trace amounts of unsaturated molecules trigger the formation of haze layer in Titan's atmosphere[1]. However, to date, none of these chemical constituents have been studied in relation to the understanding of haze formation under collisionless conditions.

Chapter 3 presents first experimental results for primary C_4H_2 photodissociation and metastable lifetimes under collisionless conditions. Chapter 4 is a detail study of the photodissociation dynamics of cyanoacetylene. Chapter 5 contains photodissociation studies of variety of heptane isomers. Heptane is of great importance for astrochemical and planetary sciences and

believed to be present in Titan. Objectives of these studies are to obtain a deep understanding of the chemical dynamics of these components in Titan's atmosphere in relation to haze formation.

Diacetylene is also believed to play a key role in the formation of polyynes and polycyclic aromatic hydrocarbons (PAH) that partially comprise the haze layer in Titan's upper atmosphere[2,3,4]. It is well established that the formation of diacetylene is initiated by photodissociation of acetylene below 217nm light [2,5,6,7,8] according to the following reaction mechanism:

$$C_2H_2 \ + \ h\nu \ \longrightarrow \ C_2H \ + \ H \ (\lambda < 217nm)$$

$$C_2H \ + \ C_2H_2 \ \longrightarrow C_4H_2 \ + \ H$$
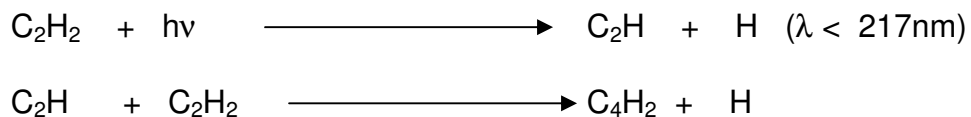
The importance ascribed to diacetylene arises in part owing to the fact that it absorbs light at longer wavelengths, where the solar flux is higher, than any other major constituents of Titan's atmosphere; moreover, experimental results suggest it is still be photochemically reactive even well below the threshold for dissociation[9,10,11,12]. Understanding the dynamics of diacetylene photoexcitation is thus key in revealing the factors driving the chemistry of Titan's atmosphere.

In a pioneering study, Glicker and Okabe determined a quantum yield of 2.0 ± 0.5 for diacetylene photodissociation in the wavelength region of 147 nm - 254 nm[9]. Between 184 and 254 nm, no free radical products were detected and polymeric material was found to coat the inside of the reaction cell. The upper

limit for the quantum yield of C_4H formation was then determined to be only 0.06 at 228 nm based on experimental uncertainty. However, at the time the published thermochemical thresholds were in error, and it is now known that the threshold for H elimination is 5.8 eV (214.1 nm), significantly higher than the energy assumed by Okabe. The diacetylene dissociation quantum yield was ascribed to reactivity of a long-lived metastable form. Subsequently Zwier and co-workers extensively investigated the UV photoinduced chemistry of diacetylene through reactions[10, 13] in a ceramic nozzle with VUV probe of the products downstream. Following excitation of the $^1\Delta_u$ excited state, secondary reactions, likely involving the lowest triplet state, were found to lead to the formation of various larger hydrocarbons[12,14,15]. These laser-based studies, principally at 231 and 243 nm, also found no evidence for radical products proceeding from primary photodissociation of diacetylene[16,11,17,18]. Although metastable diacetylene reactions invoked to account for the observed chemistry are now often incorporated in models of Titan's atmosphere, with an assumed metastable lifetime of 1 ms or more, to clarify their role the triplet lifetime must be measured directly and as a function of excitation energy[19].

Several theoretical models and experiments have examined the secondary photochemistry of C_4H_2[2,20,21]. However, for a clear understanding of the role of diacetylene in Titan's atmosphere it is essential to have a better knowledge of its primary photochemistry (product branching and energy dependence), in addition to the electronic decay pathways and rates. Therefore,

a series of experiments are carried out to understand the photodissociation dynamics of diacetylene under collisionless condition. All these results are supported by a series of ab initio and RRKM calculations, which have been done by Mebel and coworkers, to assist in interpretation of the results[22]

3.2   Experimental

The detailed DC slice imaging experimental set-up has been reported in chapter two and in previous publications[23,24]. Here, only the essential components of the present configuration are given. The molecular beam containing ~40% diacetylene seeded in Ar. The laser and molecular beam delay is adjusted to access the earlier portion of the molecular beam pulse in order to eliminate the contribution from diacetylene dimer or clusters. Two counterpropagating laser beams of different wavelengths are focused onto the molecular beam in the interaction region. The C_4H_2 is excited and dissociated to produce H-atoms which are then probed by a two-color reduced-Doppler (TCRD) REMPI[25,26] scheme, or 1+1' ionization in the case of the Lyman-α dissociation.

The 243 nm laser beam is produced by frequency doubling of the output of a dye laser pumped by a 308 nm XeCl excimer laser. Lyman-α radiation is generated by frequency tripling of 364.7 nm laser light in a VUV cell containing 30% xenon gas, phase matched with argon at a total pressure of 900 torr. The 364.7 nm beam is focused to the center of the VUV cell using a tight focusing

quartz lens. The resultant Lyman-α light is then loosely focused to the center of the interaction region by a MgF_2 lens. No H^+ signal is seen when the TCRD or Lyman-α resonant condition is not met.

In the lifetime measurements, a tunable, narrow-linewidth (0.07 cm-1) OPO laser that is frequency doubled to provide the pump light at 230-250 nm was used. The probe light is an F_2 excimer laser beam at 157 nm. Both lasers are unfocused and directed at right angles mutually perpendicular to the diacetylene beam. The power in each beam is attenuated to the point that negligible signal is seen from either laser alone. For the UV beam this corresponds to 0.3 mJ in a spot of 1 cm diameter (~150 $\mu J/cm^2$), while the VUV probe is estimated to be roughly half this value. Total ion yield at the parent C_4H_2 mass is then recorded as a function of delay between the two lasers.

3.3   Results and discussion

DC-sliced images of H atoms from diacetylene photodissociation at three different wavelengths were recorded (Figure 3.2). Background signals were subtracted from the raw images and total center-of-mass translational energy distributions were derived from the refined data (Figure 3.3). The images all show isotropic angular distributions. The distributions at all three wavelengths studied (243 nm, 212 nm, and 121.6 nm) have peaks around 0.45 eV and decay to higher recoil energies, extending to 3-4 eV for the 243 and 121.6 nm results and
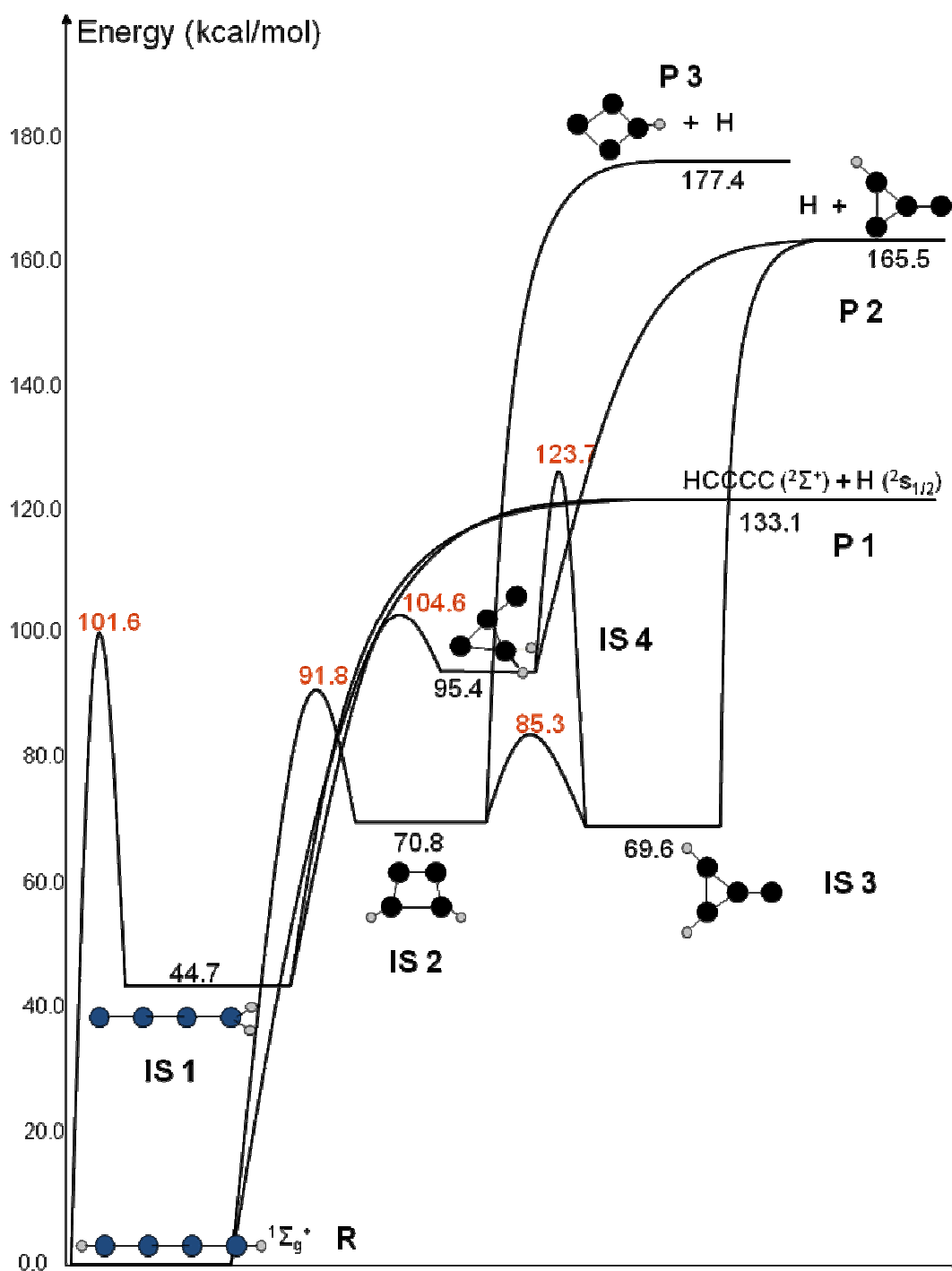
Figure 3.1 Profile of the ground state potential energy surface of diacetylene calculated by Mebel and coworkers at the CCSD(T)/CBS + ZPE(B3LYP/6-311G**) level of theory

to ~5 eV for the 212 nm dissociation. The isotropic angular distributions and structureless translational energy distributions peaking at low energy are typical of statistical, barrierless hydrogen elimination process[27] and suggest dissociation on the ground electronic state. As shown in Figure 3.1, the C-H bond in diacetylene is very strong, with dissociation energy of 133 kcal/mol. The threshold wavelength for single photon dissociation of diacetylene is thus ~215 nm, while at 243 nm the single photon energy is only 118 kcal/mol. Single photon dissociation at 243 nm is clearly not possible. However, if C_4H_2 absorbs two photons at 243 nm, dissociation to $C_4H + H$ is possible with a total excess energy of 103 kcal/mol. Such a process is consistent with the translational energy distribution in Figure 3.3, which extends nearly to this limit.

Then these results were compared to that obtained at the same two- photon energy by considering dissociation (and probe) at 121.6 nm. The kinetic energy distribution recorded at this wavelength is also shown in Figure 3.3 and is nearly superimposable on that obtained at 243 nm. Therefore, by looking at these results it is possible to conclude that 243 nm production of H atom from diacetylene likely results from absorption of two photons, while at 121.6 it is single photon dissociation. Next is to consider 212 nm, which is several kcal/mol above the threshold for H loss in diacetylene. The distribution in Figure 3.3 shows a translational energy release similar in shape but extending to even higher energy than at 243 or 121.6 nm. However, the distribution is entirely confined within the available energy (138 kcal/mol) of the two-photon excitation
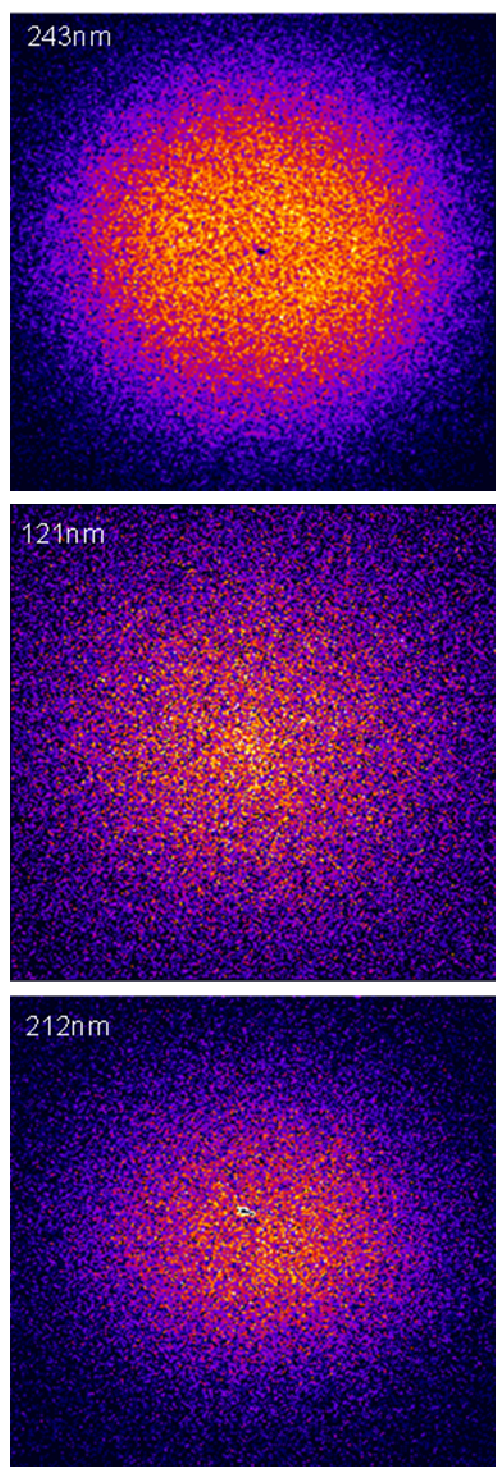
Figure 3.2 DC sliced H atom images from diacetylene excitation at (a) 243 nm (b) 121.6 nm (c) 212 nm.

at 212 nm. The conclusion is that two- photon dissociation still dominates, even though it is now certainly above the single photon dissociation threshold.

All of the observed dissociation processes appear to come from the ground state following some intramolecular electronic relaxation processes. This ground state decomposition is only a part of the picture for diacetylene. Therefore, it is also important to understand that the electronic decay dynamics leading to the ground state and the possible time spent as a potentially reactive metastable triplet species. As mentioned before, the importance is ascribed to metastable diacetylene in Titan's atmosphere. If reactive $C_4H_2^*$ is very long-lived, its contribution to the chemistry in Titan's stratosphere will clearly be much greater than if intersystem crossing (ISC) takes it to the unreactive ground state before it has an opportunity to encounter a suitable reaction partner (e.g., some other unsaturated hydrocarbon.) To examine these issues, the possible excited states involved were considered. Vila et al. have calculated energies and geometries for a range of low- lying excited states of diacetylene using CASSCF and CASMP2 methods and their results is drawn on for this discussion[22]. If first the linear geometry of the ground state is considered, the initial excitation is to the second singlet state. This is the only low-lying excited state that is linear. Internal conversion (IC) may then populate the first singlet state, or ISC may take the system to one of several triplet states. IC in the triplet manifold will then result in formation of the lowest triplet (T_1), the long-lived metastable species. It should
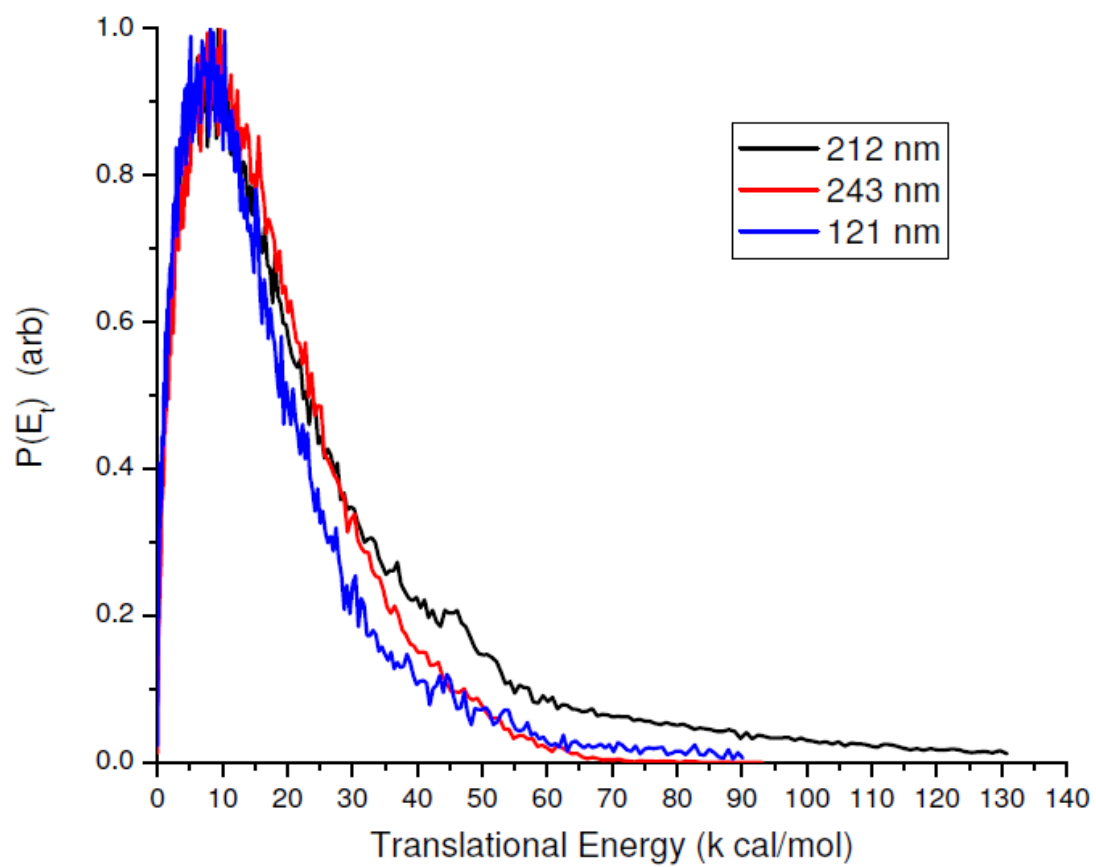
Figure 3.3 Total translational energy release spectra derived from images in Figure 3.2

be noted that these other excited states split into *cis* and *trans* isomers fairly close in energy, but with, in some cases, significant associated relaxation energy. Zwier and coworkers have shown from linewidth analysis that the initially excited state must have a sub- picosecond lifetime[28], and the spectra are in excellent agreement with their results. Relative rates for IC and ISC leading to the lowest triplet, such as could be obtained by femtosecond time-resolved photoelectron spectroscopy, would be very interesting for this system; however these measurements are not yet available. In any case, it is assumed that these processes are very rapid relative to the final step, ISC for T_1-S_0. This is the decay rate that represents the metastable lifetime for an isolated molecule, and one that we can measure using a UV-pump, VUV-probe strategy. In this approach, the nanosecond UV laser excites C_4H_2, after which it relaxes rapidly to T_1. A 7.9 eV probe laser can then ionize the electronically excited states of C_4H_2 (I.P. 10.30 eV vertical, 10.17 adiabatic[29]) but not the ground state. By monitoring the parent ion yield as a function of pump-probe delay, the lifetime of T_1 was determined. Also, this can be done for any initial UV excitation energy. Results for a typical scan at 231.5 nm are shown in Figure 3.4A. Single exponential decays are readily seen and fitted after accounting for the laser pulse duration. Experimental decay rates were determined at 231.5 nm, 243.11 and 247.6 nm and plotted in Figure 3.4B. This strong dependence of lifetime on excitation energy is a manifestation of the dependence of the T_1-S_0 ISC rate on vibrational excitation in the triplet molecule. This behavior is commonly seen, and may be ascribed to a
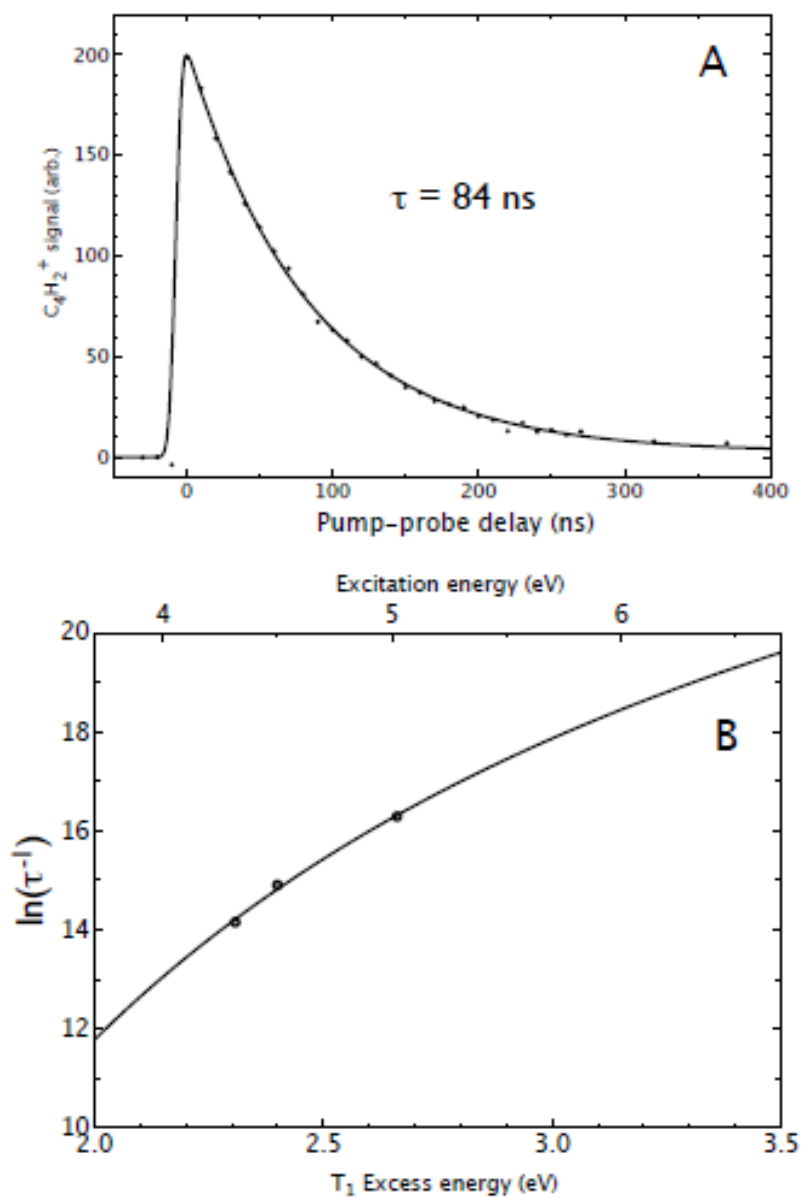
Figure 3.4 Lifetime measurements for triplet diacetylene. A) Typical pump-probe decay profile obtained following excitation at 231.5 nm. Points are experimental result and line is single exponential fit after convolution over laser pulse duration. B) Triplet decay rate plotted vs. excess energy in T_1.

barrier on the triplet surface leading to the crossing region. The barrier may be the actual crossing seam of T_1 and S_0, or it may simply be a region of T_1 that must be passed through to access a lower energy T_1/S_0 crossing. If a simple exponential dependence of the decay rate on excess energy in the lowest triplet is assumed, then it is possible to extrapolate this determination to higher excitation energies (Figure 3.4B). In here an experimental value of 2.7 eV was used for the origin of T_1[30] to obtain a lifetime of 4.6 ns at 212 nm. This indicates that at 212 nm, just above the dissociation threshold, ISC to S0 is likely to occur within the duration of our laser pulse.

The only other measurement of the triplet lifetime is a study by Vuitton et al. in argon and krypton matrices[8]. They monitored phosphorescence following excitation at 249 nm and extrapolated the results to the gas phase after accounting for the dielectric effect of the matrix on the lifetime. They obtained a value of ~70 ms. It is difficult to compare this thermalized value in a matrix at 5-30K to our microcanonical determinations at 2-3 eV vibrational energy. However, it is clear that the observation is not inconsistent with their measurement.

The most important practical issue arising from lifetime measurement is the relevant value for Titan. In attempting to incorporate metastable reactions into atmospheric models, a lifetime of 1 ms has generally been employed[10,12,31], and this has been cited as the lifetime of triplet acetylene determined by Klemperer and coworkers[32,33]. An examination of that work reveals, however, that is it not strictly a lifetime determination, rather a report that some metastable acetylene

produced by electron impact had persisted to detection for 1 ms. Recent experiments have more directly examined the triplet lifetime in acetylene following ISC from specific rovibrational levels of S_1 and obtained a value on the order of 80-100 μs that is dependent on excitation energy[34], just as seen here for diacetylene. For diacetylene, the measurement clearly shows a lifetime many orders of magnitude lower than what has been assumed at the energies relevant for UV photoexcitation on Titan. However, if collisions result in vibrational cooling of the triplet to the ambient temperature, this lifetime will be extended, perhaps to the point that triplet reactions can contribute significantly to the chemistry. However, in Titan's upper atmosphere where the UV solar flux is significant, the pressure is too low for vibrational cooling of the triplet to dominate over T_1-S_0 ISC given these sub-microsecond lifetimes.

When considering the possible H loss products and pathways on the ground state, guided by the ab initio calculations done by Mebel and coworkers as shown in Figure 3.1, the H elimination from diacetylene can occur without a barrier to the product channel P1 giving linear C_4H[35,36]. This dissociation pathway can also be accessed via an intermediate (IS1). In this case, H atom migration first occurs from one terminal carbon atom to the other terminal carbon atom with a 101 kcal/mol barrier. The intermediate product will also undergo H elimination without a barrier. At high energy (e.g., Lyman-α wavelength), all the three channels will be accessible. Starting from the diacetylene ground state, one way of producing P2 and P3 product is through the ring closing reaction which occurs

with a 91.8 kcal/mol barrier to form IS2. Finally, IS2 can undergo H elimination without a barrier to produce P3. Alternatively, IS2 can rearrange via ring contraction to IS3 with a small barrier of 15.1 kcal/mol. The IS3 intermediate finally undergoes barierlesss H elimination to produce P2. The other alternative route of forming P2 product is through intermediate IS1 followed by cyclization with a 59.9 kcal/mol barrier to IS4. The IS4 intermediate dissociates to P2 products. Finally, it is also possible to have rearrangement of IS4 to IS3 through H migration. This reaction occurs with a barrier of 28.6 kcal/mol.

To gain a sense of the relative importance of these different pathways, Mebel and coworkers have performed RRKM calculations of the dissociation rates and branching ratios to the H loss channels, as well as H_2 and C_2 elimination channels, at several energies of interest. The results are shown in Table 3.1. First they examined the total rates for H elimination summed over all C_4H product channels. Just above threshold, at 212 nm, they saw an H loss rate of 5.2×104 s-1. This very low rate readily accounts for the absence of any dissociation signal in the experiment, for which the detection window is only the 10 ns duration of the laser pulse. If the fluence at 212 nm were sufficiently low, single photon dissociation at 212 nm should be seen. However, the timescale is such that very little will be formed within the 10 ns duration of the laser pulse, so that it drops below the sensitivity limits of the experiment. At 193 nm, the rate rises rapidly to 5.3×10^7 s^{-1}. Although the dissociation at this energy has not yet been studied, it can be seen that there should be reasonable probability of

Product	Wavelength				
	212nm	193nm	157nm	121.6nm	2x212nm
Energy (eV)	5.85	6.4	7.9	10.2	11.7
HCCCC + H	100.0	88.4	82.1	86.5	84.9
$C_4(^1\Sigma_g^+)$ + H_2	0.0	0	1.5	6.1	0.1
$C_4(^1A')$ + H_2	0.0	0	0.0	0.0	0.1
$C_4(^1A_g)$ + H_2	0.0	0	0.0	0.0	0.1
C_2 + C_2H_2	0.0	11.6	16.3	7.4	5.8
HCCCC + H (From R1)	81.5	55.0	43.2	46.5	50.1
HCCCC + H (From IS1)	18.5	33.4	38.9	40.0	34.8
$k_{(H\ loss)}$, s^{-1}	5.23×10^4	5.26×10^7	2.39×10^{10}	6.88×10^{11}	1.98×10^{12}

Table 3.1 Computed branching ratios (%) and dissociation rates for indicated product channels calculated by Mebel and coworkers

decomposition within the duration of the laser pulse. At a total energy of 9-10 eV,H elimination still dominates (86%) and roughly half is formed via S3 and half via S5. The remaining branching is roughly evenly split between linear C_4 + H_2 and C_2 + C_2H_2. Branching to the lower energy rhombic isomer of C_4 is negligible in the calculations except at the highest energy studied, where is still 100-fold lower than that to the linear isomer.

These results suggest the following scenario for the observed H atom signals: the first photon excites the C_4H_2 molecule from $^1\Sigma_g$ ground state which has linear $D_{\infty h}$ symmetry, to $^1\Delta_u$ with the same symmetry. Very rapid electronic relaxation likely precedes absorption of a second photon, which then excites the molecule to one of many high-lying Rydberg states, likely now with considerable vibrational excitation[30]. This highly excited diacetylene can then undergo efficient electronic relaxation, ultimately to the ground state where dissociation takes place. This second photon absorption may be attributed to the presence of low-lying Rydberg states of C_4H_2 around 9.4 eV and below[30]. Excited state calculations done by Mebel and coworkers at CIS(D) and EOM-CCSD levels of theory have confirmed the presence of a multitude of such states in the range of 8.0-10.2 eV with significant oscillator strength.

In Okabe's work, discharge lamps were used with fluences lower by many orders of magnitude. Two-photon processes are thus unlikely in that work, and in Titan as well, we should note. However, in the previous work by Zwier and co-workers, fluences significantly greater than ours were employed, so it is

interesting that no radical processes were detected. In those experiments, it may be the number density in the irradiated nozzle extension that is key, so that the rate of vibrational quenching and reaction could exceed the rate of additional photoexcitation and decomposition to radicals. In comparing and reconciling all the various experiments performed under a wide range of conditions, there are many competing factors come into play. This underscores the importance of understanding timescales and the complex interactions between electronic and vibrational relaxation, secondary photoabsorption, and metastable reaction to determine the processes truly relevant to Titan's atmosphere.

3.4   Conclusion

The H elimination channel in C_4H_2 photodissociation was studied under isolated molecule conditions following photoexcitation at 243 nm, 212 nm, and 121.6 nm. From the translational energy and angular distributions, photodissociation was found to proceed on the ground state. At 243 nm and 212 nm, a two-photon absorption process is responsible while at Lyman-α, a one photon absorption process prevails. In separate pump-probe experiments, the lifetime of metastable diacetylene has been measured as a function of excitation energy. The values obtained for UV excitation energies are several orders of magnitude lower than assumptions generally used in modeling Titan's

atmosphere, and suggest that metastable reactions may be less important in Titan's atmosphere than previously believed.

3.5   References

1.   Gu, X.; Kaiser, R. I.; Mebel, A. M.; Kislov, V. V.; Klippenstein, S. J.; Harding, L. B.; Liang, M. C.; Yung, Y. L., A Crossed molecular beams study on the formation of the exotic cyanoethynyl radical in titan's atmosphere. *Astrophys. J.* **2009,** *701* (2), 1797-1803.

2.   Yung, Y. L.; Allen, M.; Pinto, J. P., Photochemistry Of The Atmosphere Of Titan - Comparison Between Model And Observations. *Astrophysical Journal Supplement Series* **1984,** *55* (3), 465-506.

3.   West, R. A.; Strobel, D. F.; Tomasko, M. G., Clouds, Aerosols, And Photochemistry In The Jovian Atmosphere. *Icarus* **1986,** *65* (2-3), 161-217.

4.   Thompson, W. R.; Singh, S. K.; Khare, B. N.; Sagan, C., Triton - Stratospheric Molecules And Organic Sediments. *Geophysical Research Letters* **1989,** *16* (8), 981-984.

5.   Nizamov, B.; Leone, S. R., Kinetics of C_2H reactions with hydrocarbons and nitriles in the 104-296 K temperature range. *Journal of Physical Chemistry A* **2004,** *108* (10), 1746-1752.

6.   Vakhtin, A. B.; Heard, D. E.; Smith, I. W. M.; Leone, S. R., Kinetics of reactions of C_2H radical with acetylene, O^{-2}, methylacetylene, and allene in a

pulsed Laval nozzle apparatus at T=103 K. *Chemical Physics Letters* **2001,** *344* (3-4), 317-324.

7. Pedersen, J. O. P.; Opansky, B. J.; Leone, S. R., Laboratory Studies of Low-Temperature Reactions of C_2H with C_2H_2 and Implications for Atmospheric Models of Titan. *Journal of Physical Chemistry* **1993,** *97* (26), 6822-6829.

8. Vuitton, V.; Gee, C.; Raulin, F.; Benilan, Y.; Crepin, C.; Gazeau, M. C., Intrinsic lifetime of metastable excited C_4H_2: implications for the photochemistry of C_4H_2 in Titan's atmosphere. *Planetary and Space Science* **2003,** *51* (13), 847-852.

9. Glicker, S.; Okabe, H., Photochemistry Of Diacetylene. *Journal of Physical Chemistry* **1987,** *91* (2), 437-440.

10. Bandy, R. E.; Lakshminarayan, C.; Frost, R. K.; Zwier, T. S., Direct Detection Of C_4H_2 Photochemical Products - Possible Routes To Complex Hydrocarbons In Planetary-Atmospheres. *Science* **1992,** *258* (5088), 1630-1633.

11. Bandy, R. E.; Lakshminarayan, C.; Frost, R. K.; Zwier, T. S., The Ultraviolet Photochemistry Of Diacetylene - Direct Detection Of Primary Products Of The Metastable $C_4H_2^*$ + C_4H_2 Reaction. *Journal of Chemical Physics* **1993,** *98* (7), 5362-5374.

12. Zwier, T. S.; Allen, M., Metastable diacetylene reactions as routes to large hydrocarbons in Titan's atmosphere. *Icarus* **1996,** *123* (2), 578-583.

13. Arrington, C. A.; Ramos, C.; Robinson, A. D.; Zwier, T. S., Ultraviolet photochemistry of diacetylene with alkynes and alkenes: Spectroscopic

characterization of the products. *Journal of Physical Chemistry A* **1999,** *103* (10), 1294-1299.

14.   Arrington, C. A.; Ramos, C.; Robinson, A. D.; Zwier, T. S., Aromatic ring-forming reactions of metastable diacetylene with 1,3-butadiene. *Journal of Physical Chemistry A* **1998,** *102* (19), 3315-3322.

15.   Frost, R. K.; Arrington, C. A.; Ramos, C.; Zwier, T. S., Ultraviolet photochemistry of diacetylene: The metastable $C_4H_2^*$ reaction with ethene, propene, and propyne. *Journal of the American Chemical Society* **1996,** *118* (18), 4451-4461.

16.   Wilson, E. H.; Atreya, S. K., Current state of modeling the photochemistry of Titan's mutually dependent atmosphere and ionosphere. *Journal of Geophysical Research-Planets* **2004,** *109* (E6), E06002-1-39.

17.   (a) Frost, R. K.; Zavarin, G. S.; Zwier, T. S., Ultraviolet Photochemistry Of Diacetylene - Metastahle $C_4H_2^*$+C_2H_2 Reaction In Helium And Nitrogen. *Journal of Physical Chemistry* **1995,** *99* (23), 9408-9415; (b) Robinson, A. G.; Winter, P. R.; Ramos, C.; Zwier, T. S., Ultraviolet photochemistry of diacetylene: Reactions with benzene and toluene. *Journal of Physical Chemistry A* **2000,** *104* (45), 10312-10320.

18.   Robinson, A. G.; Winter, P. R.; Zwier, T. S., The ultraviolet photochemistry of diacetylene with styrene. *Journal of Physical Chemistry A* **2002,** *106* (24), 5789-5796.

19.   Hebrard, E.; Dobrijevic, M.; Benilan, Y.; Raulin, F., Photochemical kinetics uncertainties in modeling Titan's atmosphere: A review. *Journal of Photochemistry and Photobiology C-Photochemistry Reviews* **2006,** *7* (4), 211-230.

20.   Stearns, J. A.; Zwier, T. S.; Kraka, E.; Cremer, D., Experimental and computational study of the ultraviolet photolysis of vinylacetylene. Part II. *Physical Chemistry Chemical Physics* **2006,** *8* (45), 5317-5327.

21.   Kaiser, R. I.; Stahl, F.; Schleyer, P. V.; Schaefer, H. F., Atomic and molecular hydrogen elimination in the crossed beam reaction of d1-ethinyl radicals $C_2D(X (2)Sigma(+))$ with acetylene, $C_2H_2(X (1)Sigma(+)(g))$: Dynamics of D1-diacetylene (HCCCCD) and D1-butadiynyl (DCCCC) formation. *Physical Chemistry Chemical Physics* **2002,** *4* (13), 2950-2958.

22.   Vila, F.; Borowski, P.; Jordan, K. D., Theoretical study of the low-lying electronically excited states of diacetylene. *Journal of Physical Chemistry A* **2000,** *104* (39), 9009-9016.

23.   Townsend, D.; Minitti, M. P.; Suits, A. G., Direct current slice imaging. *Review of Scientific Instruments* **2003,** *74* (4), 2530-2539.

24.   Townsend, D.; Lee, S. K.; Suits, A. G., Orbital polarization from DC slice imaging: S(D-1(2)) alignment in the photodissociation of ethylene sulfide. *Chemical Physics* **2004,** *301* (2-3), 197-208.

25.   Huang, C. S.; Li, W.; Kim, M. H.; Suits, A. G., Two-color reduced-Doppler ion imaging. *Journal of Chemical Physics* **2006,** *125* (12).

26.   Huang, C. S.; Lahankar, S. A.; Kim, M. H.; Zhang, B. L.; Suits, A. G., Doppler-free/Doppler-sliced ion imaging. *Physical Chemistry Chemical Physics* **2006,** *8* (40), 4652-4654.

27.   Feltham, E. J.; Qadiri, R. H.; Cottrill, E. E. H.; A., C. P.; P., C. J.; Balint-Kurti, G. G.; Ashfold, M. N. R., Ketene photodissociation in the wavelength range 193-215 nm: The H atom production channel. *J. Chem. Phys.* **2003,** *119*, 6017-6031.

28.   Bandy, R. E.; Lakshminarayan, C.; Zwier, T. S., Spectroscopy and Photophysics of the 1Δu<--1Σg+ Transition of Jet-Cooled C_4H_2, C_4HD, and C_4D_2. *J. Phys. Chem.* **1992,** *96*, 5337-5343.

29.   Lias, S. G., Ionization Energy Evaluation. In *Chemistry Webbook*, Linstrom, P. J.; Mallard, W. G., Eds. NIST: Gaithersburg, MD, 2005.

30.   Allan, M., The Excited-States Of 1,3-Butadiyne Determined By Electron-Energy Loss Spectroscopy. *Journal of Chemical Physics* **1984,** *80* (12), 6020-6024.

31.   Lebonnois, S.; Toublanc, D.; Hourdin, F.; Rannou, P., Seasonal variations of Titan's atmospheric composition. *Icarus* **2001,** *152* (2), 384-406.

32.   Hemminger, J. C.; Wicke, B. G.; Klemperer, W., *J. Chem. Phys.* **1976,** *65*, 2798.

33.   Lisy, J. M.; Klemperer, W., Electric Deflection Studies of Metastable Acetylene. *Journal of Chemical Physics* **1980,** *72* (7), 3880-3883.

34.   Suzuki, T.; Shi, Y.; Kohguchi, H., Detection of metastable triplet acetylene produced by intersystem crossing from the excited A((1)A(u)) state. *Journal of Chemical Physics* **1997,** *106* (12), 5292-5295.

35.   Mebel, A. M.; Kislov, V. V.; Kaiser, R. I., Ab initio/Rice-Ramsperger-Kassel-Marcus study of the singlet C_4H_4 potential energy surface and of the reactions of C^{-2}(X (1)Sigma(+)(g)) with C_4H_4(X (1)A(1g)(+)) and C(D-1) with C_3H_4 (allene and methylacetylene). *Journal of Chemical Physics* **2006,** *125* (13).

36.   Kaiser, R. I.; Balucani, N.; Charkin, D. O.; Mebel, A. M., A crossed beam and ab initio study of the C^{-2}(X-1 Sigma(+)(g)/a(3)Pi(u))+C_2H_2(X-1 Sigma(+)(g)) reactions. *Chemical Physics Letters* **2003,** *382* (1-2), 112-119.

Chapter 4

Photodissociation Dynamics of Cyanoacetylene in Titan's

Atmosphere

4.1   Introduction

Cyanoacetylene (CA), one of the key trace atmospheric constituents on Saturn's moon, Titan, is believed to be of central importance in the formation of the aerosol haze that dominates its atmosphere[1,2,3]. High energy electrons and solar UV photons initiates the dissociation pathways of N_2 and CH_4 in the upper atmosphere of Titan. These dissociation fragments are then acts as reactants for the formation unsaturated nitrile compounds including cyanoacetylene. The traces of cynoacetylene were first identified through the analysis of UV and infrared spectra obtained by Voyager mission[4,5].

Cyanoacetylene is the building block for the formation of cyanopolyines, which are then polymerizes with other organic constituents to form tholins[6]. Tholins are thought to be present in the surface of Titan and is also a major component in the formation of haze layer surrounding the upper atmosphere. However, the current understanding of the formation of haze layer is not very clear. The lack of current laboratory data with rate constants and kinetics of the

photochemical reactions of various chemical constituents such as hydrocarbons and nitriles preclude proper modeling of Titan's atmosphere. This inadequate data is also a major reason for discrepancies of the current models to the data obtained by Cassini Huygens mission.

This has motivated many experimental and theoretical investigations of cyanoacetylene photodissociation[7,8,9,10,11,12,13]. Halpern and co-workers have studied the photochemistry of CA and related compounds extensively, mostly in static cell experiments, using a variety of probe techniques but focusing mainly on the CN radical product[10,9]. Complex multiphoton processes were observed to give rise to a variety of radical products and emission from electronically excited CN and CCN. Clarke and Ferris used infrared absorption to investigate the UV photochemistry of CA by probing H-D exchange using a variety of deuterated reactants[7,14] with an interest in the role of CA photochemistry mediating ethane production on Titan. In a provocative study, Okabe and coworkers showed that UV irradiation of a cell containing a few torr CA promptly gave rise to an aerosol mist and a concomitant pressure decrease, suggesting rapid polymer formation[13]. They concluded that the primary dissociation process at 193 nm was H loss to form the radical CCCN with a quantum yield of 0.3. Radical reactions were then thought to lead to polymerization. The balance of the photoabsorption was believed to result in metastable HCCCN[*], which could undergo subsequent reactions also contributing to polymer formation. Despite this large volume of previous work, direct laboratory investigation of photochemistry of CA under

collisionless conditions in a supersonic molecular beam has not previously been undertaken.

The electronic spectrum of CA has been studied in absorption[13,15] and through excitation spectroscopy[16]. It consists of a weak band extending from 230 to 255 nm assigned to the vibronically induced $^1A'' \leftarrow {}^1\Sigma^+$ transition and a stronger, structured absorption from 190 to 225 nm assigned to a $^1\Delta \leftarrow {}^1\Sigma^+$ transition; in the vacuum ultraviolet there is a pair of broad, intense features at 146 and 141 nm as well as a series of intense Rydberg transitions beginning around 129 nm[12,17]. Significant inconsistencies in the thermochemistry and bond dissociation energies have been reported over the years, with experimental D_0 values for H-CCCN reported as low as 117 kcal/mol[10,12] or 119.9 kcal/mol[7,14], implying a dissociation threshold of 244 or 240 nm, respectively. Published theoretical values have consistently been much higher, ranging from 138 kcal/mol[18] to 130 kcal/mol[11], giving instead dissociation thresholds from 208 to 219 nm. Resolving this discrepancy is important in understanding the role of CA photolysis in Titan's atmosphere, as the solar flux decreases significantly across this range. Experiment and theory agree that the H loss channel is the lowest dissociation pathway and that the onset of CCH + CN is significantly higher. The recent high-level theoretical study by Luo et al. is noteworthy in that they characterized the stationary points in the first excited singlet and triplet states as well as the ground state[11]. For the H loss channel, they found barrierless dissociation in the ground state but modest barriers on both S_1 and T_1, with the

former correlating to electronically excited CCCN[*] ($^2\Pi$). In this paper we present direct current (dc) slice imaging results for photodissociation of CA under collisionless conditions at 121.6, 193.3, and 243.2 nm. The theoretical calculations done by mebel and coworkers augmented the experimental observations. Therefore, the chapter represents the experimental observations combined with theoretical calculations of the stationary points on the ground and excited-state surfaces (see Figure 4.1) and statistical calculations of the dissociation rates and product branching on S_0.

4.2   Experimental section

The experiment was carried out using a velocity map ion imaging[19,20] apparatus optimized for dc slice imaging[21,22]. A detail experiment set up is given in chapter 2 and only the specific details are given in here. A pulsed supersonic molecular beam containing ~2% cyanoacetylene seeded in Ar. The laser and molecular beam delay was adjusted to access the earlier portion of the molecular beam pulse in order to eliminate the contribution from cyanoacetylene dimers/clusters. After dissociation by the 193 or 121 nm laser, the H photofragments were ionized by (1 + 1′) or Doppler-free (2 + 1) REMPI schemes described previously.

For the 243 nm dissociation experiments, an alternative approach, relying on the Autler-Townes effect[23], was used to give Doppler-free detection. In this

approach, the fundamental 486 nm light was doubled and allowed to copropagate with the linearly polarized 243 nm light. The 486 nm light couples the 2s and 3d levels in atomic hydrogen, resulting in AC Stark broadening of the two-photon absorption to the 2s level.

Conditions are readily found that broaden the line sufficiently to detect the full Doppler-broadened recoil distribution, but ionization on the line's center is suppressed[24], as may be seen in the lower image in Figure 4.2. This has little effect on the reconstructed distribution.

Cyanoacetylene was synthesized by a slight modification of the published procedure[25,26]. Briefly, 5.03 g of methyl propiolate was reacted with 10 mL of ammonium hydroxide at -33 ^{0}C. The neat propiolate was added dropwise over a period of 10 minutes; the stirring bar was then removed and the water pumped off using a mechanical pump for about 8 hours. The resulting yellow propiolamide crystals were then thoroughly mixed with 40 g of P_2O_5 and sand. The solid mixture of propiolamide, P_2O_5, and sand was then placed in a round-bottom flask and heated at 180 °C for about 1 h to yield cyanoacetylene, which was collected as a white solid at -78 °C.

4.3   Results

Stationary points and dissociation asymptotes for the groundstate potential energy surface of CA are constructed by Mebel and co-workers and
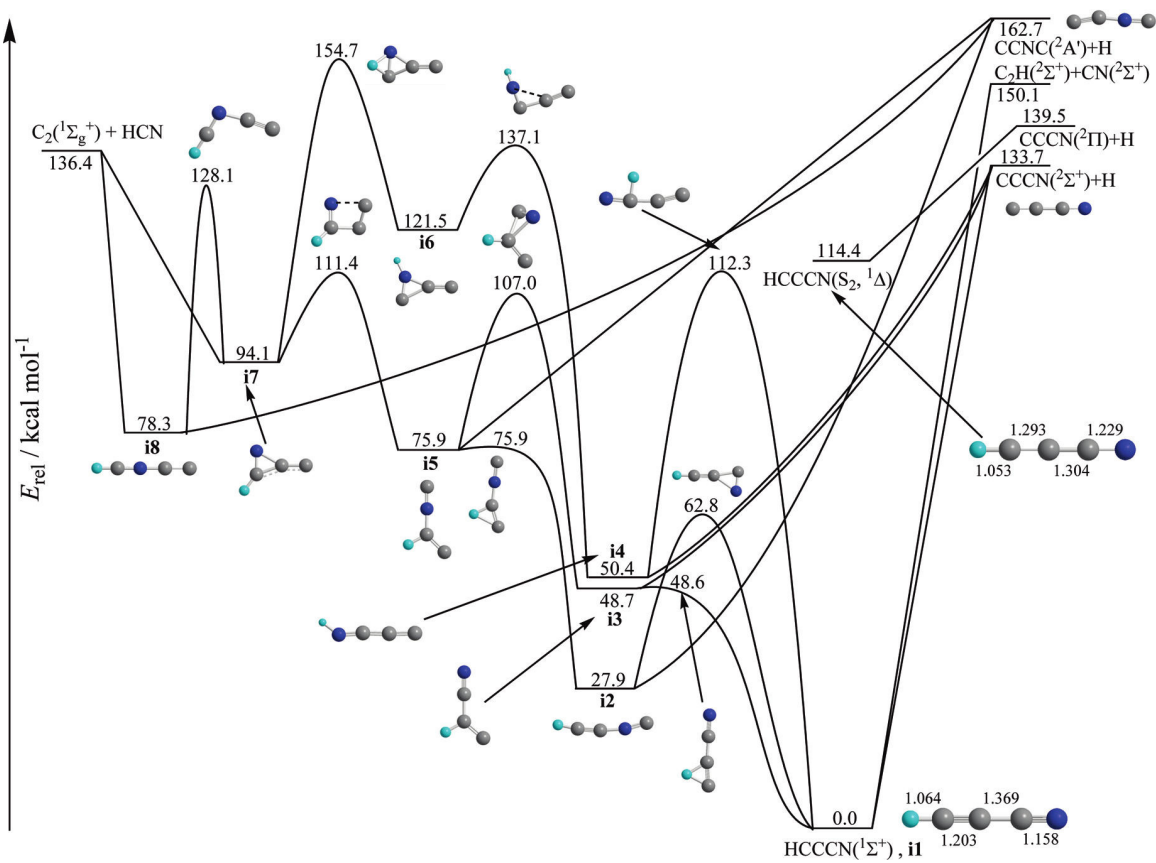
Figure 4.1 Stationary points and reaction pathways on the ground electronic state, and the S2 minimum, for HCCCN calculated by Mebel and coworkers as described in the text

given in Figure 4.1 at the CCSD(T)/CBS level of theory. One can see that HCCCN **i1** can directly decompose to $CCCN(^2\Sigma^+)$ + H or $C_2H(^2\Sigma^+)$ + $CN(^2\Sigma^+)$ by the cleavage of the C-H or the middle C-C bonds with an endothermicity of 133.7 or 150.1 kcal/mol, respectively, without exit barriers. Pathways to the other possible products, such as $CCNC(^2A')$ + H and $C_2(^1\Sigma_g^+)$ + HCN residing 162.7 and 136.4 kcal/mol above HCCCN, respectively, are more complex and will be discussed in detail elsewhere, in relation to the $C_2(^1\Sigma_g^+)$ + HCN reaction[6]. Here we only briefly mention that CCNC + H can be produced by C-H bond cleavages in HCCNC **i2**, CCHNC **i5**, and HCNCC **i8**, occurring without exit barriers. Since CCNC is computed to be 29 kcal/mol less stable than CCCN, the contribution of this product to the photodissociation of CA is expected to be insignificant. Energetically, the most favorable pathway leading to C_2 + HCN involves **i1** f **i2** rearrangement by flipping the CN group over, followed by a 1,2-H shift to **i5**, three-member ring closure to **i7**, and elimination of the C_2 fragment from the latter. **i7** can also ring open to a peculiar HCNCC isomer **i8** and then lose C_2. Since the route to C_2 + HCN is rather complicated and includes entropically unfavorable H migrations and ring openings/closures, we expect that this product channel would play a relatively minor role.

Since dissociation of HCCCN on S_1 and T_1 surfaces was considered theoretically by Luo et al.[11], here the focus is on the S_2 (B $^1\Delta$) surface. The vertical excitation energy from S_0 to S_2 computed in this work, 5.70 eV, is close to the result reported by Luo et al[11]. Geometry optimization is also an effort of

Mebel and co-workers. For S_2 gives a stable structure, shown in Figure 4.1. One can see that, upon excitation to S_2, geometric changes involve elongation of the triple C≡C and C≡N bonds by ~0.09 and ~0.07 Å, respectively, accompanied by a shortening of the C-C single bond by 0.07 Å. In contrast to the S_1 and T_1 local minima, the optimized structure for S2 maintains a linear $C_{\infty V}$ geometry. Mebel and co-workers also calculated adiabatic excitation energy to the B $^1\Delta$ state, which is 4.96 eV (114.4 kcal/mol). Due to the computed change in geometry, vibrational modes that should be active in the $^1\Delta \leftarrow {}^1\Sigma^+$ absorption spectra include combinations of C≡N, C≡C, and C-C stretching, which are displaced and distorted in the excited state, with the corresponding vibrational frequencies changing from 2377, 2172, and 906 cm^{-1} in $^1\Sigma^+$ to 2075, 1465, and 938 cm^{-1}, respectively, in $^1\Delta$. These results support the assignment of the structured absorption band from 190 to 225 nm to the $^1\Delta \leftarrow {}^1\Sigma^+$ transition. Mebel and co-workers confirm that a transition-state search for the H loss on the S_2 surface, carried out for the $^1A'$ component of $^1\Delta$ within C_s symmetry, showed that this process occurs without exit barrier and leads to the CCCN($^2\Pi$) + H products. Because of its degeneracy, the $^2\Pi$ state of the product correlates both with the S_1 ($^1A''$) and S_2 (the $^1A'$ component of $^1\Delta$ when symmetry is reduced to C_s) states of HCCCN. Thus, dissociation on the S_2 surface can also produce CCCN($^2\Pi$), but in contrast to the S_1 surface, no exit barrier was found here.

DC sliced ion images for H atom from dissociation/probe of CA at both 121.6 and 243.2 nm are shown in Figure 4.2, along with the translational energy

distributions determined from the imaging data. The images show no angular anisotropy. The translational energy distributions are nearly identical, peaking at ~0.5 eV and extending to 4-5 eV. The average translational energy release is 1.17 eV (243 nm) or 1.19 eV (121.6 nm), which is ~27% of the available energy at Lyman-α. These are typical H atom loss distributions, similar to those we have seen from a range of hydrocarbon molecules, and they suggest dissociation on the ground electronic state following internal conversion. Despite the fact that the distributions peak away from zero energy, we believe they represent simple bond fission without a barrier. Statistical ground-state treatments are able to reproduce these distributions quite well, as has been shown by Ashfold and co-workers for ketene dissociation[27]. The similarity between the 243.2 nm result and that at Lyman-α strongly suggests that the former represents a two-photon absorption process. This is analogous to the situation we recently reported for diacetylene photodissociation. Although some of the earlier experimental work indicated dissociation thresholds for CA at wavelengths as long as 244 nm, this translational energy distribution at 243 nm is clearly not consistent with single photon dissociation near threshold.

The sliced ion image and associated translational energy distribution for 193 nm dissociation of CA are shown in Figure 4.3. This distribution is quite distinct from that at Lyman-α. It peaks at ~0.2 eV and extends only to 0.5 eV, with an average of 0.30 eV. The theoretical results embodied in the energy diagram in Figure 4.1 give a dissociation energy of 133.7 kcal/ mol, with an
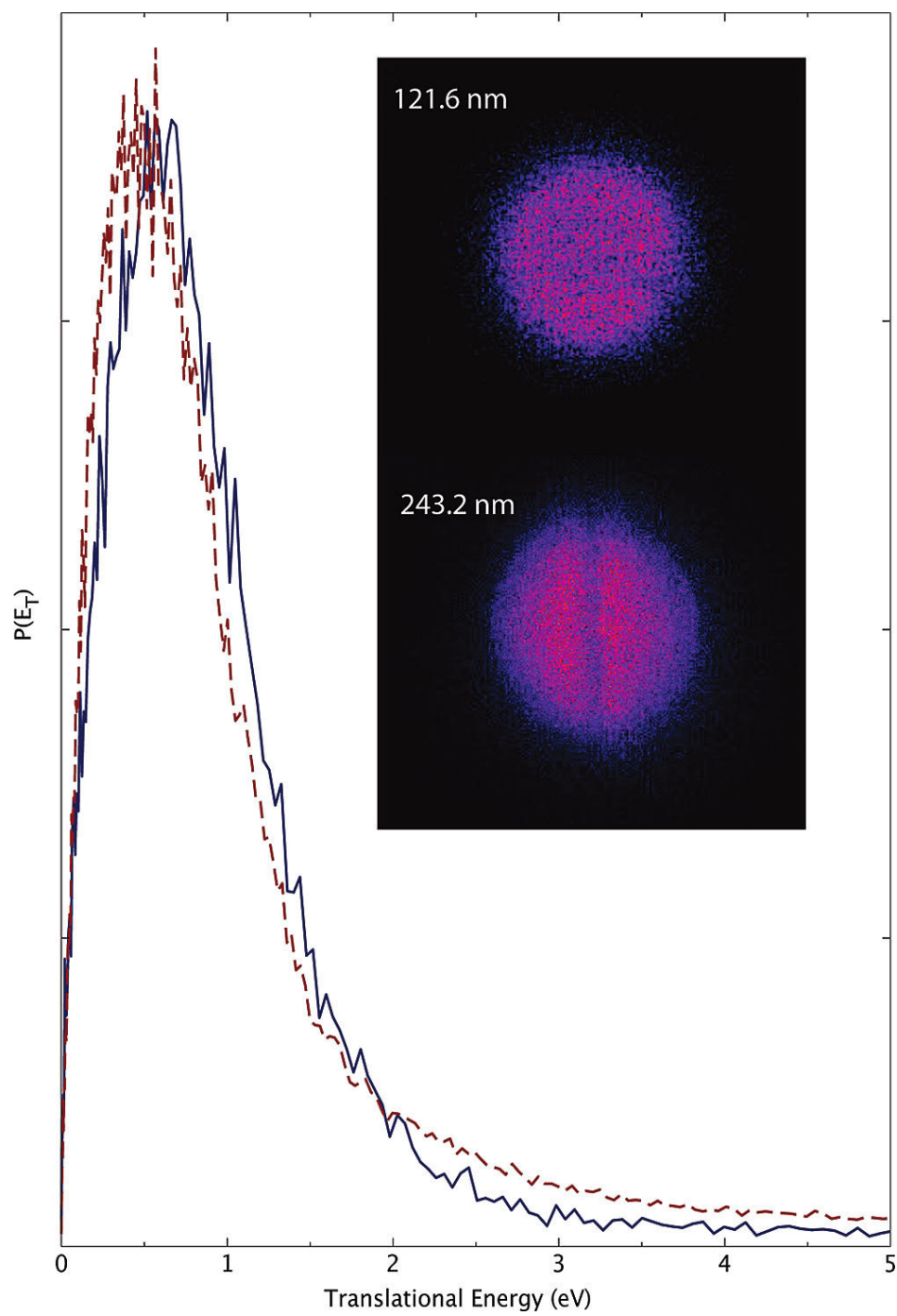
Figure 4.2 H$^+$ images at indicated wavelength and associated translational energy distributions for cyanoacetylene dissociation at 121.6 nm (solid blue line) and 243.2 nm (red dashed line).

estimated uncertainty of perhaps 1 kcal/mol. This corresponds to a maximum available energy at 193.3 nm of 14.3kcal/mol, or 0.62 eV. Our result at 193 nm thus shows roughly 50% of the available energy in translation. Alternatively, the excited-state S_1 surface correlates to electronically excited CCCN, roughly 0.2 eV higher in energy than the ground-state CCCN product (Figure 4.1). The maximum translational energy in that case would be 0.46 eV, which is very close to the observed limit. The triplet surface correlates to ground-state products and would give the higher translational energy limit. As seen in Figure 4.1, direct dissociation on S_2 also correlates to the excited CCCN radical but occurs without a barrier.

4.4   Discussion

It is instructive to compare results for UV photoexcitation of CA to those for diacetylene. In both cases, H loss is the lowest energy dissociation channel[28], but the threshold is higher than the absorption onset, and the chemistry driven by "metastable" reaction has been invoked to account for the reactive processes observed at energies below the dissociation threshold[29,30,31]. Furthermore, these dissociation thresholds were long thought to be much lower than the best current theory now suggests[28]. For CA in particular, the present theoretical value of 133.7 kcal/ mol is not likely to be significantly in error. It is also well supported by
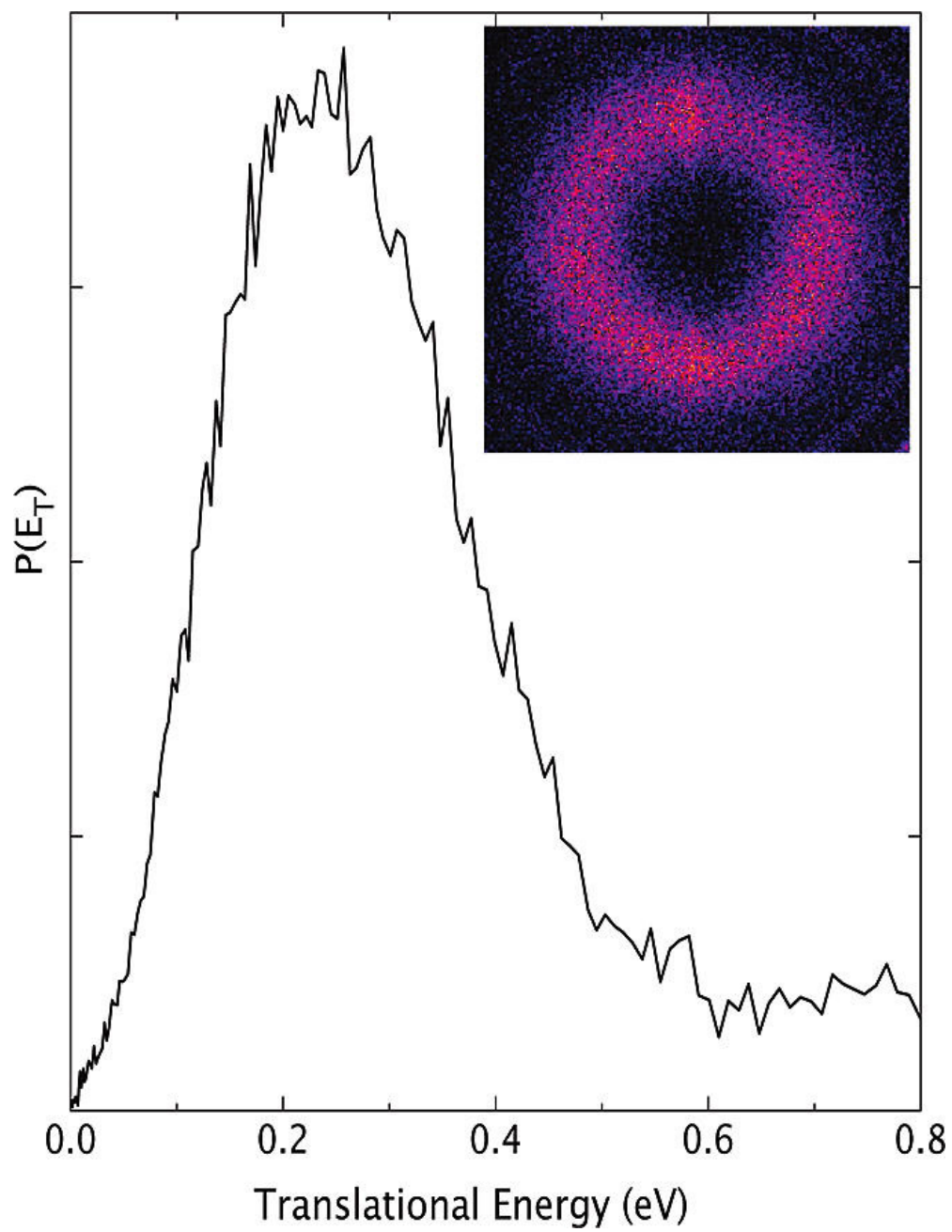
Figure 4.3 H+ images and associated translational energy distribution for cyanoacetylene dissociation at 193.3 nm probed by Doppler-free REMPI at 243 nm

the translational energy distribution in Figure 4.3. The previous experimental determinations of around 5.1 eV for the H-CCCN dissociation energy would imply a maximum translational energy limit of up to 1.3 eV for Figure 4.3. This is clearly not supported by the measurements

The VUV dissociation result shown in Figure 4.2 is consistent with ground-state dissociation following internal conversion, although dissociation from higher excited states is not explicitly ruled out by the data. To understand the ground-state dissociation dynamics, RRKM calculations of the dissociation rates and product branching were performed by Mebel and co-workers as reported for diacetylenein chapter 3[28].The results are compiled in Table 4.1. Two significant differences are immediately apparent in these results compared to those reported for diacetylene. For CA, the dissociation rate at 193 nm is 2.50 × 109 s^{-1}; this is 50 times higher than that for diacetylene. This may account, in part, for our facile detection of the H loss channel in this case, while we were unable to obtain photodissociation results for diacetylene at 193 nm. The origin of this increased rate is the lower density of states for the dissociating molecule HCCCN vs HCCCCH. The second significant difference in these results relative to those found for diacetylene is in the branching to the H loss channel. For diacetylene, H loss dominated, 80% at 157 nm and 75% at Lyman-α. For CA, we see in Table 1 that branching to H loss quickly falls to 57% once the C_2H + CN channel is open and then remains roughly independent of excitation wavelength, decreasing only slightly. The higher yield of C_2H + CN from cyanoacetylene vs C_2H + C_2H from

Wavelength (nm)	212	193	157	121.6	2x212
Available energy (kcal/mol)	134.9	148.0	182.1	235.2	269.0
Rate constants (s^{-1})					
HCCCN $\rightarrow$ C$_2$H + CN	0	4.25×10^7	1.44×10^{11}	2.20×10^{12}	5.7×10^{12}
HCCCN $\rightarrow$ CCCN + H	2.29×10^7	2.50×10^9	1.92×10^{11}	2.89×10^{12}	$7.0710 \times^{12}$
Relative yield (%)					
C$_2$H + CN	0	0	42.9	43.3	44.6
CCCN + H	100	100	57.1	56.7	55.4

Table 4.1 RRKM Calculated Rate Constants and Relative Yields for the CCCN + H and C$_2$H + CN Photodissociation Channels of Cyanoacetylene done by Mebel and co-workers

diacetylene can be understood if we compare the energy difference between C_2H+ CN and CCCN + H (16.4 kcal/mol) and that between C_2H + C_2H and CCCCH + H (26.6 kcal/mol). Thus, the C_2H + CN channel opens at a lower energy (150.1 kcal/mol), compared to 159.7 kcal/mol for C_2H + C_2H; as a result, the relative yield of the former nears its saturation earlier than that for the latter. Note also that possible minor production of C_2 + HCN (up to ~10%) is not included here.

The image at 193 nm, shown in Figure 4.3, is quite intriguing. The fraction of available energy appearing in recoil is much higher than we usually see for H loss processes on the ground state. Although peaking away from zero energy in H loss from the ground state is commonly seen, usually it represents a relatively small fraction of the available energy[27,28]. A plausible explanation for the translational energy distribution in Figure 4.3 is dissociation from an excited state with an exit barrier on the order of 0.2 eV. As mentioned above, Luo et al. found barriers of ~0.06 eV for both S_1 and T_1 dissociation[11]. Although this is a bit low to account for the observed distribution, there is likely to be some significant associated uncertainty in the magnitude of the excited-state barriers. Furthermore, the S_1 dissociation correlates to electronically excited $^2\Pi$ CCCN product. The translational energy limit is very close to the theoretical prediction for this product. These observations lead us to suggest that 193 nm excitation likely gives rise to excited-state dissociation, yielding electronically excited CCCN.

4.5 Conclusions

We have observed photodissociation of cyanoacetylene under collisionless conditions at 193.3, 243.2, and 121.6 nm. The 243 nm result is assigned to a two-photon process, and its similarity to the Lyman-α result and the fact that both are isotropic, with relatively little energy in translation, lead to the likely assignment as ground-state processes. Theoretical calculations of the groundstate dissociation rates and branching show rapid H loss at 193.3 nm and branching to HCC + CN above 40% at 157 nm and higher. The 193.3 nm result is in stark contrast, however. The sharply peaked translational energy distribution and large fraction of available energy in translation suggest excited-state dissociation, and the energetic limit leads to the likely assignment as S_1 dissociation.

At this point, the findings raise more questions than they answer for haze formation on Titan. These results are consistent with the emerging theoretical consensus that the C-H bond in CA is much stronger than previously reported, making direct dissociation above 200 nm probably of limited significance. Furthermore, the results at 193 imply excited-state dissociation to electronically excited CCCN. This indicates that internal conversion is slower than that in diacetylene, for example. One must assume, however, that below the S_1 barrier, IC or ISC must eventually occur. The timing and wavelength dependence of

these events will be important for understanding the possible role of metastable HCCCN in growth of hydrocarbons and nitriles in Titan's atmosphere.

4.6   References

1.   Wilson, E. H.; Atreya, S. K., Chemical sources of haze formation in Titan's atmosphere. *Planet Space Sci.* **2003,** *51* (14-15), 1017-1033.

2.   Coustenis, A.; Achterberg, R. K.; Conrath, B. J.; Jennings, D. E.; Marten, A.; Gautier, D.; Nixon, C. A.; Flasar, F. M.; Teanby, N. A.; Bezard, B.; Samuelson, R. E.; Carlson, R. C.; Lellouch, E.; Bjoraker, G. L.; Romani, P. N.; Taylor, F. W.; Irwin, P. G. J.; Fouchet, T.; Hubert, A.; Orton, G. S.; Kunde, V. G.; Vinatier, S.; Mondellini, J.; Abbas, M. M.; Courtin, R., The composition of Titan's stratosphere from Cassini/CIRS mid-infrared spectra. *Icarus* **2007,** *189* (1), 35-62.

3.   Clarke, D. W.; Ferris, J. P., Titan haze: Structure and properties of cyanoacetylene and cyanoacetylene-acetylene photopolymers. *Icarus* **1997,** *127* (1), 158-172.

4.   Gazeau, M. C.; Benilan, Y.; Es-Sebbar, E. T.; Ferradaz, T.; Hebrard, E.; Jolly, A.; Raulin, F.; Romanzin, C.; Guillemin, J. C.; Berteloite, C.; Canosa, A.; Le Picard, S. D.; Sims, I. R., Laboratory experiments as support to the built up of Titan's theoretical models and interpretation of Cassini-Huygens data. In *Iau:*

Organic Matter in Space, Kwok, S.; Sandford, S., Eds. Cambridge Univ Press: Cambridge, 2008; Vol. 251, pp 319-319.

5.   Hanel, R.; Conrath, B.; Flasar, F. M.; Kunde, V.; Maguire, W.; Pearl, J.; Pirraglia, J.; Samuelson, R.; Herath, L.; Allison, M.; Cruikshank, D.; Gautier, D.; Gierasch, P.; Horn, L.; Koppany, R., Infrared observations of the saturnian system from voyager-1. *Science* **1981,** *212* (4491), 192-200.

6.   Gu, X.; Kaiser, R. I.; Mebel, A. M.; Kislov, V. V.; Klippenstein, S. J.; Harding, L. B.; Liang, M. C.; Yung, Y. L., A Crossed molecular beams study on the formation of the exotic cyanoethynyl radical in titan's atmosphere. *Astrophys. J.* **2009,** *701* (2), 1797-1803.

7.   Clarke, D. W.; Ferris, J. P., Mechanism of cyanoacetylene photochemistry at 185 and 254 nm. *J. Geophys. Res.-Planets* **1996,** *101* (E3), 7575-7584.

8.   Kolos, R.; Zielinski, Z.; Grabowski, Z. R.; Mizerski, T., DIcyanoacetylene photodissociation at 193-nm and at 248-nm studied by transient absorption-spectroscopy - production of CN, C_2 and C_3N. *Chem. Phys. Lett.* **1991,** *180* (1-2), 73-80.

9.   Halpern, J. B.; Petway, L.; Lu, R.; Jackson, W. M.; McCrary, V. R.; Nottingham, W., Photochemistry of cyanoacetylene and dicyanoacetylene at 193 nm. *J. Phys. Chem.* **1990,** *94* (5), 1869-1873.

10.   Halpern, J. B.; Miller, G. E.; Okabe, H.; Nottingham, W., The UV photochemistry of cyanoacetylene. *J. Photochem. Photobiol. A-Chem.* **1988,** *42* (1), 63-72.

11. Luo, C.; Du, W. N.; Duan, X. M.; Li, Z. S., A Theoretical study of the photodissociation mechanism of cyanoacetylene in its lowest singlet and triplet excited states. *Astrophys. J.* **2008,** *687* (1), 726-730.

12. Okabe, H.; Dibeler, V. H., photon impact studies of C_2HCN and CH_3CN in vacuum ultraviolet - heats of formation of C_2H and CH_3CN. *J. Chem. Phys.* **1973,** *59*, 2430.

13. Seki, K.; He, M. Q.; Liu, R. Z.; Okabe, H., Photochemistry of cyanoacetylene at 193.3 nm. *J. Phys. Chem.* **1996,** *100* (13), 5349-5353.

14. Clarke, D. W.; Ferris, J. P., Photodissociation of cyanoacetylene - application to the atmospheric chemistry of titan. *Icarus* **1995,** *115* (1), 119-125.

15. JOB, V. A.; , Electronic spectrum of cyanoacetylene .2. Analysis of 2300-a system. *Journal of molecular spectroscopy* **1966,** *19*, 178.

16. Titarchuk, T.; Halpern, J. B., The excitation spectrum of cyanoacetylene (HC_3N) and emission from C_3N fragments. *Chem. Phys. Lett.* **2000,** *323* (3-4), 305-311.

17. Connors, R. E.; Roebber, J. L.; Weiss, K., Vacuum ultraviolet spectroscopy of cyanogen and cyanoacetylenes. *J. Chem. Phys* **1974,** *60*, 5011.

18. Francisco, J. S.; Richardson, S. L., Determination of the heats of formation of CCCN and HCCCN. *J. Chem. Phys.* **1994,** *101* (9), 7707-7711.

19. Chandler, D. W.; Houston, P. L., Two-dimensional imaging of state-selected photodissociation products detected by multiphoton ionization. *J. Chem. Phys.* **1987,** *87* (2), 1445-1447.

20.   Eppink, A.; Parker, D. H., Velocity map imaging of ions and electrons using electrostatic lenses: Application in photoelectron and photofragment ion imaging of molecular oxygen. *Rev. Sci. Instrum.* **1997,** *68* (9), 3477-3484.

21.   Townsend, D.; Minitti, M. P.; Suits, A. G., Direct current slice imaging. *Rev. Sci. Instrum.* **2003,** *74* (4), 2530-2539.

22.   Lee, S. K.; Silva, R.; Thamanna, S.; Vasyutinskii, O. S.; Suits, A. G., S(D-1(2)) atomic orbital polarization in the photodissociation of OCS at 193 nm: Construction of the complete density matrix. *J. Chem. Phys.* **2006,** *125* (14).

23.   Gray, H. R.; Stroud, C. R., Autler-townes effect in double optical resonance. *Opt. Commun.* **1978,** *25* (3), 359-362.

24.   Bowe, P.; O'Neill, R. W.; van der Burgt, P. J. M.; Slevin, J. A.; Raczynski, A.; Zaremba, J.; Chwirot, S., Two-colour intensity suppression of multiphoton ionization of atomic deuterium. *J. Phys. B-At. Mol. Opt. Phys.* **1998,** *31* (5), 1003-1010.

25.   Halter, R. J.; Fimmen, R. L.; McMahon, R. J.; Peebles, S. A.; Kuczkowski, R. L.; Stanton, J. F., Microwave spectra and molecular structures of (Z)-pent-2-en-4-ynenitrile and maleonitrile. *J. Am. Chem. Soc.* **2001,** *123* (49), 12353-12363.

26.   Moreau, C. B.; Bongrand, J. C., *Ann. Chim. (Paris)* **1920,** *14*, 47.

27.   Feltham, E. J.; Qadiri, R. H.; Cottrill, E. E. H.; Cook, P. A.; Cole, J. P.; Balint-Kurti, G. G.; Ashfold, M. N. R., Ketene photodissociation in the wavelength

range 193-215 nm: The H atom production channel. *J. Chem. Phys.* **2003,** *119* (12), 6017-6031.

28.   Silva, R.; Gichuhi, W. K.; Huang, C.; Doyle, M. B.; Kislov, V. V.; Mebel, A. M.; Suits, A. G., H elimination and metastable lifetimes in the UV photoexcitation of diacetylene. *Proc. Natl. Acad. Sci. U. S. A.* **2008,** *105* (35), 12713-12718.

29.   Bandy, R. E.; Lakshminarayan, C.; Frost, R. K.; Zwier, T. S., Direct detection of C_4H_2 photochemical products - possible routes to complex hydrocarbons in planetary-atmospheres. *Science* **1992,** *258* (5088), 1630-1633.

30.   Frost, R. K.; Arrington, C. A.; Ramos, C.; Zwier, T. S., Ultraviolet photochemistry of diacetylene: The metastable $C_4H_2^*$ reaction with ethene, propene, and propyne. *J. Am. Chem. Soc.* **1996,** *118* (18), 4451-4461.

31.   Glicker, S.; Okabe, H., Photochemistry of diacetylene. *J. Phys. Chem.* **1987,** *91* (2), 437-440.

Chapter 5

Photodissociation Dynamics of Heptane Isomers and Relative

Ionization Efficiencies of Butyl and Propyl Radicals at 157 nm

5.1   Introduction

Titan's atmosphere is continuously bombarded by high energetic electron and cosmic rays, which results in the formation of primary ions such as N_2^+, CH_4^+ [1,2]. As mentioned in chapter 1, these primary ions are undergoing a series of chemical reactions to produce stable ion clusters, which can ultimately accumulated in clouds in Titan's troposphere[3]. Gravitational settling and convection assist in charge separation, which finally leads to electric field development within the clouds and between clouds and the ground[4]. Neutralization of charge separation leads to charge discharge and stimulate variety of chemical reactions in Titan's troposphere. Laboratory investigation of corona discharge in simulated Titan's atmosphere clearly shows formation of n-heptane and its isomers[4,3]. VUV radiation in Titan's atmosphere can easily photodissociates heptane and its isomers to form alkyl radical. These alkyl radicals are   important functional intermediates not only in planetary atmospheres[5,2] such as in Titan but also in combustion[6,7], and in dissociation of

saturated hyrocarbons[8,9,10,11]. Determination of chemical and physical properties such as absolute reaction rate constants, branching ratios and ionization potentials of these alkyl products are key aspects of modeling Titan's atmosphere. Moreover, methods of determining the relative or absolute detection efficiency for reaction products provide the foundation for measuring branching ratios. A well-established approach for determining detection efficiency in electron impact ionization mass spectrometry involves accumulating the yield of all possible daughter ions arising from fragmentation in a mass-spectrometric detection system, then scaling them based on total ionization cross sections estimated from semiempirical methods[12,13,14]. However, this approach remains challenging for application to large polyatomic molecules, and in any case these determinations are associated with significant uncertainty.

Recently, a variety of related approaches have emerged based on comparing photoionization efficiencies for atomic and radical products of the same photodissociation event, notably from the Butler group[15,16]. A similar strategy has been combined with imaging to examine the internal energy dependence of 157nm ionization of butyl radical. The object in that study was simply to rule out any internal energy dependence of the VUV detection efficiency. This approach has been used extensively by Pratt and coworkers[17,18,19] in more general studies of the internal energy dependence of the photoionization efficiency. Butler's group in particular has used this approach to investigate the internal energy dependence of secondary decomposition

processes allowing them to locate ground state barriers for radical decomposition[20]. Neumark and coworkers have used tunable synchrotron radiation in related experiments, employing known atomic photoionization cross sections to place the relative VUV photoionization eficiency for radicals on an absolute scale[21,22]. Recent work from Taatjes et al. has employed this approach in a simpler imaging configuration to obtain absolute photoionization cross sections for the methyl radical[23].

In our work, photodissociation dynamics of heptane isomers and an alternative scheme to obtain relative ionization efficiency for butyl and propyl radicals' isomers of interest are studied. This approach does not offer the promise of absolute ionization efficiency as in some of the studies mentioned above. However, the objective is to examine the sensitivity of the 157 nm ionization for radical products in crossed-beam scattering experiments[24,25,26]. This strategy has the advantage that it is a simple and direct way to scale the detection under the conditions of the experiment. At the same time, it can give some insight into the VUV photodissociation of the heptane isomers used as radical precursors. Measurements and comparison of the ionization efficiencies of two major fragments i.e., butyl and propyl radicals, that result from an isolated collision free 157 nm photodissociation and ionization of several heptane isomers are presented in here. In these studies, relative detection efficiencies for separate pairs of radical products are compared; when one of the species in

each pair is identical in two measurements, the results may be scaled to give the relative detection efficiencies for the other two species.

Figure 5.1 shows results for dissociation of n-heptane (n-Hep), which yields 1-propyl and 1-butyl photofragments as the major products, to those for photodissociation of 3-methylhexane (3-M-Hex), which yields 1-propyl and 2-butyl 4 radicals as the major primary product channels. The relative 157 nm ionization efficiencies of 1-butyl and 2-butyl radicals were determined using 1-propyl radical as the reference. A similar strategy may further be used to scale the relative detection efficiency for 1-propyl and 2-propyl radicals as discussed further below.

The results reported in this study also seek to unveil the possible neutral photodissociation dynamics of heptane isomers at 157 nm with the aim of gaining a better understanding on the formation of these two radical products and their excited state behavior. Studies of the photochemistry of saturated hydrocarbons is limited to the VUV as that is the onset of the first absorption[27,28]. Studies have ranged from end-product analysis of cell experiments with VUV lamps and radical scavengers[27,29,30] to more recent Doppler[31] and photofragment translational spectroscopy studies in molecular beams[32,33,34,35]. It is worth noting that while the photodissociation dynamics of all the heptanes isomers presented here do not show any dramatic differences, the relative yields and ionization efficiencies of different dissociation pathways and radical products are distinct.
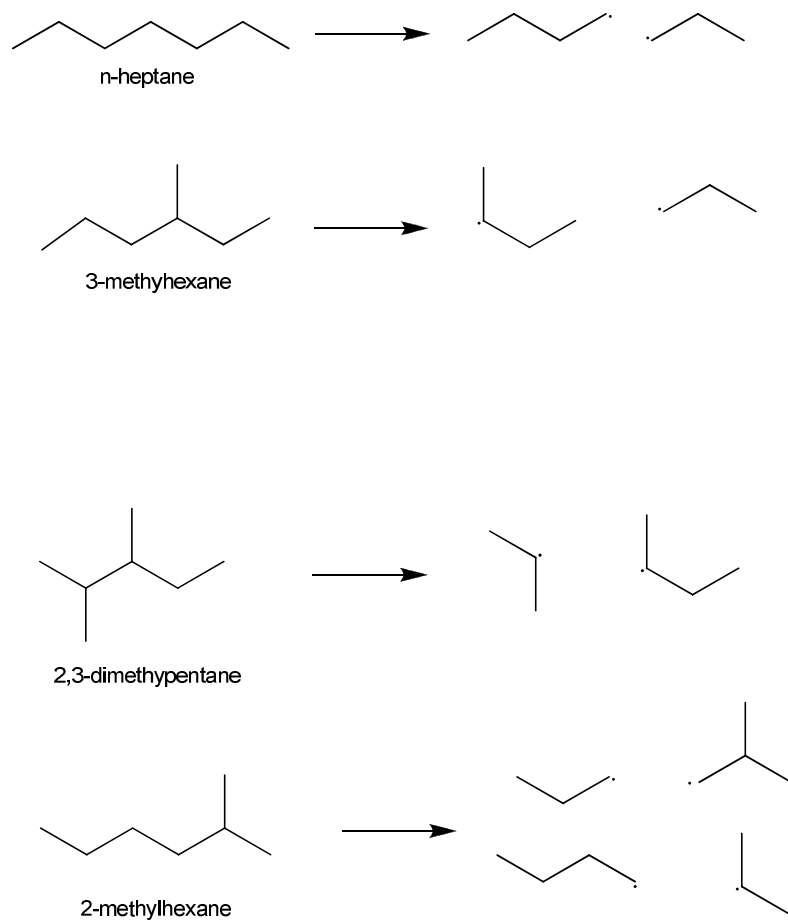
Figure 5.1 Scheme showing formation of C3 and C4 radical products from simple C-C bond fission for selected heptane isomers.

5.2 Experimental

The details of the apparatus[36] and the DC slice imaging technique[37] have been reported in previous chapters. Here, we present only the features that are essential for this experimental set up. Up to 0.5 % of a particular heptane isomer seeded in helium was supersonically expanded to the sauce chamber. The molecular beam pulse valve delay was adjusted such that 157nm laser light interacted only with the early portion of the beam to avoid the contamination with clusters. An oxygen free environment was maintained along the F_2 excimer laser path way by a continuous purge of N_2. The laser beam was loosely focused in the interaction region by a 135 cm focal length MgF_2 lens. After fragmentation and ionization, the ion cloud was accelerated to the MCP detector coupled with P-47 phosphor screen. The phosphor screen was viewed by a CCD camera which captured and recorded the ion images, and by a photomultiplier tube (PMT) to capture the integrated time-of-flight signal.

In the time of flight spectrum measurements, the MCP was un-gated and the PMT signal was sent to an oscilloscope for averaging and final transfer to the computer.

5.3 Results

To investigate the product yields resulting from the 157 nm dissociation of heptane and its isomers, time of flight mass spectra were accumulated up to 1000 shots and the accumulated intensity of selected radical products measured. This procedure was repeated for each system and the relative intensity of each fragment was then determined. At the total available energy for dissociation and ionization at 157nm, i.e., two photons, secondary H and H2 loss from the cation is possible, and the TOF data showed overlapping mass peaks for these processes. The ion yields were thus summed for all $C_4H_n^+$ and $C_3H_n^+$ species. The results are presented in Table 1 scaled for the propyl product in each case.

To confirm that these ion yields represent neutral dissociation pathways, and to investigate the photodissociation dynamics, DC sliced ion images were recorded at each mass for each parent molecule shown in Figure 5.1. The results are shown in Figure 5.2 for the propyl and butyl products from each precursor heptane molecule. In addition, imaging results are shown for the ethyl-pentyl and methyl-hexyl radical product pairs from n-heptane dissociation. Total translational energy distributions derived from the images are shown in Figure 5.3. A key point in Figure 5.3 is that the distributions are derived independently for each co-product. If the products come from the same neutral dissociation event, there should be momentum matching between the products and the two inferred translational energy distributions should agree. There is reasonable agreement

for all C3-C4 product pairs examined. The C2-C5 and C1-C6 pairs shown in Figure 5.2 e,f and Figure 5.3 e,f, however, do not show momentum matching; clearly these signals do not originate from a common neutral dissociation event. Instead, they may arise from multiphoton ionization/fragmentation processes. Nevertheless, they provide a useful contrast to the momentum matching seen for the propyl-butyl radical pairs. The average translational energy release determined for each channel and partner fragment is compiled in Table 5.2. The trends apparent from the translational energy distribution are reflected clearly in the average translational energy release.

The imaging results all show isotropic angular distributions. Although the 157 nm laser is unpolarized, any inherent anisotropy in the photodissociation event should still be manifested in the images, albeit reduced by a factor of two relative to the case of pure linear polarization. The absence of anisotropy suggests that the lifetime may be long relative to the rotational period of the molecule or that dissociation occurs from a wide range of geometries.

As outlined in the Introduction, the relative detection efficiency for radical products determined for several precursor heptane molecules may be obtained if there is a co-product in common. This is the case for n-Hep and 3-M-Hex: they both give 1- propyl radical as a product, but for n-Hep the cofragment is 1-butyl radical, while for 3-M-Hex, the cofragment is 2-butyl radical. Assuming the detection efficiency for the product 1- propyl radicals is the same for the two systems, the relative 157 nm ionization efficiency for 2-butyl vs. 1-butyl radical
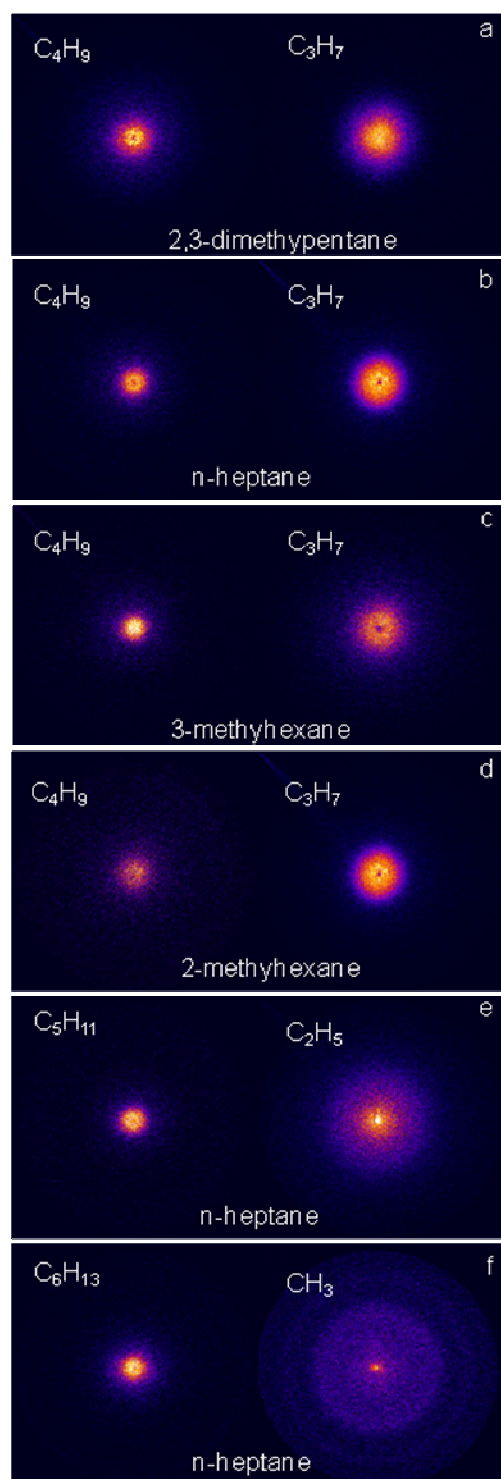
Figure 5.2 DC sliced ion images for indicated radical fragment from various heptanes precursors

are detected as 0.46:0.43 or 1.0:0.93. Similarly, 3-M-Hex and 2,3-DM-Pent both give 2-butyl as the C4 product to determine our relative detection efficiency for propyl radical products. Then, a relative 157 nm ionization efficiency of 1.0:0.96for 2-propyl:1-propyl is obtained. A similar comparison is possible for 2,3-DM-Pent and 2-M-Hex. However, this is complicated by the fact, shown in Fig. 1, that 2-M-Hex has two distinct pairs of C3-C4 products following CC bond fission: 1- propyl with iso-butyl, and 2-propyl with 1-butyl. The relative yields of these two channels are unknown, but the thermochemistry places them very close in energy. No single channel is likely to dominate. For 2-M-Hex, the C3:C4 relative detection efficiency is obtained as 1.0:0.42, certainly consistent with the other measurements. However, the relative detection efficiency for iso-butyl from these results could not be obtained, only that it is likely to be similar to the other C4 products.

5.4   Discussion

Although few studies exist on the VUV photodissociation dynamics of heptane, extensive studies have been reported over the years for simpler alkanes, methane to butane, and the close chemical relation among these make for a very useful comparison to the present results. Unfortunately there does not appear to be a consensus on the nature of the initial electronic excitation. The 157 nm excitation for heptane is on the triplet or the ground singlet state of the

	1-C$_3$H$_3$	2-C$_3$H$_3$	1-C$_4$H$_3$	iso-C$_4$H$_3$	2-C$_4$H$_3$
3-M-Hex	1.0				0.5
2,3 DM-Pent		1.0			0.47
2-M-Hex	1.0		0.42		
n-Hept	1.0		0.43		

Table 5.1 Relative signal intensity for C4H3 products from indicated heptane isomer dissociation/ionization at 157 nm

molecule. Perhaps the most useful studies for comparison to the present work is an investigation of the 157 nm dissociation of propane and other hydrocarbons by Yang and coworkers using photofragment translational spectroscopy with universal detection[33,34,35]. Although their study focused on H and H_2 loss channels, they also reported the C-C bond fission channel giving radical products in the propane case. They reported a branching of 0.22:0.46:0.32 for H, H_2 and CH_3 loss channels, respectively. In this, the focus is in considering the C-C bond fission channel to give radical products readily detected at 157 nm. Nevertheless, by analogy, the propane results suggest this is likely a significant reaction channel.

The propane study inspired a theoretical examination of the ground state surface of methane, ethane and propane by Morokuma and coworkers. For propane, they characterized the energetics of the H and H_2 dissociation asymptotes and the barrier for 1,1 or 1,2 H_2 elimination. The located the lowest barrierless H loss pathway at 99.4 kcal/mol to make 2-propyl, the 2,2 elimination transition state at 97.3 kcal/mol, the 1,2 pathway at 104.3 kcal/mol, and they found the C-C bond fission reaction to be barrierless and located at 89 kcal/mol. The energetics for analogous processes in heptanes do not differ greatly. In all of the heptane systems, following 157 nm excitation there are many similar competing reactions involving H or H_2 loss or other C-C bond fission processes, possibly followed by secondary decomposition. At the same time there may also be complex multiphoton dissociative ionization processes. The signals we
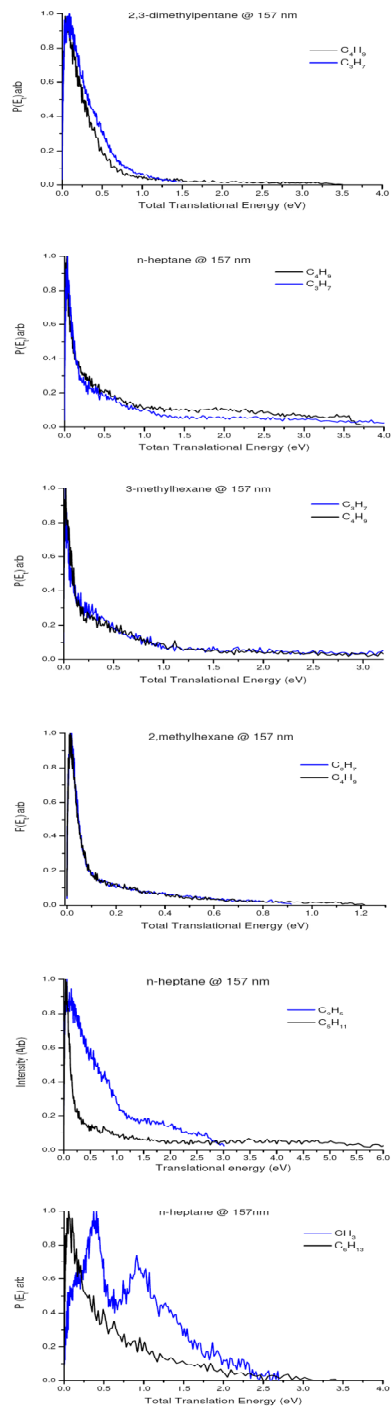
114

Figure 5.3 Total translational energy distributions derived from the corresponding images in Figure 5.2

observe will simply reflect the dominant pathways for combined fragmentation and ionization. The results obtained by this study clearly suggest that the facile detection for C3 and C4 radical products at 157 nm (7.9 eV) means that for these, neutral dissociation followed by ionization dominates relative to dissociative ionization. This is plausible given the ionization energies: roughly 7.3 eV for 2-propyl or 2-butyl, 7.9 eV for iso-butyl and 8.1 eV for 1-propyl or 1-butyl (adiabatic values)[38].

For CH_3 and C_2H_5, the dissociative ionization processes appear to dominate over direct detection of these radicals. However, it is likely that the results obtained for the heavy fragment in these reactions still reflects the underlying neutral dissociation event. This is supported by the translational energy distributions shown in Figure 5.3 and the average translational energy release in Table 5.2, closely resembling results for C3 and C4 products. A key question that has not yet addressed is the possibility of rearrangement in the product radicals to give the lowest energy isomers, a 2-1 H migration in 1-propyl for example. This would certainly undermine the determination of the relative detection efficiencies presented in this study. Calculations by Noler and Fisher[39] place this at just 38 kcal/mol relative to the 1-propyl minimum, and calculated values range from this to even 50 kcal/mol for 1,2 H migration in hexyl radicals[40]. H migration may thus be possible for some subset of the radical products. At 157 nm there is 182 kcal/mol excitation energy, C-C bond fission requires ~89 kcal/mol. Our experiments suggest an average of ~7 kcal/mol in translation. This leaves ~ 86

	C4	C3
3-M-Hex	0.33	0.27
2,3 DM-Pent	0.26	0.31
2-M-Hex	0.24	0.19
n-Hept	0.32	0.31
n-Hept	C5	C2
	0.28	0.52
n-Hept	C6	C1
	0.37	0.69

Table 5.2 Average total translational energy release (eV) determined from each product from the indicated heptane isomer dissociation/ionization at 157nm.

kcal/mol to be distributed between the two radical products. The most likely partitioning of energy places roughly half of this in each product, so that, given enough time, some fraction of the radical products could relax to the lowest energy isomers. However, in our study the total available time is limited to the duration of the laser pulse, less than 20 ns, and this includes the time for dissociation of the parent molecule and possible rearrangement of the radical.

Noller and Fischer measured H loss rates for propyl radicals at 112 kcal/mol and higher excitation energies (significantly higher than available in the present experiment) and obtained values below 108 s^{-1}, much lower than predicted by RRKM theory. The lifetime for rearrangement is likely on a similar timescale. In the present study, the average available energy is only slightly higher than the barrier so the lifetime is expected to be much longer. These considerations suggest that, although some radical rearrangement is possible, on the timescale of the experiment it is not likely to be the dominant process. Therefore, the reported detection efficiencies of this study thus represent the indicated radicals inferred from the parent geometries.

5.5   Conclusion

Ion imaging and time-of-flight mass spectra for one-color laser dissociation of a variety of heptane isomers were obtained under collisionless conditions at

157 nm. Momentum matching results for the C3 and C4 product radicals suggest that those signals are dominated by neutral dissociation with single photon ionization of the products. This is in clear contrast to the results for C2-C5 and C1-C6 products of n-heptane dissociation, in which momentum matching was not demonstrated. The isotropic angular distributions and very low translational energy release suggest dissociation on the ground state following internal conversion. Results for four different heptane isomers allowed for calibration of the relative detection efficiency for the different C3 and C4 radical isomers at 157 nm.

5.6   References

1.   Wilson, E. H.; Atreya, S. K., Current state of modeling the photochemistry of Titan's mutually dependent atmosphere and ionosphere. *J. Geophys. Res.-Planets* **2004,** *109* (E6).

2.   Yung, Y. L.; Allen, M.; Pinto, J. P., Photochemistry of the atmosphere of titan - comparison between model and observations. *Astrophysical Journal Supplement Series* **1984,** *55* (3), 465-506.

3.   Ramirez, S. I.; Navarro-Gonzalez, R.; Coll, P.; Raulin, F., Organic chemistry induced by corona discharges in Titan's troposphere: Laboratory simulations. In *Space Life Sciences: Astrobiology: Steps toward Origin of Life*

and Titan before Cassini, Bernstein, M.; NavarroGonzalez, R.; Raulin, R., Eds. Elsevier Science Ltd: Oxford, 2005; Vol. 36, pp 274-280.

4.   NavarroGonzalez, R.; Ramirez, S. I., Corona discharge of Titan's troposphere. In *Life Sciences: Complex Organics in Space*, Raulin, F.; Greenberg, J. M., Eds. Pergamon Press Ltd: Oxford, 1997; Vol. 19, pp 1121-1133.

5.   Lavvas, P. P.; Coustenis, A.; Vardavas, I. M. In *Coupling photochemistry with haze formation in Titan's atmosphere, part I: Model description*, Pergamon-Elsevier Science Ltd: 2008; pp 27-66.

6.   Ross, P. L.; Johnston, M. V., Production and decomposition of large alkyl radicals. *Journal of Physical Chemistry* **1995,** *99* (45), 16507-16510.

7.   Cool, T. A.; Nakajima, K.; Mostefaoui, T. A.; Qi, F.; McIlroy, A.; Westmoreland, P. R.; Law, M. E.; Poisson, L.; Peterka, D. S.; Ahmed, M., Selective detection of isomers with photoionization mass spectrometry for studies of hydrocarbon flame chemistry. *Journal of Chemical Physics* **2003,** *119* (16), 8356-8365.

8.   Billaud, F.; Elyahyaoui, K.; Baronnet, F.; Kressmann, S., Chemical kinetic modeling of normal-hexane pyrolysis by acuchem, chemkin and morse software packages. *Chemical Engineering Science* **1991,** *46* (11), 2941-2946.

9.   Pant, K. K.; Kunzru, D., Pyrolysis of n-heptane: Kinetics and modeling. *Journal of Analytical and Applied Pyrolysis* **1996,** *36* (2), 103-120.

10.   Chen, J. H.; Dunbar, R. C., Fragmentation of n-heptane ions by photodissociation. *International Journal of Mass Spectrometry and Ion Processes* **1986,** *72* (1-2), 115-123.

11.   Lemonidou, A. A.; Koulouris, A. P.; Varvarezos, D. K.; Vasalos, I. A., Mechanistic model for the catalytic cracking of normal-hexane over calcium aluminate catalysts for producing light alkenes. *Applied Catalysis* **1991,** *69* (1), 105-123.

12.   Mandl, R. E. C. a. A., Ionization cross-sections of F_2 and Cl_2 by electron-impact. *Journal of chemical physics* **1972,** *57*, 4104.

13.   Bouma, W. J.; Poppinger, D.; Radom, L., The ionization of alkanes. *Israel Journal of Chemistry* **1983,** *23* (1), 21-36.

14.   Fitch, W. L.; Sauter, A. D., Calculation of relative electron-impact total ionization cross-sections for organic-molecules. *Analytical Chemistry* **1983,** *55* (6), 832-835.

15.   Kitchen, D. C.; Myers, T. L.; Butler, L. J., Determination of absolute product branching ratios in mass spectrometric experiments: Detecting acetyl radicals at CH_2CO+. *Journal of Physical Chemistry* **1996,** *100* (13), 5200-5204.

16.   Forde, N. R.; Morton, M. L.; Curry, S. L.; Wrenn, S. J.; Butler, L. J., Photodissociating trimethylamine at 193 nm to probe dynamics at a conical intersection and to calibrate detection efficiency of radical products. *Journal of chemical physics* **1999,** *111* (10), 4558-4568.

17.   Aguirre, F.; Pratt, S. T., Photoionization and photodissociation dynamics of the B-1 Sigma(+)(u) and C-1 Pi(u) states of H-2 and D-2. *Journal of Chemical Physics* **2004,** *121* (20), 9855-9864.

18.   Aguirre, F.; Pratt, S. T., Photoionization of vibrationally hot CH_3 and CF_3. *Journal of Chemical Physics* **2005,** *122* (23).

19.   Fan, H. Y.; Pratt, S. T., Photoionization of hot radicals: C_2H_5,n-C_3H_7, and i-C3H7. *Journal of Chemical Physics* **2005,** *123* (20).

20.   Lau, K. C.; Liu, Y.; Butler, L. J., Probing the barrier for CH_2CHCO -> CH_2CH+CO by the velocity map imaging method. *Journal of Chemical Physics* **2005,** *123* (5).

21.   Robinson, J. C.; Sveum, N. E.; Neumark, D. M., Determination of absolute photoionization cross sections for vinyl and propargyl radicals. *Journal of Chemical Physics* **2003,** *119* (11), 5311-5314.

22.   Robinson, J. C.; Sveum, N. E.; Neumark, D. M., Determination of absolute photoionization cross sections for isomers of C_3H_5: allyl and 2-propenyl radicals. *Chemical Physics Letters* **2004,** *383* (5-6), 601-605.

23.   Taatjes, C. A.; Osborn, D. L.; Selby, T. M.; Meloni, G.; Fan, H. Y.; Pratt, S. T., Absolute photoionization cross-section of the methyl radical. *Journal of Physical Chemistry A* **2008,** *112* (39), 9336-9343.

24.   Willis, P. A.; Stauffer, H. U.; Hinrichs, R. Z.; Davis, H. F., Rotatable source crossed molecular beams apparatus with pulsed ultraviolet vacuum ultraviolet

photoionization detection. *Review of Scientific Instruments* **1999,** *70* (6), 2606-2614.

25.   Ahmed, M.; Peterka, D. S.; Suits, A. G., H abstraction dynamics by crossed-beam velocity map imaging: Cl+CH₃OH -> CH₂OH+HCl. *Chemical Physics Letters* **2000,** *317* (3-5), 264-268.

26.   Huang, C.; Li, W.; Estillore, A. D.; Suits, A. G., Dynamics of CN plus alkane reactions by crossed-beam dc slice imaging. *Journal of Chemical Physics* **2008,** *129* (7).

27.   Ausloos, P., Far Ultraviolet Photolysis of Alkanes [1]. *Mol.Photochem* **1972,** *4* (1), 39.

28.   Au, J. W.; Cooper, G.; Burton, G. R.; Olney, T. N.; Brion, C. E., The valence shell photoabsorption of the linear alkanes, CNH₂N+2(N=1-8) - absolute oscillator-strengths (7-220 EV). *Chemical Physics* **1993,** *173* (2), 209-239.

29.   Okabe , H. a. M., R, *J.Chem.Phys* **1962,** *37*, 1340.

30.   Obi, K., *J.Chem.Phys* **1971,** *55*, 3822.

31.   Tonokura, K.; Matsumi, Y.; Kawasaki, M.; Kasatani, K., Doppler spectroscopy of hydrogen-atoms from the photodissociation of saturated-hydrocarbons and methyl halides at 157 nm. *Journal of Chemical Physics* **1991,** *95* (7), 5065-5071.

32.   Lin, J. J.; Harich, S.; Hwang, D. W.; Wu, M. S.; Lee, Y. T.; Yang, X. M., Dynamics of atomic and molecular hydrogen elimination from hydrocarbons at VUV excitation. *Journal of the Chinese Chemical Society* **1999,** *46* (3), 435-444.

33. Wu, S. M.; Lin, J. J.; Lee, Y. T.; Yang, X., Site specificity in molecular hydrogen elimination from photodissociation of propane at 157 nm. *Journal of Chemical Physics* **1999,** *111* (5), 1793-1796.

34. Wu, S. M.; Lin, J. J.; Lee, Y. T.; Yang, X., Dynamics of atomic and molecular hydrogen elimination from small alkanes following 157-nm excitation. *Journal of Physical Chemistry A* **2000,** *104* (31), 7189-7199.

35. Wu, S. M.; Lin, J. J.; Lee, Y. T.; Yang, X., Site specific dissociation dynamics of propane at 157 nm excitation. *Journal of Chemical Physics* **2000,** *112* (18), 8027-8037.

36. Lee, S. K.; Silva, R.; Thamanna, S.; Vasyutinskii, O. S.; Suits, A. G., S(D-1(2)) atomic orbital polarization in the photodissociation of OCS at 193 nm: Construction of the complete density matrix. *Journal of Chemical Physics* **2006,** *125* (14).

37. Townsend, D.; Minitti, M. P.; Suits, A. G., Direct current slice imaging. *Review of Scientific Instruments* **2003,** *74* (4), 2530-2539.

38. Lias, S. G., Ionization energy evaluation. *NIST Chemistry WebBook, NIST Standard Reference Database Number 69* **2008**.

39. Noller, B.; Fischer, I., Photodissociation dynamics of the 2-propyl radical, C3H7. *Journal of Chemical Physics* **2007,** *126* (14).

40. Viskolcz, B.; Lendvay, G.; Seres, L., Ab initio barrier heights and branching ratios of isomerization reactions of a branched alkyl radical. *Journal of Physical Chemistry A* **1997,** *101* (38), 7119-7127.

ABSTRACT

PHOTODISSOCIATION DYNAMICS IN TITAN'S ATMOSPHERE

by

W. RUCHIRA SILVA

December 2010

Advisor: Dr. Arthur.G.Suits

Major: Chemistry (Physical)

Degree: Doctor of Philosophy

Photodissociation dynamics of molecules relevant to understanding Titan's atmosphere (diacetylene, cyanoacetylene and heptane isomers) are carried out under collisionless condition using the DC slice imaging technique. In diacetylene photodissociation, two-photon processes dominate at 243 nm and 212 nm whereas at 121.6 nm, a one-photon dissociation process dominates. Direct measurement of the lifetime of metastable triplet diacetylene confirms sub-microsecond lifetimes. Photodissociation of cyanoacetylene at 193.3 nm proceeds on the S_1 potential energy surface with an exit barrier. In heptane photodissociation, the dissociation occurs on the ground state or low-lying triplet states with nonradiative electronic relaxation. Time-of-flight mass spectroscopy studies in this system yield the relative ionization efficiencies of 1- and 2-butyl and propyl radicals at 157 nm.

AUTOBIOGRAPHICAL STATEMENT

I was born in Colombo, Sri Lanka. I have received my primary education from Sri Dharmaloka College, Kelaniya. Next I moved to St. Peters College, Bambalapitiya to complete my high school education. I have completed my undergraduate studies in Chemistry from University of Peradeniya. During my graduate studies in Wayne State University, I have contributed to the following publications.

1. Huang, C; Zhang, F; Kaiser, R.I; Kislov, V.V; Mebel, A.M; Silva, R; Gichuhi, W.K; Suits, A.G: *"Photodissociation of diacetylene dimer and implication for hydrocarbon growth in Titan atmosphere"* Astrophysical journal **2010**, 714, 1249-1255

2. Silva, R; Gichuhi, W.K; Kislov, V.V; Mebel, A.M; Suits, A.G: *"UV Photodissociation of cyanoacetylene: A combined ion imaging and theoretical investigation"* J.Phys.Chem. A **2009**, 113, 11182-11186

3. Silva, R; Gichuhi, W.K; Doyle, M.B; Winney, A.H; Suits, A.G: *"Photodissociation of heptane isomers and relative ionization efficiencies of butyl and propyl radicals at 157 nm"* Physical Chemistry Chemical Physics **2009**, 11, 4777-4781

4. Silva, R; Gichuhi, W.K; Huang, C; Doyle, M.B; Kislov, V.V; Mebel, A.M; Suits, A.G: *"H elimination and metastable lifetimes in the UV photoexcitation of diacetylene"* PNAS **2008**, 105, 12713-12718

5. Lee, S.K; Silva, R; Kim, M.H; Shen, L; Suits, A.G: *"Photodissociation of spatially aligned acetaldehyde cations"* J.Phys.Chem. A **2007**, 111, 6741-6745

6. Lee, S.K; Silva, R; Thamnna, S; Vasyutinski, O.S; Suits, A.G: "*S(D-1(2)) atomic orbital polarization in the photodissociation of OCS at 193 nm: Construction of the complete density matrix"* J. Chem. Phys **2006**, 125, 144318 (1-12)

7. Huang, C; Li, W; Silva, R; Suits, A.G: "*DC slice ion imaging of the ultraviolet photodissociation of BrCN"* Chemical Physics Letters **2006**, 426, 242-247